

## Physical Results from 2+1 Flavor Domain Wall QCD and SU(2) Chiral Perturbation Theory

C. Allton,<sup>1</sup> D.J. Antonio,<sup>2</sup> Y. Aoki,<sup>3</sup> T. Blum,<sup>3,4</sup> P.A. Boyle,<sup>2</sup> N.H. Christ,<sup>5</sup> S.D. Cohen\*,<sup>5</sup>  
M.A. Clark,<sup>6</sup> C. Dawson<sup>†,3</sup>, M.A. Donnellan,<sup>7</sup> J.M. Flynn,<sup>7</sup> A. Hart,<sup>2</sup> T. Izubuchi,<sup>3,8</sup> A. Jüttner<sup>‡,7</sup>,  
C. Jung,<sup>9</sup> A.D. Kennedy,<sup>2</sup> R.D. Kenway,<sup>2</sup> M. Li,<sup>5</sup> S. Li,<sup>5</sup> M.F. Lin<sup>§,5</sup>, R.D. Mawhinney,<sup>5</sup>  
C.M. Maynard,<sup>10</sup> S. Ohta,<sup>11,12,3</sup> B.J. Pendleton,<sup>2</sup> C.T. Sachrajda,<sup>7</sup> S. Sasaki,<sup>3,13</sup>  
E.E. Scholz,<sup>9</sup> A. Soni,<sup>9</sup> R.J. Tweedie,<sup>2</sup> J. Wennekers,<sup>2</sup> T. Yamazaki,<sup>4</sup> and J.M. Zanotti<sup>2</sup>  
(RBC and UKQCD Collaborations)

<sup>1</sup>*Department of Physics, Swansea University, Swansea SA2 8PP, UK*

<sup>2</sup>*SUPA, School of Physics, The University of Edinburgh, Edinburgh EH9 3JZ, UK*

<sup>3</sup>*RIKEN-BNL Research Center, Brookhaven National Laboratory, Upton, NY 11973, USA*

<sup>4</sup>*Physics Department, University of Connecticut, Storrs, CT 06269-3046, USA*

<sup>5</sup>*Physics Department, Columbia University, New York, NY 10027, USA*

<sup>6</sup>*Center for Computational Science, 3 Cummington Street, Boston University, MA 02215, USA*

<sup>7</sup>*School of Physics and Astronomy, University of Southampton, Southampton SO17 1BJ, UK*

<sup>8</sup>*Institute for Theoretical Physics, Kanazawa University, Kakuma, Kanazawa, 920-1192, Japan*

<sup>9</sup>*Brookhaven National Laboratory, Upton, NY 11973, USA*

<sup>10</sup>*EPCC, School of Physics, The University of Edinburgh, Edinburgh EH9 3JZ, UK*

<sup>11</sup>*Institute of Particle and Nuclear Studies, KEK, Tsukuba, 305-0801, Japan*

<sup>12</sup>*Physics Department, Sokenkai Graduate U. Adv. Studies, Hayama, Kanagawa, 240-0193, Japan*

<sup>13</sup>*Department of Physics, University of Tokyo, Tokyo 113-003, Japan*

(Dated: April 2, 2008)

---

\* Present address: Jefferson Lab, 12000 Jefferson Avenue, Newport News, VA 23606

† Present address: Dept. of Physics, University of Virginia, 382 McCormick Rd. Charlottesville, VA 22904-4714

‡ Present address: Institut für Kernphysik, Johannes Gutenberg-Universität Mainz, Johann-Hoachim-Becher-Weg 45, D-55099 Mainz, Germany

§ Present address: Center for Theoretical Physics, Massachusetts Institute of Technology, 77 Massachusetts Ave., 6-319, Cambridge, MA 02139

## ABSTRACT

We have simulated QCD using 2+1 flavors of domain wall quarks on a  $(2.74 \text{ fm})^3$  volume with an inverse lattice scale of  $a^{-1} = 1.729(28) \text{ GeV}$ . The up and down (light) quarks are degenerate in our calculations and we have used four values for the ratio of light quark masses to the strange (heavy) quark mass in our simulations: 0.217, 0.350, 0.617 and 0.884. We have measured pseudoscalar meson masses and decay constants, the kaon bag parameter  $B_K$  and vector meson couplings. We have used SU(2) chiral perturbation theory, which assumes only the up and down quark masses are small, and SU(3) chiral perturbation theory to extrapolate to the physical values for the light quark masses. While next-to-leading order formulae from both approaches fit our data for light quarks, we find the higher order corrections for SU(3) very large, making such fits unreliable. We also find that SU(3) does not fit our data when the quark masses are near the physical strange quark mass. Thus, we rely on SU(2) chiral perturbation theory for accurate results. We use the masses of the  $\Omega$  baryon, and the  $\pi$  and  $K$  mesons to set the lattice scale and determine the quark masses. We then find  $f_\pi = 124.1(3.6)_{\text{stat}}(6.9)_{\text{syst}} \text{ MeV}$ ,  $f_K = 149.6(3.6)_{\text{stat}}(6.3)_{\text{syst}} \text{ MeV}$  and  $f_K/f_\pi = 1.205(0.018)_{\text{stat}}(0.062)_{\text{syst}}$ . Using non-perturbative renormalization to relate lattice regularized quark masses to RI-MOM masses, and perturbation theory to relate these to  $\overline{\text{MS}}$  we find  $m_{ud}^{\overline{\text{MS}}}(2 \text{ GeV}) = 3.72(0.16)_{\text{stat}}(0.33)_{\text{ren}}(0.18)_{\text{syst}} \text{ MeV}$ ,  $m_s^{\overline{\text{MS}}}(2 \text{ GeV}) = 107.3(4.4)_{\text{stat}}(9.7)_{\text{ren}}(4.9)_{\text{syst}} \text{ MeV}$ , and  $\tilde{m}_{ud} : \tilde{m}_s = 1 : 28.8(0.4)_{\text{stat}}(1.6)_{\text{syst}}$ . For the kaon bag parameter, we find  $B_K^{\overline{\text{MS}}}(2 \text{ GeV}) = 0.524(0.010)_{\text{stat}}(0.013)_{\text{ren}}(0.025)_{\text{syst}}$ . Finally, for the ratios of the couplings of the vector mesons to the vector and tensor currents ( $f_V$  and  $f_V^T$  respectively) in the  $\overline{\text{MS}}$  scheme at 2 GeV we obtain:  $f_\rho^T/f_\rho = 0.687(27)$ ;  $f_{K^*}^T/f_{K^*} = 0.712(12)$  and  $f_\phi^T/f_\phi = 0.750(8)$ .

## I. INTRODUCTION

Numerical simulations of Quantum Chromodynamics (QCD) conventionally discretize four-dimensional space-time by introducing a lattice scale,  $a$ , which yields a well-defined path integral formulation appropriate for study via importance sampling techniques. Measurements of observables at non-zero values of  $a$  can then be extrapolated to  $a = 0$  to produce continuum results and, if discretization errors are small, the continuum extrapolation is better controlled. An important aspect of simulating QCD is choosing a lattice discretization which reduces the  $a$  dependence of observables [1]. Here, one is helped by knowing that if an  $O(a^2)$  accurate gauge action is used, such as the Wilson action, and a discretization of QCD preserves the continuum chiral symmetries of massless QCD, then the lattice theory can only have errors quadratic in  $a$ , in combinations such as  $(a\Lambda_{\text{QCD}})^2$ , and  $(ma)^2$ , where  $m$  is a quark mass. These errors are much smaller than the  $O(am)$  discretization errors which can occur if the lattice theory breaks chiral symmetry. Additionally, if chiral symmetry is broken at non-zero lattice spacing, renormalization of the simplest operators, while straightforward, is involved [2]. (For a recent review, see [3].)

Preserving chiral symmetry at non-zero lattice spacing has a large impact on many of the more complicated observables, such as matrix elements of operators, that one wants to determine from lattice QCD. For observables such as hadron masses, which do not require any renormalization, controlling non-zero lattice spacing effects in the discretized theory is helpful. For observables requiring renormalization, such as weak matrix elements in hadronic states, the presence of chiral symmetry at non-zero lattice spacing can be vital to the renormalization and mixing of the relevant operators [4]. The chiral symmetries control the allowed operator mixings, so simplifications take place. Without this control, the number of operators and mixings amongst them can make renormalization very difficult, if not practically impossible. Chiral symmetry can now be preserved at non-zero lattice spacing with a variety of formulations [5, 6, 7, 8, 9, 10]. (It is important to point out that some of the benefits of chiral symmetry can be achieved without its presence at non-zero lattice spacing. For example, twisted mass Wilson fermion discretizations [11] make judicious use of chiral transformations to calculate quantities without linear dependence on  $a$  and continuum-like renormalization properties, without having full chiral symmetry.)

In addition to taking the limit  $a \rightarrow 0$ , to achieve accurate physical results lattice simulations must reach the large volume ( $V \rightarrow \infty$ ) limit and also the limit of physical light quarks. For discretizations which preserve chiral symmetry at non-zero  $a$ , simulations with arbitrarily light quarks can be

done before taking the continuum limit – without chiral symmetry, lattice artifacts can alter the chiral limit at non-zero  $a$  and make the limits non-commuting. Current computer power does not allow simulations with physically light up and down quarks, so an extrapolation from masses used in the simulations to physical light quark masses must be done. Chiral perturbation theory [12, 13] provides a theoretical framework for these extrapolations and, for lattice QCD discretizations which preserve chiral symmetry, the chiral perturbation theory is very similar to the continuum theory, since there are only a few lattice alterations to it.

Of long recognized importance, the preservation of the global chiral symmetries in discretized QCD has been achieved by Kaplan’s proposal [5] of four-dimensional fermions resulting from a defect in a five-dimensional theory. Further developments led to the domain wall fermions of Shamir and Furman [6, 7], that we use here, the overlap formulation of Neuberger and Narayanan [8, 9] and the perfect actions of Hasenfratz [10]. To date, the domain-wall formulation has proven to be the most numerically feasible. In this approach, one introduces a fifth dimension (which we label by the index  $s$  and which has extent  $L_s$ ) and only achieves exact chiral symmetry in the  $L_s \rightarrow \infty$  limit. However, for finite  $L_s$ , chiral symmetry breaking effects can be made small enough to be easily controlled, as we will discuss in subsequent sections. The presence of the fifth dimension (we use  $L_s = 16$  in this work) increases the number of floating point operations required in a calculation by a factor of  $O(L_s)$  over conventional QCD discretizations such as Wilson and staggered fermions, which do not preserve continuum chiral symmetries.

The domain wall fermion formulation has been used extensively in numerical simulations for about a decade. The original works were primarily in the quenched approximation, although some early work did involve QCD with two light quark flavors [14]. More extensive 2 flavor simulations were done [15] and, with recent improvements in algorithms and computers, 2+1 flavor QCD simulations have been completed [16, 17, 18, 19, 20]. These previous calculations demonstrated that domain wall fermion QCD shows the expected consequences of having a controlled approximation to the full chiral symmetries of continuum QCD. In particular, the following important features were observed.

1. A mild dependence on  $a$  in the  $a \rightarrow 0$  limit in the quenched approximation.
2. For both quenched and unquenched QCD, the residual chiral symmetry breaking at non-zero  $a$ , as measured by the additive contribution to the quark mass  $m_{\text{res}}$ , is readily made a small fraction of the input bare quark mass at practical values for  $L_s$ .

3. The operator mixing problem for domain wall fermion QCD is essentially the same as the continuum problem.

These previous calculations were not able to fully exploit one of the main benefits of domain wall fermion QCD – the ability to probe the chiral limit of the theory at non-zero lattice spacing – and hence make accurate contact with the physical quark mass region. With recent advances in computers and algorithms, we have made considerable progress in simulating with light quarks and on large volumes. In this paper, we report on simulations of domain wall fermion QCD, with two light degenerate quarks and a single flavor heavier quark (a 2+1 flavor simulation) at a single inverse lattice spacing of  $a^{-1} = 1.729(28)$  GeV in a  $(2.74 \text{ fm})^3$  spatial volume. We used four different light dynamical quark masses in our simulations and the ratios of these light masses to the physical strange quark mass is 0.217, 0.350, 0.617 and 0.884. A single value for the heavy quark mass was used in all our simulations and its ratio to the physical strange quark mass is 1.150. (An accurate value for the physical strange quark mass was, of course, not known until after our simulation was complete.) For mesons made of degenerate light quarks, the corresponding pseudoscalar meson masses are 331 MeV, 419 MeV, 557 MeV and 672 MeV. We have also done measurements with a variety of valence quark masses, with a ratio of the smallest mass to the physical strange quark mass of 0.110, corresponding to a pseudoscalar meson with a mass of 242 MeV. In a previous paper [16], we have given results from simulations with the same gauge coupling constant, but on a smaller volume, which gives us some understanding of finite volume effects.

To extrapolate from our simulation quark masses to the physical values, we use chiral perturbation theory (ChPT), which is an expansion of low energy QCD observables in powers of the meson masses and momenta over the pseudoscalar decay constant. Within the general framework of ChPT one can consider only the pions to be light particles, yielding an  $SU(2)_L \times SU(2)_R$  ChPT (which we will call  $SU(2)$  ChPT) or one can also consider the kaons as light, yielding an  $SU(3)_L \times SU(3)_R$  ChPT (which we will call  $SU(3)$  ChPT). In Section II, we discuss the DWF corrections to ChPT and develop  $SU(2)$  ChPT for the kaon sector, which we will later use to fit our data.

In Section III we give details of our simulations, including the Rational Hybrid Monte Carlo (RHMC) algorithm that we use to generate our lattices. Section IV describes the sources and sinks we use for our pseudoscalar observables, our methods of determining desired quantities and results in lattice units. We will also use the mass of the  $\Omega$  baryon, which has no corrections from chiral logarithms, as part of our scale setting and the details of the measurement of  $m_\Omega$  are given

in Section V.

In Section VI we fit our lattice values for the masses and decay constants of pseudoscalars to partially quenched SU(2) ChPT at NLO. We find our data is well described by the theoretical formula from Section II, provided the pions have masses below about 420 MeV. We use the fits to SU(2) ChPT as the most accurate way to extrapolate our data to the chiral limit, since SU(2) ChPT does not require the kaon mass to be small, but only requires  $m_\pi \ll m_K$ . Using the results for pseudoscalar masses from our SU(2) ChPT fits and our lattice values for the  $\Omega$  baryon mass, we fix the lattice scale and bare quark masses using the known masses of the  $\pi$ ,  $K$  and  $\Omega$ . We find that our inverse lattice spacing is  $a^{-1} = 1.729(28)$  GeV. In a separate work [21], we have used non-perturbative renormalization to calculate the multiplicative renormalization factor needed to relate our bare lattice quark masses to continuum  $\overline{\text{MS}}$  masses. We find

$$m_{ud}^{\overline{\text{MS}}}(2 \text{ GeV}) = 3.72(0.16)_{\text{stat}}(0.33)_{\text{ren}}(0.18)_{\text{syst}} \text{ MeV}, \quad (1)$$

$$m_s^{\overline{\text{MS}}}(2 \text{ GeV}) = 107.3(4.4)_{\text{stat}}(9.7)_{\text{ren}}(4.9)_{\text{syst}} \text{ MeV}, \quad (2)$$

$$\tilde{m}_{ud} : \tilde{m}_s = 1 : 28.8(0.4)_{\text{stat}}(1.6)_{\text{syst}}. \quad (3)$$

where  $(\dots)_{\text{stat}}$ ,  $(\dots)_{\text{ren}}$  and  $(\dots)_{\text{syst}}$  show the statistical error, the error from renormalization and the systematic error. We assume the light quarks to be degenerate in this work. We now predict values for  $f_\pi$  and  $f_K$  and find  $f_\pi = 124.1(3.6)_{\text{stat}}(6.9)_{\text{syst}} \text{ MeV}$  and  $f_K = 149.6(3.6)_{\text{stat}}(6.3)_{\text{syst}} \text{ MeV}$ . Our fits to SU(2) ChPT also determine the low energy constants (LECs) for pseudoscalar masses and decay constants in SU(2) ChPT. Furthermore, implications of our results to CKM matrix elements are discussed.

In Section VII we fit our light pseudoscalar data to SU(3) ChPT. Here we also find that our data is well represented by SU(3) ChPT at NLO, provided our pseudoscalars have masses below about 420 MeV. The failure of NLO SU(3) ChPT to fit our data when pseudoscalar masses are near the physical kaon mass rules out using NLO SU(3) ChPT in this mass region. With light masses, we determine values for the SU(3) LECs which agree well with values determined by others. However, we find a small value for the decay constant in the SU(3) chiral limit, which we denote by  $f_0$  (a complete description of our notation is given in the Appendix). Our fits give  $f_0 = 94$  MeV, with conventions such that the physical value is  $f_\pi = 131$  MeV, and this value is smaller than generally found phenomenologically, which we discuss further in Section VII. Along with this we find that the size of the NLO corrections to SU(3) ChPT, relative to the leading order term, are in the range of 50% or more. This makes the convergence of SU(3) ChPT for these quark

masses unreliable. Thus, although it represents our data well and the parameters we find generally agree with others, we find the systematic errors in SU(2) ChPT substantially smaller and use it as our most accurate means of extrapolating our data to the chiral limit.

In section VIII, we discuss our determination of the kaon bag parameter,  $B_K$ , which is needed to relate indirect CP violation in the standard model to experimental measurements. This section expands upon the data and analysis presented in [19]. Here we also find extrapolations to the physical quark masses to be under much better control with SU(2) than with SU(3) ChPT. We present our estimates of systematic errors, including finite size effects. We find  $B_K^{\overline{\text{MS}}}(2\text{ GeV}) = 0.524(0.010)_{\text{stat}}(0.013)_{\text{ren}}(0.025)_{\text{syst}}$ .

In Section IX we present results for the couplings of light vector mesons to vector and tensor currents. The results for the ratios of the couplings of the vector mesons to the vector and tensor currents ( $f_V$  and  $f_V^T$  respectively) in the  $\overline{\text{MS}}$  scheme at 2 GeV are:  $f_\rho^T/f_\rho = 0.687(27)$ ;  $f_{K^*}^T/f_{K^*} = 0.712(12)$  and  $f_\phi^T/f_\phi = 0.750(8)$ .

## II. CHIRAL PERTURBATION THEORY

In this section, we discuss chiral perturbation theory for domain wall fermions in subsection II A. We develop SU(2) ChPT for kaons in II B. Our notation and an extensive list of the formulae from SU(2) and SU(3) ChPT that we use in this work are given in the Appendix.

### A. Chiral Perturbation Theory for Domain Wall Fermions

Our simulations are done with domain wall fermions, which have explicit chiral symmetry breaking effects at non-zero lattice spacing. These effects are controlled by the extent of the lattice in the fifth dimension, denoted by  $L_s$ , whose value is chosen to make such terms small, consistent with current computer power. The small chiral symmetry breaking that remains can be measured and its effects taken into account, as has been discussed extensively in the literature. A recent review of this topic is available in [22].

As previously discussed in [4, 23], for a theory with  $N$  quarks these explicit symmetry breaking effects can be easily included by introducing an  $N \times N$  matrix parameter  $\Omega$  into the domain wall fermion action. This parameter connects four-dimensional planes at the mid-point of the fifth

dimension and is included into the action by adding

$$S_\Omega = - \sum_x \left\{ \bar{\Psi}_{x,L_s/2-1} P_L (\Omega^\dagger - 1) \Psi_{x,L_s/2} + \bar{\Psi}_{x,L_s/2} P_R (\Omega - 1) \Psi_{x,L_s/2-1} \right\} \quad (4)$$

to the conventional action for domain wall fermions [24]. Here,  $\Psi_{x,s}$  represents a five-dimensional fermion field with four spin components and suppressed flavor indices. We recover the conventional domain wall fermion action when we set  $\Omega = 1$ .

If we let  $\Omega$  transform as

$$\Omega \rightarrow V_R \Omega V_L^\dagger \quad (5)$$

under  $SU(N)_L \times SU(N)_R$ , then the domain wall fermion Dirac operator possesses exact chiral symmetry. Thus we can use  $\Omega$  to track the explicit chiral symmetry breaking from domain wall fermions, in both the Symanzik style effective Lagrangian for domain wall fermion QCD and in Green functions. However, we note that  $\Omega$  itself is not a small quantity, since a general Green function involving the five-dimensional fermion fields does not have any approximate chiral symmetry. However, for the effective action and low momentum limit of Green functions made from the four-dimensional fields at the boundaries of the fifth dimension, each power of  $\Omega$  that enters should come with a suppression related to the ratio of amplitudes of the low-energy fermion modes between the boundaries and the midpoint in the fifth dimension.

Consider a non-zero  $a$  effective Lagrangian description of QCD with domain wall fermions at finite  $L_s$ . The presence of the parameter  $\Omega$  implies that the terms containing fermions, up to operators of dimension five, are

$$\frac{Z_m m_f}{a} \bar{\Psi} \Psi + \frac{c_3}{a} \left\{ \bar{\Psi} \Omega^\dagger P_R \Psi + \bar{\Psi} \Omega P_L \Psi \right\} + ac_5 \left\{ \bar{\Psi} \sigma_{\mu\nu} F_{\mu\nu} \Omega^\dagger P_R \Psi + \bar{\Psi} \sigma_{\mu\nu} F_{\mu\nu} \Omega P_L \Psi \right\}. \quad (6)$$

Here  $m_f$  is the dimensionless input bare quark mass in the domain wall fermion formulation, and  $c_3$  and  $c_5$  are dimensionless parameters that represent the mixing of left- and right-handed quarks between the five-dimensional boundaries. These parameters are of  $O(e^{-\alpha L_s})$  at weak coupling; for coarse lattices where there are localized dislocations in the gauge fields corresponding to changes in the topology, they are generically  $O(a_1 e^{-\alpha L_s} + a_2)/L_s$ , where  $a_2 \neq 0$  is due to the density of localized topological dislocations [17].

Setting  $\Omega = 1$ , we have

$$\frac{Z_m m_f}{a} \bar{\Psi} \Psi + \frac{c_3}{a} \bar{\Psi} \Psi + ac_5 \bar{\Psi} \sigma_{\mu\nu} F_{\mu\nu} \Psi. \quad (7)$$

The combination  $Z_m m_f + c_3$  is the total (dimensionless) quark mass and we choose  $L_s$  to control the contribution of the second term, by changing the size of  $c_3$ . Eq. (7) is identical to the result



for Wilson fermions, except that the coefficients  $c_3$  and  $c_5$  are expected to be small,  $O(10^{-3})$ , for realistic domain wall fermion simulations, compared to being  $O(1)$  as for Wilson fermions.

We can now discuss the application of chiral perturbation theory to our domain wall fermion simulations at a fixed lattice spacing. Our discussion will be for SU(3), but the results are easily generalized. We start from the conventional QCD SU(3) chiral Lagrangian in the continuum and make use of the presence of the  $\Omega$  spurion field to add all additional terms to it. Initially we power count only in  $\Omega$  and defer, for the moment, the additional question of power counting in  $a$ . We choose  $\Sigma(x) = e^{2i\phi(x)/f_0}$ , where  $\Sigma$  transforms as:  $\Sigma \rightarrow V_L \Sigma V_R^\dagger$ ,  $V_L, V_R \in \text{SU}(3)$ . We define  $\widehat{\chi} = 2B_0 \text{diag}(m_u, m_d, m_s)$ , where  $B_0$  is one of the low energy constants (LECs) that enters in chiral perturbation theory. To  $O(p^4)$  the continuum Lagrangian is:

$$\begin{aligned}
\mathcal{L} = & \frac{f_0^2}{8} \text{Tr}[\partial_\mu \Sigma \partial^\mu \Sigma^\dagger] + \frac{f_0^2}{8} \text{Tr}[\widehat{\chi} \Sigma + (\widehat{\chi} \Sigma)^\dagger] \\
& + L_1^{(3)} \left\{ \text{Tr}[\partial_\mu \Sigma (\partial^\mu \Sigma)^\dagger] \right\}^2 + L_2^{(3)} \text{Tr} \left[ \partial_\mu \Sigma (\partial_\nu \Sigma)^\dagger \right] \text{Tr} \left[ \partial^\mu \Sigma (\partial^\nu \Sigma)^\dagger \right] \\
& + L_3^{(3)} \text{Tr} \left[ \partial_\mu \Sigma (\partial^\mu \Sigma)^\dagger \partial_\nu \Sigma (\partial^\nu \Sigma)^\dagger \right] + L_4^{(3)} \text{Tr} \left[ \partial_\mu \Sigma (\partial^\mu \Sigma)^\dagger \right] \text{Tr} \left( \widehat{\chi} \Sigma + (\widehat{\chi} \Sigma)^\dagger \right) \\
& + L_5^{(3)} \text{Tr} \left[ \partial_\mu \Sigma (\partial^\mu \Sigma)^\dagger (\widehat{\chi} \Sigma + (\widehat{\chi} \Sigma)^\dagger) \right] + L_6^{(3)} \left[ \text{Tr} \left( \widehat{\chi} \Sigma + (\widehat{\chi} \Sigma)^\dagger \right) \right]^2 \\
& + L_7^{(3)} \left[ \text{Tr} \left( \widehat{\chi} \Sigma - (\widehat{\chi} \Sigma)^\dagger \right) \right]^2 + L_8^{(3)} \text{Tr} \left( \widehat{\chi} \Sigma \widehat{\chi} \Sigma + (\widehat{\chi} \Sigma \widehat{\chi} \Sigma)^\dagger \right). \tag{8}
\end{aligned}$$

For the domain wall fermion case, we can generate the new terms that arise by starting from the Lagrangian in Eq. (8). Since  $\Omega$  transforms as  $\widehat{\chi}$  or  $\Sigma^\dagger$  does, new terms can be created by substituting  $\Omega$  for  $\widehat{\chi}$  and  $\Sigma^\dagger$  in Eq. (8), remembering that derivatives acting on  $\Omega$  vanish. Since the dominant contribution of explicit chiral symmetry breaking in Eq. (7) is an additive contribution to the quark mass, we power count  $\Omega$  as  $O(p^2)$ . Keeping terms of  $O(p^4)$  and using  $D_i, \tilde{D}_i$  for the LEC's for these terms, we have additional contributions to Eq. (8) of

$$\begin{aligned}
& \frac{f^2}{8} D_0 \text{Tr}[\Omega \Sigma + (\Omega \Sigma)^\dagger] + \frac{f^2}{8} \tilde{D}_0 \text{Tr}[\Omega \widehat{\chi}^\dagger + \Omega^\dagger \widehat{\chi}] \\
& D_4 \text{Tr} \left[ \partial_\mu \Sigma (\partial^\mu \Sigma)^\dagger \right] \text{Tr} \left( \Omega \Sigma + (\Omega \Sigma)^\dagger \right) + D_5 \text{Tr} \left[ \partial_\mu \Sigma (\partial^\mu \Sigma)^\dagger (\Omega \Sigma + (\Omega \Sigma)^\dagger) \right] \\
& + D_6 \left[ \text{Tr} \left( \Omega \Sigma + (\Omega \Sigma)^\dagger \right) \right] \left[ \text{Tr} \left( \widehat{\chi} \Sigma + (\widehat{\chi} \Sigma)^\dagger \right) \right] + \tilde{D}_6 \left[ \text{Tr} \left( \Omega \Sigma + (\Omega \Sigma)^\dagger \right) \right]^2 \\
& + D_7 \left[ \text{Tr} \left( \Omega \Sigma - (\Omega \Sigma)^\dagger \right) \right] \left[ \text{Tr} \left( \widehat{\chi} \Sigma - (\widehat{\chi} \Sigma)^\dagger \right) \right] + \tilde{D}_7 \left[ \text{Tr} \left( \Omega \Sigma - (\Omega \Sigma)^\dagger \right) \right]^2 \\
& + D_8 \text{Tr} \left( \widehat{\chi} \Sigma \Omega \Sigma + (\widehat{\chi} \Sigma \Omega \Sigma)^\dagger \right) + \tilde{D}_8 \text{Tr} \left( \Omega \Sigma \Omega \Sigma + (\Omega \Sigma \Omega \Sigma)^\dagger \right). \tag{9}
\end{aligned}$$

Terms which involve two derivatives, a factor of  $\widehat{\chi}$  and a factor of  $\Omega$  will be  $O(p^6)$  and have been neglected. Note that we have kept the term involving  $\tilde{D}_0$ , even though it does not involve any  $\Sigma$

fields. Such a term does play a role in determining the value for the chiral condensate through the variation of the partition function with respect to the quark mass.

We would seem to have many new low energy constants to determine with domain wall fermions at non-zero  $a$ . However, the form of the Symanzik effective Lagrangian for DWF QCD shows that the leading order (in  $a$ ) chiral symmetry breaking effect is a universal shift in the quark mass, *i.e.*  $c_3/a$  multiplies the dimension three operator  $\bar{\psi}\psi$ . Thus, there is no difference in ChPT between  $m_f$  and  $c_3$ , and we can rewrite the terms in Eq. (9) in terms of the original LEC's of QCD, with a shifted quark mass, plus higher order corrections. Letting  $\chi = 2B_0[\text{diag}(m_u, m_d, m_s) + c_3\text{diag}(1, 1, 1)]$  and looking at the  $D_4$  term as an example, we have

$$D_4\text{Tr} \left[ \partial_\mu \Sigma (\partial^\mu \Sigma)^\dagger \right] \text{Tr} \left( \Omega \Sigma + (\Omega \Sigma)^\dagger \right) = L_4^{(3)} \text{Tr} \left[ \partial_\mu \Sigma (\partial^\mu \Sigma)^\dagger \right] \text{Tr} \left( \chi \Sigma + (\chi \Sigma)^\dagger \right) + O(ac_5) L_4^{(3)} \text{Tr} \left[ \partial_\mu \Sigma (\partial^\mu \Sigma)^\dagger \right] \text{Tr} \left( \Sigma + \Sigma^\dagger \right). \quad (10)$$

The last term is  $O(a) \times O(c_5) \times O(p^2)$ . It is customary to power count  $O(a)$  and  $O(p^2)$  terms as the same size for unimproved Wilson fermions, and this same term appears there [25], except that  $c_5^{\text{Wilson}}$  is  $O(1)$ . While for Wilson fermions, this term must be kept at NLO in the chiral Lagrangian, for domain wall fermions, where  $c_5$  is very small, it can be neglected.

Examining all the terms in Eq. (9), we see that the complete NLO chiral Lagrangian for domain wall fermions is given by Eq. (8), with  $\hat{\chi} \rightarrow \chi$ , where  $\chi$  is proportional to the sum of the input bare quark mass,  $m_f$ , and the additive quark mass contribution which comes from  $c_3$ . Since we will be working to NLO order of ChPT in this work, domain wall fermions at non-zero lattice spacing should be described by the chiral Lagrangian given in Eq. (8). When we fit our data for specific quantities to the chiral formula following from Eq. (8), the LEC's  $L_i$  will differ at  $O(a^2)$  from their continuum values. Since we work at a single lattice spacing, we will not be able to correct for these deviations from continuum QCD.

The size of the residual symmetry breaking terms represented by  $c_3$  and  $c_5$  in Eq. (6) is most easily studied by examining the five-dimensional current  $\mathcal{A}_\mu^a$  which can be easily defined for domain wall fermions and is exactly conserved in the limit  $m_f \rightarrow 0$  and  $L_s \rightarrow \infty$  [7]. The DWF equations of motion imply that this current obeys the divergence condition

$$\Delta_\mu \mathcal{A}_\mu^a(x) = 2m_f J_5^a(x) + 2J_{5q}^a(x), \quad (11)$$

where  $J_5^a$  is a pseudoscalar density made up of quark fields on the boundary of the fifth dimension and  $J_{5q}^a$  is a pseudoscalar density containing quark fields at  $L_s/2 - 1$  and  $L_s/2$ . While the  $J_5^a$  term is

the result of the usual chiral non-invariance of the mass term, the  $J_{5q}^a$  operator is expected to have vanishing matrix elements at low energy as  $L_s \rightarrow \infty$ . It represents the effects of residual, finite- $L_s$ , chiral symmetry breaking. For low energy Green functions, the midpoint term in Eq. (11) can be expanded as

$$J_{5q}^a \sim m_{\text{res}} J_5^a - \frac{(Z_{\mathcal{A}} - 1)}{2} \Delta_\mu \mathcal{A}_\mu^a + c'_5 O_5^a. \quad (12)$$

Here we have introduced the  $m_f$ -independent parameter  $m_{\text{res}}$ , related to the constant  $c_3$  in Eq. (6). We also have a new lattice operator,  $O_5^a$ , similar to the axial transform of the  $c_5$  term in Eq. (6), which is carefully subtracted so that its matrix elements are of order  $a^2$  smaller than those of the operator  $J_5^a$  at long distances. Since the low energy matrix elements of the midpoint operator on the left-hand side of Eq. (12) will be suppressed by a factor  $\exp(-\alpha L_s)$  we expect the quantities  $m_{\text{res}}$ ,  $(Z_{\mathcal{A}} - 1)$  and  $c'_5$  to all be of this order (at least in the perturbative regime).

While an expansion such as that written in Eq. (12) is typically written in terms of the operators of the effective theory, the present form of this equation is useful because it can be combined with Eq. (11) to yield:

$$Z_{\mathcal{A}} \Delta_\mu \mathcal{A}_\mu^a(x) = 2(m_f + m_{\text{res}}) J_5^a(x) + c'_5 O_5^a. \quad (13)$$

As is well known from the classic analysis of the case of Wilson fermions [2], the conservation of the vector current and the vector Ward identities imply that product  $m_f J_5^a(x)$  in Eq. (13) approaches its continuum counterpart without multiplicative renormalization. This equation then implies that the product  $Z_{\mathcal{A}} \mathcal{A}_\mu^a(x)$  will reproduce the standard continuum axial current when evaluated in low energy Greens functions.

The appearance of the  $(Z_{\mathcal{A}} - 1)$  term on the right-hand side of Eq. (12) and the consequent renormalization of the five-dimensional DWF axial current is an effect that was not recognized in earlier RBC or RBC-UKQCD work. Such a possibility was raised by Steve Sharpe [22]. However, in this paper, Sharpe argues that  $(Z_{\mathcal{A}} - 1)$  is expected to be of order  $m_{\text{res}}^2$ , not the order  $m_{\text{res}}$  scale suggested by the above argument. Sharpe's argument relies on the chiral character of the operators  $V_\mu \pm A_\mu$ , defined in terms of fields on the boundaries of the fifth dimension. The mixing between these operators implied by  $Z_{\mathcal{A}} \neq 1$  can arise only if a fermion and an antifermion move from one wall from the other, a situation suppressed as  $m_{\text{res}}^2$ . We believe that this generally very useful argument does not apply in the present case because the right- and left-handed currents under consideration each span one-half of the entire five dimensions and are not localized on the left and right walls. For example, two fermions can propagate from the midpoint operator  $J_{5q}$  to the same wall with

only a suppression of  $[\exp(-\alpha L_s/2)]^2 = \exp(-\alpha L_s)$ . Note, this argument only applies to the perturbative piece. For tunneling caused by near-zero modes of the four-dimension Wilson operator, two such modes are needed implying a suppression more like  $m_{\text{res}}^2$ .

Finally it is informative to consider the implications of this more complete analysis on the conventional calculation of the residual mass from a ratio of low energy pion to vacuum matrix elements.

We measure a quantity commonly called  $m'_{\text{res}}(m_f)$  and given by

$$m'_{\text{res}}(m_f) = \frac{\langle 0 | J_{5q}^a | \pi \rangle}{\langle 0 | J_5^a | \pi \rangle} \quad (14)$$

$$= \frac{\langle 0 | \left( m_{\text{res}} J_5^a - \frac{(Z_{\mathcal{A}} - 1)}{2} \Delta_{\mu} \mathcal{A}_{\mu}^a + c'_5 O_5^a \right) | \pi \rangle}{\langle 0 | J_5^a | \pi \rangle} \quad (15)$$

We can then use the lattice equations of motion to evaluate the  $\Delta_{\mu} \mathcal{A}_{\mu}^a$  term so that Eq. (15) takes the form:

$$m'_{\text{res}}(m_f) = m_{\text{res}} + \left( \frac{1}{Z_{\mathcal{A}}} - 1 \right) (m_f + m_{\text{res}}) + \frac{c'_5}{2} \left( 1 + \frac{1}{Z_{\mathcal{A}}} \right) \frac{\langle 0 | O_5^a | \pi \rangle}{\langle 0 | J_5^a | \pi \rangle} \quad (16)$$

This equation governs the  $m_f$  dependence of  $m'_{\text{res}}(m_f)$ . Since, by construction, the third term on the right-hand side is of order  $a^2$ , we might be tempted to neglect it and use Eq. (16) to relate the  $m_f$  dependence of  $m'_{\text{res}}(m_f)$  to the difference  $(1/Z_{\mathcal{A}} - 1)$ . However, we can distinguish the dependence of  $m'_{\text{res}}(m_f)$  on the valence and sea masses,  $m_f^{\text{val}}$  and  $m_f^{\text{sea}}$  ( $m_x$  and  $m_l$  in the general notation of the rest of this paper). We see that there is valence quark mass dependence in both the  $1/Z_{\mathcal{A}} - 1$  term and in the term containing  $c'_5$ , while the sea quark mass dependence is only in the  $c'_5$  term. As will be shown in Section IV B,  $m'_{\text{res}}$  depends to a roughly equal degree on both  $m_f^{\text{val}}$  and  $m_f^{\text{sea}}$ . In particular, we find that  $d \ln(m'_{\text{res}}) / dm_f^{\text{val}} \approx -4$  and  $d \ln(m'_{\text{res}}) / dm_f^{\text{sea}} \approx 6$ . This implies that the third term in Eq. (16), which can depend on both the valence and sea quark masses, must be of an equal size to the second. In fact, if we introduce physical dimensions, we expect the ratio  $\langle 0 | O_5^a | \pi \rangle / \langle 0 | J_5^a | \pi \rangle$  to be of  $O((a\Lambda_{\text{QCD}})^2)$ . The effect of the quark masses on this ratio will be to replace one of the factors of  $\Lambda_{\text{QCD}}$  by the dimensioned factor  $m_f^{\text{val}}/a$  or  $m_f^{\text{sea}}/a$ . Thus, the quark mass dependent terms coming from the third term in Eq. (16) are suppressed by only by  $O(a\Lambda_{\text{QCD}})$  relative to the second term, which is apparently insufficient to permit them to be neglected, a fact already pointed out by Sharpe[22].

The arguments above show that we expect  $Z_{\mathcal{A}} - 1$  to be  $O(m_{\text{res}})$ . If all of the unitary mass dependence of  $m'_{\text{res}}(m_f)$  came from the  $1/Z_{\mathcal{A}} - 1$  term, this would give  $Z_{\mathcal{A}} - 1 = -0.003$ . Similarly, the valence mass dependence would give  $Z_{\mathcal{A}} - 1 = 0.01$ . At present, we do not have sufficient data to measure  $Z_{\mathcal{A}} - 1$  without contamination from the  $c'_5$  term. Thus, for the remainder of this

work, we take  $Z_{\mathcal{A}} = 1$  and we expect this to introduce an error of 1% or less in our axial current normalization.

We also work with a local, four-dimensional axial current  $A_\mu^a$ , which we renormalize so that  $Z_A A_\mu^a = \mathcal{A}_\mu^a$ , so that

$$Z_A \Delta_\mu A_\mu^a(x) = 2\tilde{m} J_5^a(x). \quad (17)$$

## B. $SU(2)_L \times SU(2)_R$ Chiral Perturbation Theory for Kaon Physics

### 1. Introduction

An important goal of this paper is the comparison of the mass dependence of our lattice results with both  $SU(3)_L \times SU(3)_R$  and  $SU(2)_L \times SU(2)_R$  chiral perturbation theory (ChPT) at NLO (*i.e.* at one-loop order). For compactness of notation, throughout the remainder of this section we will simply refer to  $SU(3)$  and  $SU(2)$  ChPT. We will see that our data for pseudoscalar masses and decay constants only agrees with NLO  $SU(3)$  ChPT with good precision when the quark masses are small. This will be quantified in detail in Sec. VII, where we will see that NLO  $SU(3)$  ChPT provides a good description of our data when the average, dimensionless, input valence mass satisfies  $m_{\text{avg}} < 0.01$  (all our results will be obtained using data for valence  $u$  and  $d$  quark masses below this value). In order to attempt to extend the range of agreement to heavier masses (to include the strange quark for example), one possible approach is to use NNLO (or even higher order) ChPT. This introduces many additional low energy constants (LECs) and we find that we have insufficient data to determine all of these with sufficient precision.

Instead of attempting to fit our data using NNLO (or even higher order) ChPT, we propose to use  $SU(2)$  ChPT at NLO. For pion physics, where it is possible to satisfy the condition,  $m_{\text{avg}} < 0.01$  for the valence quarks, both  $SU(2)$  and  $SU(3)$  ChPT provide a good description of our data. Moreover, we will see in Secs. VI and VII that the  $SU(2)$  LECs obtained directly are consistent with those obtained by “converting” the  $SU(3)$  LECs to  $SU(2)$  [13, 26] (conversion formulae appear in Appendix B 2 c). For kaons on the other hand, the presence of the valence strange quark means that we do not satisfy the condition  $m_{\text{avg}} < 0.01$  and so we propose to use  $SU(2)$  ChPT at NLO. The effects of the strange quark mass are now absorbed into the LECs of the  $SU(2)$  ChPT. This eliminates the errors due to neglected higher powers of  $\chi_s/\Lambda_{\text{CSB}}^2$  present when using  $SU(3)$  ChPT, but now one has to ensure that the  $u$  and  $d$  quark masses are sufficiently small to be able to

neglect higher order terms in  $\chi_{ud}/\chi_s$ . Here  $\Lambda_{\text{CSB}} \sim 4\pi f_\pi$  is the chiral symmetry breaking scale, while  $\chi_{ud}$  and  $\chi_s$  are tree level masses of pseudoscalars made of  $ud$  and  $s$  quarks (see Appendix A). In this section we derive the NLO formulae for the behavior of the kaon's leptonic decay constant  $f_K$ , its mass  $m_K$ , and the bag parameter  $B_K$  as a function of the light-quark masses in SU(2) ChPT. At each stage, we start by presenting the arguments and calculations in the unitary theory, with valence and sea quark masses equal, and then proceed to the partially quenched theory. In the partially quenched theory in general the valence and sea strange quark masses,  $m_y$  and  $m_h$  respectively, are also different and the SU(2) LECs depend on both these masses. For compactness of notation, we write these LECs with a single argument  $m_h$ , but it should be remembered that if  $m_y \neq m_h$ , then  $m_h$  should be replaced by the pair of variables  $m_y, m_h$ . We note that in this subsection quark masses written without a tilde have their usual interpretation as lagrangian mass parameters in continuum ChPT or PQChPT (a change from the notation defined in Appendix A and used elsewhere in this paper).

We start by introducing our notation. In the unitary effective theory, the pion matrix, quark-mass matrix and the kaon fields are written in the form:

$$\phi = \begin{pmatrix} \pi^0/\sqrt{2} & \pi^+ \\ \pi^- & -\pi^0/\sqrt{2} \end{pmatrix}, \quad M = \begin{pmatrix} m_l & 0 \\ 0 & m_l \end{pmatrix}, \quad K = \begin{pmatrix} K^+ \\ K^0 \end{pmatrix}. \quad (18)$$

We work in the isospin limit in which the two light quarks are degenerate with mass  $m_l$ . The pion matrices  $\xi$  and  $\Sigma$  are defined in the standard way:

$$\xi = \exp(i\phi/f) \quad \text{and} \quad \Sigma = \xi^2, \quad (19)$$

where the constant  $f$  is the pion decay constant ( $f_\pi$ ) at lowest order in the chiral expansion (we use the convention in which  $f_\pi = 132 \text{ MeV}$ ). Under global left- and right-handed transformations,  $L$  and  $R$  respectively, these quantities transform as follows:

$$\Sigma \rightarrow L\Sigma R^\dagger, \quad \xi \rightarrow L\xi U^\dagger = U\xi R^\dagger \quad \text{and} \quad K \rightarrow UK, \quad (20)$$

where  $U$  is a function of  $L$ ,  $R$  and the meson fields, but reduces to a global vector transformation when  $L = R$ . The pion Lagrangian at lowest order is

$$L_{\pi\pi}^{(2)} = \frac{f^2}{8} \text{tr} \partial_\mu \Sigma \partial^\mu \Sigma^\dagger + \frac{f^2 B}{4} \text{tr} (M^\dagger \Sigma + M \Sigma^\dagger) \quad (21)$$

where  $f$  and  $B$  are the usual leading order LECs and, to this order,  $m_\pi^2 = 2Bm_l$ .

The results for  $m_\pi^2$  and  $f_\pi$  at NLO in the chiral expansion are well known [12] and are presented in Eqs. (B34) and (B38) in the appendix. We now turn our attention to kaon physics using ‘‘Kaon ChPT’’ (KChPT). The corresponding chiral Lagrangian has already been introduced by Roessl [27] in order to study  $\pi K$  scattering close to threshold. At leading order the interaction of kaons with soft pions is described by the Lagrangian

$$L_{\pi K}^{(1)} = D_\mu K^\dagger D^\mu K - M^2 K^\dagger K, \quad (22)$$

where the covariant derivative  $D_\mu$  is constructed using the vector field  $V_\mu$  so that  $D_\mu K$  transforms like  $K$  under chiral transformations:

$$D_\mu K = \partial_\mu K + V_\mu K \rightarrow U D_\mu K. \quad (23)$$

$V_\mu$  itself is constructed from the pion fields and transforms as

$$V_\mu = \frac{1}{2} \left( \xi^\dagger \partial_\mu \xi + \xi \partial_\mu \xi^\dagger \right) \rightarrow U V_\mu U^\dagger + U \partial_\mu U^\dagger. \quad (24)$$

We refer the reader to Eq. (11) of [27] for the higher order terms in the  $K\pi$  Lagrangian (terms up to  $O(m_l^4)$  are explicitly listed). For completeness we also present the axial field:

$$A_\mu = \frac{i}{2} \left( \xi^\dagger \partial_\mu \xi - \xi \partial_\mu \xi^\dagger \right) \rightarrow U A_\mu U^\dagger. \quad (25)$$

In the following, when constructing Feynman diagrams from the  $K\pi$  Lagrangian and the effective-theory local operators, we expand the vector and axial fields in terms of pion fields:

$$V_\mu = [\phi, \partial_\mu \phi]/2f^2 + \dots \quad \text{and} \quad A_\mu = -\partial_\mu \phi/f + \dots. \quad (26)$$

The use of Partially Quenched Chiral Perturbation Theory (PQChPT), in which we vary the valence quark masses independently of those of the sea quarks, gives us more scope to determine the low-energy constants of the unitary chiral theory and in this paper we will profit from this opportunity. We consider the case with two degenerate light sea quarks, two degenerate light valence quarks and two ‘ghost’ degenerate light commuting quarks to cancel the loop effects of the valence quarks. Thus we are using the graded symmetry method [28, 29], based on Morel’s ghost-quark trick [30]. See the lectures by Sharpe [31] for a recent review of PQChPT and references to the original literature (as well as many other applications of chiral perturbation theory to lattice QCD). We let the sea quarks have mass  $m_l$  while the valence and ghost quarks have mass  $m_\chi$ . Thus we build an  $SU(4|2)_L \times SU(4|2)_R$  effective theory. We identify the quark flavors using the ordered list

$$u_v, d_v, u_s, d_s, \tilde{u}_v, \tilde{d}_v \quad (27)$$

where subscripts  $v$  and  $s$  are for valence and sea respectively, while the tilde denotes a ghost quark. We remind the reader that the strange quark mass does not appear explicitly here; rather, the LECs are functions of the strange quark mass.

The matrix of Goldstone fields is written in block form

$$\Phi = \begin{pmatrix} \phi & \eta_1 \\ \eta_2 & \tilde{\phi} \end{pmatrix} \quad (28)$$

where  $\phi$  is a  $4 \times 4$  block containing normal mesons,  $\eta_1 = \eta_2^\dagger$  is a  $4 \times 2$  block of normal-ghost mesons and  $\tilde{\phi}$  is a  $2 \times 2$  block of ghost-ghost mesons. The QCD pions are present in the central  $2 \times 2$  block of  $\Phi$ . As before, we work with the quantities  $\xi$  and  $\Sigma$

$$\xi = \exp(i\Phi/f) \quad \text{and} \quad \Sigma = \xi^2, \quad (29)$$

in terms of which the leading order PQ chiral Lagrangian is

$$\mathcal{L}_{\text{PQ}}^{(2)} = \frac{f^2}{8} \text{str}(D_\mu \Sigma)^\dagger D^\mu \Sigma + \frac{f^2 B}{4} \text{str}(\mathcal{M} \Sigma^\dagger + \Sigma \mathcal{M}^\dagger), \quad (30)$$

where  $\mathcal{M}$  is the mass matrix

$$\mathcal{M} = \text{diag}(M_v, M_s, M_v), \quad \text{with} \quad M_v = \text{diag}(m_x, m_x) \quad \text{and} \quad M_s = \text{diag}(m_l, m_l). \quad (31)$$

The quadratic terms in  $\mathcal{L}_{\text{PQ}}^{(2)}$  are

$$\begin{aligned} \mathcal{L}_{\text{PQ,quad}}^{(2)} &= \frac{1}{2} \text{str}(\partial_\mu \Phi \partial^\mu \Phi) - B \text{str}(\mathcal{M} \Phi^2) \\ &= \frac{1}{2} \text{tr}(\partial_\mu \phi \partial^\mu \phi + \partial_\mu \eta_1 \partial^\mu \eta_2 - \partial_\mu \eta_2 \partial^\mu \eta_1 - \partial_\mu \tilde{\phi} \partial^\mu \tilde{\phi}) \\ &\quad - B \text{tr} \left( (\phi \phi + \eta_1 \eta_2) \begin{pmatrix} M_v & 0 \\ 0 & M_s \end{pmatrix} - \eta_2 \eta_1 M_s - \tilde{\phi} \tilde{\phi} M_s \right). \end{aligned} \quad (32)$$

The Lagrangian in Eq. (32) leads to a number of propagators which appear in the Feynman diagrams in the following sections. We distinguish the propagators for the following mesons:

- normal ‘charged’ (off-diagonal) mesons ( $\sim q_1 \bar{q}_2$ ):

$$\frac{i}{p^2 - m_{12}^2}, \quad m_{12}^2 = B(m_1 + m_2) = (\chi_1 + \chi_2)/2, \quad (33)$$

where  $m_{1,2}$  are valence or sea masses;



- ‘charged’ ghost mesons: ( $\sim \tilde{q}_1 \bar{\tilde{q}}_2$ )

$$\frac{-i}{p^2 - m_{12}^2}, \quad m_{12}^2 = B(m_1 + m_2) = (\chi_1 + \chi_2)/2. \quad (34)$$

Here  $m_{1,2}$  are valence masses;

- ‘charged’ quark-ghost mesons ( $\sim q_1 \bar{\tilde{q}}_2$  or  $\sim \tilde{q}_1 \bar{q}_2$ )

$$\frac{i}{p^2 - m_{12}^2}, \quad m_{12}^2 = B(m_1 + m_2) = (\chi_1 + \chi_2)/2, \quad (35)$$

where  $m_{1,2}$  are a valence mass from the ghost and a valence or sea mass from the quark;

- ‘neutral’ mesons from diagonal parts of  $\phi$  and  $\tilde{\phi}$ :

$$\langle \Phi_{ii} \Phi_{jj} \rangle = i \frac{\varepsilon_i \delta_{ij}}{p^2 - \chi_i} - \frac{i}{N} \frac{p^2 - \chi_l}{(p^2 - \chi_i)(p^2 - \chi_j)}, \quad (36)$$

for  $N$  sea quarks which are all degenerate with mass  $m_l$ , with  $N = 2$  here and

$$\varepsilon_i = \begin{cases} +1 & \text{valence or sea} \\ -1 & \text{ghost} \end{cases}. \quad (37)$$

Note that the neutral propagators are determined after implementing the constraint  $\text{str}[\Phi] = 0$ , which has the effect that neutral valence-valence meson propagators can have contributions from neutral sea quark states (see [31] for example).

We now add a kaon matter field

$$K = \begin{pmatrix} K_v^+ \\ K_v^0 \\ K^+ \\ K^0 \\ \tilde{K}^+ \\ \tilde{K}^0 \end{pmatrix} \sim \begin{pmatrix} \bar{s}u_v \\ \bar{s}d_v \\ \bar{s}u_s \\ \bar{s}d_s \\ \bar{s}\tilde{u}_v \\ \bar{s}\tilde{d}_v \end{pmatrix}. \quad (38)$$

The partially quenched  $K\pi$  Lagrangian is the generalization of Eq. (22) written in terms of the partially quenched fields.

In the following three subsections we derive the mass dependence of  $f_K$ ,  $m_K^2$  and  $B_K$  respectively.

## 2. Chiral Behavior of $f_K$

The kaon decay constant,  $f_K$ , is defined by the matrix element of the axial vector current:

$$\langle 0 | \bar{u} \gamma_\mu \gamma_5 s | K^-(p) \rangle \equiv -i f_K p_\mu. \quad (39)$$

We now need to match the QCD axial vector current to operators in KChPT. We start by doing this for left and right handed currents and then build the axial vector current. The left-handed QCD current for kaon decay is

$$\frac{1}{2} \bar{q} \gamma_\mu (1 - \gamma_5) s \quad (40)$$

where  $q = u$  or  $d$ . It is convenient to promote  $q$  to be a 2-component vector with components  $u$  and  $d$  and to introduce a constant 2-component spurion vector  $h$  in order to be able to project  $u$  or  $d$  as required; specifically we write the left-handed current as:

$$\frac{1}{2} \bar{q} h \gamma_\mu (1 - \gamma_5) s \quad (41)$$

The current in Eq. (41) would be invariant under  $SU(2)_L$  transformations if  $h$  transformed as  $h \rightarrow Lh$ .

We match to the effective theory by building quantities linear in  $h$  and with a single Lorentz index, which would also be invariant if  $h$  transformed as above. At lowest order, we identify two terms:

$$(D_\mu K)^\dagger \xi^\dagger h, \quad \text{and} \quad K^\dagger A_\mu \xi^\dagger h. \quad (42)$$

By using equations of motion, operators with more covariant derivatives acting on the kaon field (which transform in the same way under chiral transformations) can be reduced to ones of higher order in the chiral expansion.

For a right-handed current we simply take the  $h$ -transformation to be  $h \rightarrow Rh$  and obtain the two operators

$$(D_\mu K)^\dagger \xi h, \quad \text{and} \quad K^\dagger A_\mu \xi h, \quad (43)$$

which transform in the same way as  $\bar{q} h \gamma_\mu (1 + \gamma_5) s$ .

Under a parity transformation, the quantities in the effective theory transform as:

$$K \rightarrow -K, \quad \xi \rightarrow \xi^\dagger, \quad A_\mu \rightarrow -A_\mu. \quad (44)$$

Noting that parity transforms the left-handed current into the right-handed current and vice-versa, we deduce that the currents are of the form:

$$J_\mu^L = -L_{A1} (D_\mu K)^\dagger \xi^\dagger h + iL_{A2} K^\dagger A_\mu \xi^\dagger h \quad (45)$$

$$J_\mu^R = L_{A1} (D_\mu K)^\dagger \xi h + iL_{A2} K^\dagger A_\mu \xi h, \quad (46)$$

where  $L_{A1}$  and  $L_{A2}$  are low-energy constants. To the extent that the kaon is regarded as heavy, the  $L_{A2}$  term is subleading (and in any case does not contribute to  $f_K$  at tree or one-loop level). The axial vector current  $J_\mu^R - J_\mu^L$  is therefore

$$J_\mu^5 = L_{A1} (D_\mu K)^\dagger (\xi + \xi^\dagger) h + iL_{A2} K^\dagger A_\mu (\xi - \xi^\dagger) h. \quad (47)$$

We have introduced a factor of  $i$  in the  $L_{A2}$  term to make the low energy constants real. This can be seen by considering charge conjugation  $\mathcal{C}$ . For the quark current (taking  $h$  to be real), we have

$$J_\mu^5 = \bar{q} h \gamma_\mu \gamma_5 s \xrightarrow{\mathcal{C}} \bar{s} \gamma_\mu \gamma_5 h^T q = (J_\mu^5)^\dagger. \quad (48)$$

In the effective theory, the charge conjugation transformations are

$$\xi \rightarrow \xi^T, \quad A_\mu \rightarrow A_\mu^T, \quad V_\mu \rightarrow -V_\mu^T \quad (49)$$

together with

$$K_a \rightarrow K_a^\dagger, \quad (D_\mu K)_a = \partial_\mu K_a + (V_\mu K)_a \rightarrow \partial_\mu K_a^\dagger - (K^\dagger V_\mu)_a = (D_\mu K)_a^\dagger, \quad (50)$$

where  $a$  is a flavor label. Using these transformations, the current in the effective theory is transformed into its Hermitian conjugate under charge conjugation provided  $L_{A1}$  and  $L_{A2}$  are both real. The leading contribution to  $f_K$  in the chiral expansion can be readily deduced. The first term in the axial current has a  $\partial_\mu K$  factor with no pion fields, so that at tree level  $f_K$  is fixed by  $L_{A1}$ , specifically

$$f^{(K)}(m_h) = 2L_{A1}, \quad (51)$$

where  $m_h$  is the mass of the strange quark (we are using the notation defined in Appendix A).

The NLO contribution to  $f_K$  is obtained from the tadpole diagram in Fig. 1(a). From the  $K\pi\pi$  vertex in the  $L_{A1}$  term in the axial current we obtain the contribution

$$2L_{A1}(-ip_\mu) \frac{-iC_F}{f^2} \int \frac{d^4k}{(2\pi)^4} \frac{1}{k^2 - m_\pi^2} = 2L_{A1}(-ip_\mu) \frac{-iC_F}{(4\pi f)^2} m_\pi^2 \left( \log \frac{m_\pi^2}{\Lambda_\chi^2} + \text{constant} \right), \quad (52)$$

where  $C_F = 3/4$  is the eigenvalue of the quadratic Casimir operator for SU(2) in the fundamental representation and  $\Lambda_\chi$  is an arbitrary renormalization scale. There is no contribution at one-loop order from the term in the axial current proportional to  $L_{A2}$  and so we have shown that the chiral behavior of  $f_K$  is of the form:

$$f_K = f^{(K)}(m_h) \left\{ 1 + c(m_h) \frac{m_\pi^2}{f^2} - \frac{m_\pi^2}{(4\pi f)^2} \frac{3}{4} \log \frac{m_\pi^2}{\Lambda_\chi^2} \right\}, \quad (53)$$

where  $c(m_h)$  is a low-energy constant and  $m_\pi^2 = \chi_l$ .

Before proceeding to discuss the chiral behavior of  $f_K$  in partially quenched SU(2) ChPT, we compare the above calculation with that of  $f_B$  in Heavy Meson ChPT [32]. In that case the NLO contribution has the corresponding contribution to Eq. (53), but in addition it has a second contribution from the self-energy diagram in Fig. 1(b). To discuss this for both  $f_B$  and  $f_K$  simultaneously, let  $P$  and  $P^*$  be pseudoscalar and vector mesons containing a light quark ( $u$  or  $d$ ) and a heavier antiquark (*e.g.*  $s$  or  $b$ ). Let the masses of the  $P$  and  $P^*$  mesons be  $M$  and  $M_*$  respectively. The interaction of pions with pseudoscalar and vector mesons,  $P$  and  $P^*$ , takes the form  $Mg \partial^\mu \pi P P_\mu^*/f$ , where the  $1/f$  arises because there is one pion and the  $Mg$  is put in for compatibility with heavy meson chiral perturbation theory (where the fields are usually normalized with an implicit factor of  $\sqrt{M}$ ) so that the coupling constant  $g$  is dimensionless. The diagram in Fig. 1(b), for a  $P$  meson with momentum  $p$ , is proportional to  $(Mg/f)^2 I$  where  $I$  is the Feynman integral:

$$I = \int \frac{d^4 l}{(2\pi)^4} \frac{l^\mu l^\nu [g_{\mu\nu} - (p-l)_\mu (p-l)_\nu / M_*^2]}{(l^2 - m_\pi^2)((p-l)^2 - M_*^2)}. \quad (54)$$

We now compare the behavior of this integral with  $m_\pi^2$  in the two cases: i) the heavy quark limit in which  $M \rightarrow \infty$  with  $M_*^2 - M^2 = O(\Lambda_{\text{QCD}}^2)$  which is an approximation for  $B$ -physics and ii)  $M$  and  $M_*$  both of  $O(\Lambda_{\text{QCD}})$  and not degenerate, a situation which is appropriate for kaon physics.

In the heavy quark limit, we write  $p = Mv + k$ , where  $v$  is the meson's four-velocity ( $v^2 = 1$ ) and the leading term in  $I$  in the  $1/M$  expansion is:

$$I \simeq \frac{1}{2M} \int \frac{d^4 l}{(2\pi)^4} \frac{l^\mu l^\nu [g_{\mu\nu} - v_\mu v_\nu]}{(l^2 - m_\pi^2)(v \cdot (k-l) - \Delta)}, \quad (55)$$

where  $\Delta = (M_*^2 - M^2)/2M$  which is of  $O(\Lambda_{\text{QCD}}^2/M)$  and hence negligible compared to  $m_\pi$  in the heavy quark limit. We stress that in this analysis we take the heavy-quark limit before the chiral limit, *i.e.* we keep  $\Lambda_{\text{QCD}}/M \ll m_\pi/\Lambda_{\text{QCD}}$ . By power counting we see that the component of  $I$  contributing to the wavefunction renormalization can have a term proportional to

$$\frac{v \cdot k}{M} m_\pi^2 \log \frac{m_\pi^2}{\Lambda_\chi^2} \quad (56)$$

and so can lead to terms proportional to  $(g^2/f^2)m_\pi^2 \ln(m_\pi^2/\Lambda_\chi^2)$  in the behavior of  $f_B$ . An explicit evaluation of the diagram confirms that such terms are indeed present [32].

In contrast, there is no contribution of the form  $m_\pi^2 \log m_\pi^2$  in KChPT, *i.e.* when we take the chiral limit of small  $m_\pi^2$  while keeping  $M$  and  $M_*$  fixed, non-degenerate and neither especially large or small. To see this we combine the denominators in  $I$  using Feynman parametrization and write

$$I = \int_0^1 d\alpha \int \frac{d^4 l}{(2\pi)^4} \frac{N(\alpha)}{D^2(\alpha)}, \quad (57)$$

where  $\alpha$  is the Feynman parameter,

$$N(\alpha) = (l + \alpha p)^2 - \frac{((l + \alpha p) \cdot (l - (1 - \alpha)p))^2}{M_*^2} \quad (58)$$

and

$$D(\alpha) = l^2 + \alpha(1 - \alpha)p^2 - (1 - \alpha)m_\pi^2 - \alpha M_*^2. \quad (59)$$

The question we are addressing is whether there is a contribution to  $I$  of the form  $m_\pi^2 \log m_\pi^2$ . If there is such a term then we can isolate it by differentiating with respect to  $m_\pi^2$ , setting  $m_\pi^2 \rightarrow 0$  and searching for a logarithmic (infrared) divergence in

$$\left. \frac{dI}{dm_\pi^2} \right|_{m_\pi^2=0} = -2 \int_0^1 d\alpha (1 - \alpha) \int \frac{d^4 l}{(2\pi)^4} \frac{N(\alpha)}{D^3(\alpha, m_\pi^2=0)}. \quad (60)$$

We use dimensional regularization in  $D = 4 + 2\varepsilon$  dimensions. The contribution from the first term in  $N$  in Eq. (58) is

$$\begin{aligned} \left. \frac{dI_1}{dm_\pi^2} \right|_{m_\pi^2=0} &= -2 \int_0^1 d\alpha (1 - \alpha) \int \frac{d^D l}{(2\pi)^D} \frac{l^2 + \alpha^2 p^2}{[l^2 + \alpha(1 - \alpha)p^2 - \alpha M_*^2]^3} \\ &= \frac{-i}{(4\pi)^{2+\varepsilon}} \int_0^1 d\alpha (1 - \alpha) \alpha^\varepsilon [M_*^2 - (1 - \alpha)p^2]^\varepsilon \left\{ (2 + \varepsilon)\Gamma(-\varepsilon) - \frac{\alpha p^2}{M_*^2 - (1 - \alpha)p^2} \right\}. \end{aligned} \quad (61)$$

The contribution to the self-energy is the coefficient of  $p^2$  at  $p^2 = M^2$ , which we can isolate by differentiating with respect to  $p^2$  and setting  $p^2 = M^2$ . By inspection we can readily verify that there are no infrared singular terms and hence no term proportional to  $m_\pi^2 \log m_\pi^2$  in  $I$ . Note that  $M_* > M$  and hence  $M_*^2 - (1 - \alpha)p^2 > 0$  for  $p^2 = M^2$  throughout the integration region in  $\alpha$ . A parallel argument shows that there is also no contribution to  $I$  of the form  $m_\pi^2 \log m_\pi^2$  from the second term in  $N(\alpha)$  on the right-hand side of Eq. (58).

Note also that  $I$  does contain a term proportional to  $m_\pi^4 \log m_\pi^2$ . In this case we seek an infra-red divergence after differentiating  $I$  twice with respect to  $m_\pi^2$  and setting  $m_\pi^2 \rightarrow 0$ . The power of

$l^2 + \alpha(1 - \alpha)p^2 - \alpha M_*^2$  in the integrand is  $-4$  as compared to  $-3$  in Eq. (61). After performing the  $l$ -integration, we find that for small  $\alpha$  the integrand  $\sim \alpha^{-1+\varepsilon}$ , which diverges in 4 dimensions and is a signature of the presence of a  $\log m_\pi^2$  term (*i.e.* a  $m_\pi^4 \log m_\pi^2$  term in  $I$ ).

There are also no chiral logarithms from the tadpole diagram in Fig. 1(c). The  $KK\pi\pi$  term in  $L_{\pi K}^{(1)}$  in Eq. (22) is proportional to  $K(\partial_\mu K)[\phi, \partial^\mu \phi]$  and so the integrand is an odd function of the pion's momentum and the integral vanishes.

Finally in this section we derive the behavior of  $f_K$  in the partially quenched case, *i.e.* in PQKChPT. The axial vector current is of the form of that in Eq. (47), but uses the PQ  $K$  and  $\xi$  fields. As before, the spurion  $h$  is chosen to pull out the appropriate flavor. The tree and quadratic terms from this current are

$$J_\mu^{5a} = 2L_{A1} \partial_\mu K_b^\dagger \left( 1 - \frac{\Phi^2}{2f^2} \right)_{ba} + \dots \quad (62)$$

where we have dropped terms with a single derivative acting on a Goldstone field.

To calculate the decay constant for a kaon containing a valence light quark, we take the flavor index  $a = 1$  or 2. Choosing, for illustration,  $a = 1$  we find

$$2L_{A1} \partial_\mu K_1^\dagger \left[ 1 - \frac{1}{2f^2} (\eta_{1,11} \eta_{2,11} + \eta_{1,12} \eta_{2,21} + \phi_{11}^2 + \phi_{12} \phi_{21} + \phi_{13} \phi_{31} + \phi_{14} \phi_{41}) \right]. \quad (63)$$

There are also terms containing  $\partial_\mu K_2^\dagger$ , but these have Goldstone field pairings which cannot be contracted to give a one-loop tadpole contribution and thus are not listed above. The one-loop tadpole contribution to  $f_{K_v^+}$  is

$$-L_{A1} \frac{1}{f^2} \int \frac{d^4 l}{(2\pi)^4} \left\{ -\frac{2i}{l^2 - \chi_x} + \frac{i}{l^2 - \chi_x} + \frac{2i}{l^2 - (\chi_x + \chi_l)/2} + \frac{i}{l^2 - \chi_x} - \frac{1}{2} \frac{l^2 - \chi_l}{(l^2 - \chi_x)^2} \right\}. \quad (64)$$

The 5 terms in the integrand of Eq. (64) have the following origin:

1. The first term comes from the quark-ghost mesons in the tadpole loop. These have valence-quark masses and the minus sign arises from the closed loop of anticommuting fields.
2. The second term has the  $\phi_{12} \phi_{21}$  propagator with both quarks having valence masses.
3. The third term has the  $\phi_{13} \phi_{31} + \phi_{14} \phi_{41}$  propagators with one quark having the valence-quark mass and the other the sea-quark mass.
- 4&5. The final two terms have a neutral propagator in the tadpole diagram from the  $\phi_{11}^2$  term on the rhs of Eq. (63). Both quarks have valence-quark masses.

We observe, as expected, that the tadpole contribution with the valence-ghost propagator cancels that with the valence-valence one. Extracting the chiral logarithms from the loop integrals we arrive at the expression:

$$f_{xh} = 2L_{A1} \left\{ 1 - \frac{1}{(4\pi f)^2} \left[ \frac{\chi_l + \chi_x}{2} \log \frac{\chi_l + \chi_x}{2\Lambda_\chi^2} + \frac{\chi_l - 2\chi_x}{4} \log \frac{\chi_x}{\Lambda_\chi^2} \right] \right\} + \dots \quad (65)$$

The analytic terms can be proportional to  $\chi_l$  and  $\chi_x$  and so we obtain the final result for the mass behavior of a meson with a light valence quark  $x$  and a heavier (strange) valence quark  $h$ :

$$f_{xh} = f^K(m_h) \left\{ 1 + \frac{\lambda_3(m_h)}{f^2} \chi_l + \frac{\lambda_4(m_h)}{f^2} \chi_x - \frac{1}{(4\pi f)^2} \left[ \frac{\chi_x + \chi_l}{2} \log \frac{\chi_x + \chi_l}{2\Lambda_\chi^2} + \frac{\chi_l - 2\chi_x}{4} \log \frac{\chi_x}{\Lambda_\chi^2} \right] \right\}, \quad (66)$$

where  $\lambda_{3,4}$  are LEC's and we remind the reader that if the valence and sea strange quark masses are different then the LECs  $f^{(K)}$  and  $\lambda_{3,4}$  depend on both these masses. Eq. (66) agrees with the corresponding calculation of the chiral behavior of  $f_B$  [32], when the terms proportional to the square of the  $BB^*\pi$  coupling are neglected. The right-hand side of Eq. (66) reduces to Eq. (53) in the unitary limit  $\chi_x = \chi_l$ .

### 3. Chiral Behavior of $m_K^2$

We now consider the chiral behavior of  $m_K^2$ , starting in the unitary theory in which the valence and sea masses are equal. In principle the chiral logarithms could come from the tadpole diagram in Fig. 1(c). However, just as for the wavefunction renormalization, there is no such contribution at one-loop order. The  $KK\pi\pi$  term in  $L_{\pi K}^{(1)}$  in Eq. (22) is proportional to  $K(\partial_\mu K)[\phi, \partial^\mu \phi]$  and so the integrand is an odd function of the pion's momentum and the integral vanishes. This is also the case in the partially quenched theory and so, at NLO in the chiral expansion, the mass-dependence of  $m_K^2$  comes from the analytical terms coming from the higher order terms in the  $K\pi$  Lagrangian. For the partially quenched theory at NLO

$$m_{xh}^2 = B^{(K)}(m_h) \tilde{m}_h \left\{ 1 + \frac{\lambda_1(m_h)}{f^2} \chi_l + \frac{\lambda_2(m_h)}{f^2} \chi_x \right\}. \quad (67)$$

In the unitary theory we have the natural simplification of only a single low-energy constant.

#### 4. Chiral Behavior of $B_K$

The non-perturbative strong interaction effects in neutral kaon mixing are contained in the matrix elements of the QCD operator

$$\bar{s}_L \gamma_\mu d_L \bar{s}_L \gamma^\mu d_L, \quad (68)$$

between  $K^0$  and  $\bar{K}^0$  states. This operator is part of a multiplet transforming under  $SU(2)_L$  on the two down quarks and is symmetric under the interchange of the two  $d_L$ 's. Hence it transforms as a triplet under  $SU(2)_L$  and is a singlet under  $SU(2)_R$  (the analogous situation for neutral  $B$ -meson mixing is that the corresponding operator is part of a 6 representation of  $SU(3)_L$  [33]).

In our effective kaon theory the combination  $\xi K$  transforms as  $\xi K \rightarrow L \xi K$  under  $SU(2)_L$ , and we can use it to build the leading  $\Delta S = 2$  operator,

$$\mathcal{O}_{ab} = 2\beta (\xi K)_{\{a} (\xi K)_{b\}}, \quad (69)$$

which is symmetrised in the flavor indices  $a$  and  $b$  and has a LEC  $\beta$  (the analogous construction for neutral  $B$ -meson mixing in  $SU(3)_L \times SU(3)_R$  heavy meson chiral perturbation theory leads to an operator  $4\beta_Q (\xi P^{(Q)\dagger})_{\{a} (\xi P^{(\bar{Q})})_{b\}$  [33], where  $P^{(Q)}$  and  $P^{(\bar{Q})}$  destroy mesons containing heavy  $Q$  and  $\bar{Q}$  quarks respectively). As in the discussion of the axial current, operators with one or both of the kaon fields on the right hand side of Eq. (69) replaced by  $D^n K$ , where  $D$  is the covariant derivative (the Lorentz indices have been suppressed) transform in the the same way as  $\mathcal{O}_{ab}$ . Again, by using the equations of motion, the leading component of these operators can be reduced to  $\mathcal{O}_{ab}$ . In order to evaluate  $B_K$  we will need the matrix element  $\langle \bar{K}^0 | \mathcal{O}_{22} | K^0 \rangle$  and thus need to use the  $K^0 K^0$  piece of  $\mathcal{O}_{22}$ . At tree level we find

$$4\beta = \frac{8}{3} m_K^2 f_K^2 B_K. \quad (70)$$

In order to evaluate the one-loop contributions to the matrix element (see Fig. 2) we expand  $\mathcal{O}_{22}$  up to second order in the pion fields:

$$\mathcal{O}_{ab} = 2\beta K_a K_b - \frac{2\beta}{f^2} \left\{ (\phi K)_a (\phi K)_b + \frac{1}{2} [(\phi^2 K)_a K_b + K_a (\phi^2 K)_b] \right\} + \dots \quad (71)$$

We observe, by comparing to the expansion of the axial vector current in Eq. (47), that the two terms containing  $\phi^2$  lead to relative one-loop corrections each of which is the same as the relative one-loop correction for  $f_K$ . Since we are calculating a matrix element proportional to  $f_K^2 B_K$ , these



two corrections will not affect  $B_K$  and we need only calculate the one-loop correction from the  $(\phi K)_a(\phi K)_b$  term. Thus the relevant component of  $\mathcal{O}_{22}$  is the  $K^0 K^0$  term in

$$-\frac{2\beta}{f^2}(\phi K)_2(\phi K)_2 = -\frac{2\beta}{f^2} \frac{\pi^0 \pi^0}{2} K^0 K^0 + \dots \quad (72)$$

Contracting the two pions into a loop leads to a contribution

$$-\frac{2\beta}{f^2} \int \frac{d^4 k}{(2\pi)^4} \frac{i}{k^2 - m_\pi^2} = -\frac{2\beta}{f^2} \frac{1}{(4\pi f)^2} m_\pi^2 \log \frac{m_\pi^2}{\Lambda_\chi^2} + \text{analytic terms.} \quad (73)$$

Hence we find that

$$B_K = B_K^{\text{tree}} \left\{ 1 - \frac{1}{2} \frac{1}{(4\pi f)^2} m_\pi^2 \log \frac{m_\pi^2}{\Lambda_\chi^2} \right\} + \dots \quad (74)$$

This agrees with the result for  $B_B$  in Eq. (3.8) of Sharpe and Zhang [32] when the  $BB^*\pi$  coupling  $g \rightarrow 0$ .

We now promote the above discussion to the partially quenched case. The effective theory operator is still of the form of Eq. (69), but now the flavor labels take 6 values and  $\xi$  is expanded in terms of  $\Phi$  in Eq. (28). This echoes the discussion for partially-quenched neutral  $B$ -meson mixing in Sharpe and Zhang [32], starting from the QCD discussion in [33].

To obtain the mixing matrix element for neutral kaons with valence down quarks, we look at the  $K_2 K_2$  piece of the  $\mathcal{O}_{22}$  operator, expanded up to second order in the Goldstone fields:

$$\mathcal{O}_{22} = 2\beta K_2 K_2 - \frac{2\beta}{f^2} \left\{ (\Phi K)_2 (\Phi K)_2 + \frac{1}{2} [(\Phi^2 K)_2 K_2 + K_2 (\Phi^2 K)_2] \right\} + \dots \quad (75)$$

As in the unquenched calculation above, the  $(\Phi^2 K)_2 K_2$  terms lead to chiral logarithms which are cancelled by those from  $f_K^2$  when extracting  $B_K$  from the  $\Delta S = 2$  matrix element. Hence the pieces of the partially-quenched operator we need are:

$$2\beta \left( 1 - \frac{1}{f^2} \phi_{22}^2 \right) K_2 K_2. \quad (76)$$

The  $\phi_{22}$  field is a valence-valence neutral meson, so we find a one-loop correction

$$-\frac{4\beta i}{f^2} \int \frac{d^4 l}{(2\pi)^4} \left\{ \frac{1}{l^2 - \chi_x} - \frac{1}{2} \frac{l^2 - \chi_l}{(l^2 - \chi_x)^2} \right\} = -\frac{2\beta}{(4\pi f)^2} \chi_l \log \frac{\chi_x}{\Lambda_\chi^2} + \dots \quad (77)$$

For  $B_K$  the result is:

$$B_{xh} = B_{\text{PS}}^{(K)} \left\{ 1 - \frac{1}{2} \frac{1}{(4\pi f)^2} \chi_l \log \frac{\chi_x}{\Lambda_\chi^2} \right\} + \dots$$

This agrees with Eq. (3.9) in Sharpe and Zhang [32] with  $g \rightarrow 0$  and  $N_f = 2$ . It also reduces to the QCD result above, Eq. (74), when  $\chi_x = \chi_l = m_\pi^2$ . Noting that there are analytic terms proportional to both  $\chi_l$  and  $\chi_x$  the final result for the mass dependence of  $B_K$  is that in Eq. (B48) of the appendix

$$B_{xh} = B_{\text{PS}}^{(K)}(m_h) \left\{ 1 + \frac{b_1(m_h)}{f^2} \chi_l + \frac{b_2(m_h)}{f^2} \chi_x - \frac{\chi_l}{32\pi^2 f^2} \log \frac{\chi_x}{\Lambda_\chi^2} \right\}, \quad (78)$$

where  $b_{1,2}$  are LECs.

### 5. Comments

We conclude this section with the observation that for all the physical quantities considered in this section the chiral logarithms in the SU(2) theory can be simply deduced from those in the SU(3) theory. In all these cases the chiral behavior is of the generic form:

$$O = O_{\text{LO}} (1 + \text{chiral logarithms} + \text{analytic terms}), \quad (79)$$

where  $O$  is the physical quantity (pseudoscalar mass-squared, decay constant or bag parameter) and there is a single LEC at lowest order ( $O_{\text{LO}}$ ). The generic form in Eq. (79) holds in both the SU(2) and SU(3) theories. As an example consider the pseudoscalar decay constant  $f_{xh}$ , with a degenerate heavy (strange) valence and sea quark with mass  $m_h$  and partially quenched up and down quarks. In the partially quenched SU(3) theory at NLO we have from Eq. (B18):

$$\begin{aligned} f_{xh} = f_0 \left\{ 1 - \frac{1}{8\pi^2 f_0^2} \left[ \frac{\chi_x + \chi_l}{4} \log \frac{\chi_x + \chi_l}{2\Lambda_\chi^2} + \frac{\chi_h + \chi_l}{4} \log \frac{\chi_h + \chi_l}{2\Lambda_\chi^2} \right. \right. \\ \left. \left. + \frac{\chi_x + \chi_h}{8} \log \frac{\chi_x + \chi_h}{2\Lambda_\chi^2} + \frac{\chi_h}{4} \log \frac{\chi_h}{\Lambda_\chi^2} \right] \right. \\ \left. + \frac{1}{96\pi^2 f_0^2} \left[ \left( \chi_x - \chi_h - \chi_x \frac{\chi_l - \chi_x}{\chi_\eta - \chi_x} \right) \log \frac{\chi_x}{\chi_h} \right. \right. \\ \left. \left. + \chi_\eta (\chi_h - \chi_x) \frac{\chi_\eta - \chi_l}{\chi_\eta - \chi_x} \left( \frac{\log \frac{\chi_\eta}{\chi_x}}{\chi_x - \chi_\eta} - \frac{\log \frac{\chi_\eta}{\chi_h}}{\chi_h - \chi_\eta} \right) \right] + \text{analytic terms} \right\}. \quad (80) \end{aligned}$$

“Converting” to the SU(2) theory, we can expand in  $m_x/m_h$  and  $m_l/m_h$  obtaining:

$$\begin{aligned} f_{xh} = f_0 \left\{ 1 - \frac{1}{8\pi^2 f_0^2} \frac{\chi_x + \chi_l}{4} \log \frac{\chi_x + \chi_l}{2\Lambda_\chi^2} + \frac{1}{64\pi^2 f_0^2} (2\chi_x - \chi_l) \log \frac{\chi_x}{\Lambda_\chi^2} \right. \\ \left. + \text{analytic and higher order terms} \right\}. \quad (81) \end{aligned}$$

The analytic terms now include contributions proportional to  $\chi_h$  which do not vanish in the SU(2) chiral limit. They are absorbed into the lowest order SU(2) LEC  $f$ , which now depends on  $m_h$ . Whether or not the relation between  $f$  and  $f_0$  is well approximated by one-loop SU(3) ChPT or whether higher order ( $\chi_h^2$  and higher powers) terms must be included depends on  $m_h$  and on the convergence of the series. In any case, if  $f_{xh}$  is to satisfy the generic form dictated by SU(2) ChPT given in Eq. (79) the chiral logs are fixed from Eq. (81):

$$f_{xh} = f \left\{ 1 - \frac{1}{8\pi^2 f^2} \frac{\chi_x + \chi_l}{4} \log \frac{\chi_x + \chi_l}{2\Lambda_\chi^2} + \frac{1}{64\pi^2 f^2} (2\chi_x - \chi_l) \log \frac{\chi_x}{\Lambda_\chi^2} \right. \\ \left. + \text{analytic and higher order terms} \right\}, \quad (82)$$

which agrees with the result from the direct evaluation in the SU(2) theory (see Eq. (66)). The same is true for the other quantities being studied here. Of course, in general there may be more than one operator in the effective theory with the same quantum numbers as the QCD operator whose matrix element is to be evaluated. In such cases there are more than one LEC at leading order, Eq. (79) does not apply and the simple arguments presented here have to be generalized.

### III. SIMULATION DETAILS AND ENSEMBLE PROPERTIES

Following the work in [16, 34] we have used the Iwasaki gauge action and the domain wall fermion action. By producing smoother gauge fields at the lattice scale, for a fixed lattice spacing in physical units, the Iwasaki action removes some of the gauge field dislocations that contribute to the residual chiral symmetry breaking for domain wall fermions at finite  $L_s$ . While suppressing such dislocations improves residual chiral symmetry breaking, it also suppresses topology change in the evolution [17]. Since we want our ensembles to sample topological sectors of the theory as well as possible, we have found the Iwasaki gauge action to provide a reasonable balance between these two, contradictory goals.

We generate ensembles with two degenerate light quarks, whose bare input mass is given by  $m_l$ , and one heavy strange quark of mass  $m_h$ . We use the exact Rational Hybrid Monte Carlo (RHMC) algorithm to generate ensembles. During the course of this work, we made improvements to the RHMC algorithm, as detailed in [34], yielding three variants of the RHMC algorithm, 0, I and II. The original RHMC 0 algorithm [35, 36] was used for the 2+1 flavor simulations in [16] and the RHMC I was used for most of the simulations in [34]. We also compared the RHMC I and

II algorithms in [34]. We find the RHMC II algorithm to be the best version to date. It uses a single stochastic noise source to estimate ratios of determinants, which reduces the size of the forces in the molecular dynamics integration [15]. It produces ensembles that change topology more rapidly than RHMC I, likely due to this decrease in the fermionic force. It uses a multiple time scale Omelyan integrator and light quark preconditioning [37, 38], which has the effect of making the time spent solving the light quark Dirac equation less than the time spent solving for heavier quarks.

We can briefly define the RHMC II algorithm. Letting  $\mathcal{D}(m_i) = D_{\text{DWF}}^\dagger(M_5, m_i)D_{\text{DWF}}(M_5, m_i)$ , where  $D_{\text{DWF}}(M_5, m_i)$  is the domain wall fermion Dirac operator,  $M_5$  is the domain wall height and  $m_i$  is the mass of the quark we wish to simulate, we write the fermionic contribution to the path integral as

$$\det \left\{ \frac{\mathcal{D}(m_l)}{\mathcal{D}(1)} \right\} \det \left\{ \frac{\mathcal{D}(m_h)}{\mathcal{D}(1)} \right\}^{1/2} = \det \left\{ \frac{\mathcal{D}(m_l)}{\mathcal{D}(m_h)} \right\} \left[ \det \left\{ \frac{\mathcal{D}(m_h)}{\mathcal{D}(1)} \right\}^{1/2} \right]^3. \quad (83)$$

(Recall that for domain wall fermions, a regulator must be added to remove the bulk infinity that would arise as  $L_s \rightarrow \infty$ . The  $\mathcal{D}(1)$  terms in Eq. (83) are this regulator.) Each ratio of determinants on the right-hand side of Eq. (83) is represented by a single stochastic estimator, *i.e.* a single estimator is used for the ratio involving  $m_l$  and  $m_h$  and three estimators are used for the three, fractional power determinants involving  $m_h$  and 1. The light quark ratio is integrated on the coarsest time scale, using a conventional Hybrid Monte Carlo algorithm. The three 1/2 powers of ratios involving the heavy dynamical quark are integrated on a 2 times finer time scale using the RHMC algorithm. For each integration step of the RHMC and for each field, a single solution of the Dirac equation is required with mass  $m_h$  and two solutions with the regulator mass of 1. (The solutions are found with the conjugate gradient algorithm.) The regulator mass solutions take roughly half as many conjugate gradient iterations in the RHMC as the  $m_h$  solutions, but there are twice as many required. Thus the time spent solving the Dirac equation in the two cases is comparable. Because of the three different stochastic estimators needed in the RHMC, and the coarser time step for the HMC, the number of conjugate gradient iterations in the RHMC are larger than in the HMC part of the algorithm for the quark masses currently used. This has made simulating at lighter quark masses much less expensive. The gauge field is integrated on an even finer time scale than the RHMC. For a further review of the RHMC, see [39].

As mentioned, we had already begun evolving configurations with the RHMC 0 algorithm as improved versions were being developed. Table I gives the molecular dynamics time when we

changed from one algorithm to the next, for each of our ensembles. Since, the RHMC II gives more decorrelated lattices than earlier versions, all of the observables in this paper have been measured only on configurations generated by the RHMC II algorithm. The configurations generated with the earlier algorithms are being used only for equilibration.

As one indicator of how well the RHMC II algorithm is decorrelating our ensembles, we have measured the global topological charge. Of course, for infinite volumes, global topological charge is not relevant to local physics. However, in finite volume knowing that global topology is changing gives us evidence that there are local topological fluctuations. To calculate the topological charge the configurations are first cooled by applying 30 updates with a quenched, 5 loop improved gauge action with zero coupling strength,  $\beta = \infty$ . After cooling, the topological charge is measured using a 5 loop improved gluonic topological charge operator, the 5Li method of [40] and the results are shown in Fig. 3. This figure shows that the RHMC algorithm is sampling different topological sectors for each of our ensembles and the histograms indicate, by their symmetry and shape, that the topological landscape has been sampled reasonably well.

Figures 4 and 5 show the integrated autocorrelation time for the pion correlator at a separation of 12 lattice spacings for the  $m_l = 0.005$  ensemble. Both show an integrated autocorrelation time for this quantity of 10 to 15 molecular dynamics time units. Figure 6 shows the evolution of the plaquette for the  $m_l = 0.02$  ensemble. For this short-distance observable, equilibration took a few hundred molecular dynamics time units.

## IV. LATTICE RESULTS FOR PSEUDOSCALAR MASSES AND DECAY CONSTANTS

### A. Measurements

Since we are most interested in the light quark limit where pion masses are close to the physical values, we put significant computational effort into the measurements on the two lightest ensembles with  $m_l = 0.005$  and  $m_l = 0.01$ . On these two ensembles, three separate measurements have been done, which we shall refer to as Full-Partially-Quenched (FPQ), Degenerate (DEG) and Unitary (UNI). In the FPQ measurement we computed hadron two-point correlators for all the combinations with valence quark masses  $m_x, m_y \in \{0.001, 0.005, 0.01, 0.02, 0.03, 0.04\}$ . The DEG dataset consists of hadron correlators with *degenerate* quarks with the same list of masses. In the UNI dataset only quark propagators with masses equal to the light and strange sea quark

masses were calculated, and the light-light, light-strange and strange-strange meson correlators were then constructed. On the  $m_l = 0.02$  and  $m_l = 0.03$  ensembles, only the DEG and UNI calculations were performed. Details of the measurements, including the gauge configurations used, separation of each measurement and the total number of measurements, can be found in Table II. For the  $m_l = 0.005$  and  $m_l = 0.01$  ensembles, we blocked the data so that each block contains measurements from every 80 molecular-dynamics time units, while for the  $m_l = 0.02$  and  $0.03$  ensembles the block size was chosen to be 40 time units to yield a reasonable number of jackknife blocks to perform the analysis.

In each of the FPQ measurements, we used Coulomb gauge fixed wall (W) sources of size  $24^3$ , which were placed at  $t = 5$  and  $t = 59$ . For each source, two quark propagators were calculated, one with the periodic, and the other anti-periodic, boundary condition in the temporal direction. The sum of these two quark propagators (as a single quark propagator) was then used to construct the meson correlators. The resulting cancellation of backward propagating states has the effect of doubling the temporal extent of the lattice, so over much of the lattice volume, there is no excited state contribution to the hadron propagator. We find this works well with our Coulomb gauge fixed wall sources, which generally have small statistical errors but are not tuned to remove excited state contaminations. The long plateaus and small statistical errors allow us to work far enough from the source that excited states are not a worry.

The DEG measurements used a Coulomb gauge fixed box source (B) of size  $16^3$  which we have found to give the optimal early onset of the plateaus for pseudoscalar mesons. The sources were placed at two timeslices,  $t = 0$  and  $32$ .

In the UNI measurements, the propagators were calculated from Coulomb gauge fixed hydrogen S-wavefunction (H) sources [41], with radius  $r = 3.5$ , in lattice units, or gauge invariant gaussian (G) sources and sinks with radius  $r = 4$ . Again the sources were placed at multiple timeslices for a better sampling over the gauge fields.

We also used two different interpolating operators for the pseudoscalar state, namely, the pseudoscalar operator  $P^a(x) = \bar{q}(x)\gamma_5(\tau^a/2)q(x)$ , which we refer to using a short-hand notation  $P$ , and the axialvector operator  $A_\mu^a(x) = \bar{q}(x)\gamma_\mu\gamma_5(\tau^a/2)q(x)$ , which we refer to as  $A$ . Here  $\tau^a$  is a flavor symmetry generator. Unless otherwise specified, we only consider the time component of  $A_\mu^a(x)$ , *i.e.*,  $A_4^a(x)$ . Together with the different source/sink smearings described above, this allows us to construct several different pseudoscalar meson correlators, which are tabulated in Table III. (Table IV has similar information for vector and tensor correlators, which are discussed in detail in

Section IX.) The notation in Table III follows Ref.[16], where quark propagators are specified by the smearings applied in the source and sink. For example, WL means a quark propagator calculated with a wall (W) source and a local (L) sink. Meson correlators are then denoted by the type of quark propagators used in the contraction, *e.g.*, WL-WL refers to a meson correlator with two WL quark propagators. In this case we may also use WL to refer to the meson correlator unless ambiguities arise.

In this paper we only consider meson correlators with zero momentum projection. Our meson states are normalized such that the time dependence of the correlators in the large  $t$  limit can be expressed as

$$\mathcal{C}_{O_1 O_2}^{s_1 s_2}(t) = \frac{\langle 0 | O_1^{s_1} | \pi \rangle \langle \pi | O_2^{s_2} | 0 \rangle}{2m_{xy} V} \left[ e^{-m_{xy} t} + (-1)^p e^{-m_{xy}(T-t)} \right], \quad (84)$$

where the superscripts specify the smearings for the quark propagators, and the subscripts specify the interpolating operators used.  $m_{xy}$  is the ground-state mass of a pseudoscalar meson composed of two valence quarks with masses  $m_x$  and  $m_y$ . For convenience the amplitude of the correlator will be denoted as

$$\mathcal{N}_{O_1 O_2}^{s_1 s_2} \equiv \frac{\langle 0 | O_1^{s_1} | \pi \rangle \langle \pi | O_2^{s_2} | 0 \rangle}{2m_{xy} V}. \quad (85)$$

## B. Residual Chiral Symmetry Breaking

As discussed in Section II A, the finite size in the fifth dimension of the domain wall fermion formulation in our current simulations permits the mixing between the two light quark states bound to the boundary walls, resulting in a residual chiral symmetry breaking [7, 14, 17]. Close to the continuum limit, this effect can be quantified as a residual mass term (denoted as  $m_{\text{res}}$ ), which, up to  $O(a^2)$ , behaves as a regular quark mass, making the total quark mass effectively the sum of the bare input quark mass and the residual mass. We determine the residual mass by computing the ratio [14, 16]:

$$R(t) = \frac{\langle \sum_{\vec{x}} J_{5q}^a(\vec{x}, t) P^a(\vec{0}, 0) \rangle}{\langle \sum_{\vec{x}} P^a(\vec{x}, t) P^a(\vec{0}, 0) \rangle}, \quad (86)$$

where  $J_{5q}^a$  is the ‘‘mid-point’’ operator which mixes the quark states from the left and right walls [7, 14], and  $P^a$  is the pseudoscalar operator defined earlier. For  $t$  large enough that only pions contribute to the correlators in Eq. (86),  $R(t) \rightarrow m'_{\text{res}}(m_f)$ . From the DEG data sets, we obtained the residual mass for each pair of valence quark masses by averaging the plateaus of  $R(t)$  from  $t = 10$  to  $t = 32$ . Figure 7 shows the residual mass as a function of the valence quark mass.

We can see that the residual mass has a linear dependence on the input quark masses, and the magnitude of the slope is larger in the valence sector than the sea sector. The slopes have opposite signs, as was also observed in our previous simulations on smaller volumes [16, 34]. In particular,  $d\ln(m'_{\text{res}})/dm_f^{\text{val}} = -4.1$  for the ensemble with  $m_l = 0.005$  and  $-4.5$  for the  $m_l = 0.03$  ensemble. We also find  $d\ln(m'_{\text{res}})/dm_f^{\text{sea}} = 6$  and, for the dynamical quark mass dependence in the unitary case, the result is  $d\ln(m'_{\text{res}})/dm_l = 1.1$ . In terms of the discussion at the end of Section II A, it appears that the  $Z_{\mathcal{A}} - 1$  and dimension five terms are comparable in magnitude. We define a mass-independent residual mass for our simulations by evaluating  $m_{\text{res}}(m_l)$  at the  $m_l = 0$  limit. The straight line in Fig. 7 shows a linear fit to the four unitary points with  $m_x = m_y = m_l$ . And the star is the resulting residual mass at  $m_l = 0$ , which we determined to be

$$m_{\text{res}} = 0.00315(2). \quad (87)$$

It is worth noting that this result is in decent agreement with that obtained from earlier simulations at the same gauge coupling but with a smaller lattice volume [34], indicating that the finite volume effect for the residual mass is small.

### C. Pseudoscalar Meson Masses and Decay Constants

#### 1. Results from the $m_l = 0.005$ and $0.01$ ensembles

To obtain the masses and decay constants for the pseudoscalar mesons from the  $m_l = 0.005$  and  $m_l = 0.01$  ensembles, we focus on the FPQ data sets, since the long plateaus of the FPQ data sets lessen the uncertainty in choosing the fit ranges. In fact, including the UNI and DEG measurements in the simultaneous fits (described below) does not change significantly either the central values or statistical errors of the final results. Thus here we only quote results from the FPQ data sets.

For each mass combination in the FPQ data sets, we performed a simultaneous fit to the five correlators as specified in the second column of Table III, to determine a common mass and a different amplitude for each correlator. This approach has the advantage of averaging out the systematic uncertainties due to different characteristics of the interpolating operators ( $P$  or  $A$ ), and reducing the uncertainty of fit range choices. One drawback is that, as the number of data points included in the fit ( $\sim 220$ ) is greater than the number of independent measurements we have in hand, the covariance matrix is poorly resolved, and we lean on uncorrelated fits to obtain results.



The resulting pseudoscalar meson masses for all the mass combinations of the  $m_l = 0.005$  and  $0.01$  ensembles are given in Table V. Note that the quoted  $\chi^2/\text{dof}$ 's only give a qualitative indication of how different fits compare to each other. They are not meaningful quantitative indications of the goodness of the fits.

Besides a common mass for each valence mass combination, we also obtained an amplitude for each correlator included in the simultaneous fit, namely

$$\mathcal{N}_{AA}^{LW}, \mathcal{N}_{PP}^{LW}, \mathcal{N}_{AP}^{LW}, \mathcal{N}_{PP}^{WW} \text{ and } \mathcal{N}_{AP}^{WW}. \quad (88)$$

Combinations of these amplitudes can be used to determine the pseudoscalar decay constant, which we will describe in the following.

The pseudoscalar decay constant can be determined by

$$f_{xy} = \frac{Z_A |\langle \pi | A_4 | 0 \rangle|}{m_{xy}}, \quad (89)$$

where  $Z_A$  is the axial vector current renormalization constant which relates the (partially) conserved axial vector current in the original five-dimensional theory of domain wall fermions to the local four-dimensional axial vector current [4]. Alternatively, the axial Ward identity in Eq. (11) connects the divergence of the partially conserved axial vector current to the pseudoscalar density, allowing us to determine the pseudoscalar decay constant through

$$f_{xy} = \frac{(\tilde{m}_x + \tilde{m}_y) |\langle \pi | P | 0 \rangle|}{m_{xy}^2}, \quad (90)$$

where  $\tilde{m}_{x,y} = m_{x,y} + m_{\text{res}}$ .

We determined  $Z_A$  from the DEG data sets using the improved ratio [4] of  $\langle \mathcal{A}_4(t) P(0) \rangle$  to  $\langle A_4(t) P(0) \rangle$ , where  $\mathcal{A}_\mu(x)$  is the partially conserved axial vector current for domain wall fermions [4, 7]. Similar to the residual mass, we computed the value of  $Z_A$  at each unitary quark mass, and extrapolated it to the chiral limit at  $m_l = -m_{\text{res}}$ , finding

$$Z_A = 0.7161(1), \quad (91)$$

which agrees very well with the result of our smaller-volume simulations [34].

There are in principle five methods [42] to determine the matrix element necessary for the  $f_{xy}$  calculation in Eq. (89) or (90). These use jackknife ratios of different amplitudes in Eq. (88). We found that different methods give statistically consistent results for all quark masses except for the lightest or heaviest quark masses, where systematic deviations for results obtained using

Eq. (89) and Eq. (90) are observed. The methods where the pseudoscalar density is used make use of the equation of motion for the conserved axial current and are more indirect, since we have not systematically controlled higher order renormalization effects here. As was discussed in Section II A, the renormalization of the conserved axial current is known to  $O(m_{\text{res}})$ , and we know the renormalization between the local and conserved current to high accuracy. Therefore, we have chosen as our preferred result a determination of  $f_{xy}$  using axial current matrix elements and postpone further investigation of the differences we are seeing for future work. We also find that the statistical errors are the smallest when only the axial vector current matrix elements are used in the analysis. Thus, we determine  $f_{xy}$  by

$$f_{xy} = Z_A \sqrt{\frac{2}{m_{xy}} \frac{\mathcal{N}_{AP}^{LW^2}}{\mathcal{N}_{PP}^{WW}}}. \quad (92)$$

The final results for the  $m_l = 0.005$  and  $0.01$  ensembles are shown in Table VI.

Comparing the results from the  $m_l = 0.01$  ensemble with those obtained from a smaller volume reported in Ref.[34], we find that there is a statistically significant 4% difference at the unitary point of  $m_x = m_y = m_l = 0.01$ , as shown in Fig. 8. As we shall see in Section VI A, such a difference is about twice as large as predicted by finite volume chiral perturbation theory. While it is possible that ChPT still underestimates the finite volume effect for  $f_{xy}$ , we want to point out that the  $16^3 \times 32$  gauge configurations were generated using RHMC I which could intrinsically induce long-range autocorrelations. Another difference is that there we determined  $f_{xy}$  using correlators with much shorter plateaus compared to the  $24^3 \times 64$  ensembles discussed here, which means the smaller-volume results may suffer from larger systematic errors. Although we tried our best to estimate uncertainties on the physical quantities of the  $16^3 \times 32$  simulations, the errors might still be underestimated. With these factors taken into account, the discrepancy between the lattice data and the predictions of the finite volume ChPT may not be as significant as it appears.

## 2. Results from the $m_l = 0.02$ and $0.03$ ensembles

For the two heavy ensembles with  $m_l = 0.02$  and  $0.03$  we performed uncorrelated simultaneous fits to four correlators from the DEG data sets:  $\mathcal{C}_{AA}^{LB}(t)$ ,  $\mathcal{C}_{PP}^{LB}(t)$ ,  $\mathcal{C}_{AP}^{LB}(t)$  and  $\mathcal{C}_{AP}^{BB}(t)$ . The time slices included in the fits are from  $t = 10$  to  $32$  for each correlator. The pseudoscalar meson masses obtained this way are presented in Table VII. The corresponding amplitudes of these correlators

can be used to determine the pseudoscalar meson decay constants by the following relation:

$$f_{xy} = Z_A \sqrt{\frac{2}{m_{xy}} \frac{\mathcal{N}_{AA}^{LB} \mathcal{N}_{AP}^{LB}}{\mathcal{N}_{AP}^{BB}}}, \quad (93)$$

the results of which are given in Table VIII.

## V. RESULTS FOR THE OMEGA BARYON MASS

We have chosen to set the lattice scale using the  $\Omega^-$  baryon mass because it is made of three strange valence quarks and so does not have non-analytic light quark mass terms at NLO in chiral perturbation theory[43, 44]. Thus, it is justified to linearly extrapolate in  $m_l$  to obtain the physical value.

The interpolating field for the decuplet baryons is

$$\chi_{\text{dec}} = \varepsilon_{abc} [q_a^T C \gamma_\mu q_b] q_c, \quad (94)$$

which couples to both spin 3/2 and 1/2 states, the former being the ground state [45]. For  $q = s$ , the strange quark, the operator destroys an  $\Omega^-$  baryon.

The correlation function is constructed using the BL quark propagator described in Section IV computed from sources set at time slices 0 and 32 for every twentieth trajectory, starting from a thermalized one. Results are averaged over these sources and blocked in bins of size 80 trajectories to reduce auto-correlations. The total number of measurements made varies between about 100 and 200, depending on the light sea quark mass (see Table IX). To avail ourselves of all possible statistics, we average over forward propagating particle states, and backward propagating anti-particle states, as well as all three spatial directions for the interpolating operator.

The average correlation function is fit using a jackknife procedure where the covariance matrix is estimated for each jackknife block. The minimum time slice used in the fit was varied in the range  $4 \leq t_{\text{min}} \leq 10$ ; the maximum was fixed to 14. Though the mass values do not depend sensitively on the choice of  $t_{\text{min}}$ , we chose to take as central values the masses obtained from  $t_{\text{min}} = 8$  to minimize excited state contamination without losing control of the statistical error and because  $\chi^2$  is acceptable for this  $t_{\text{min}}$  value. The baryon mass values for valence quark masses  $m_x = 0.03$  and 0.04 are summarized in Table IX and plotted in Fig. 9.

Also shown in the figure is a linear extrapolation, for each degenerate valence mass, to the physical value of the light sea quark mass (solid lines). The linear fit to the  $m_x = 0.03$  data has a  $\chi^2/\text{d.o.f.}$

of 1.2 and the  $m_s = 0.04$  data has a  $\chi^2/\text{d.o.f.}$  of 1.4. In the next section we use these values to interpolate to the physical strange quark mass in order to set the lattice scale using the  $\Omega^-$  baryon mass.

A systematic error in the  $\Omega^-$  mass, and hence in the lattice spacing, results from the fixed unphysical value of the strange sea quark mass in the simulation. This effect can be estimated from the slope of the baryon mass with respect to the light sea quark mass (see Fig. 9). The effect, which is similar for both valence quark masses, is about 2–3 % for a (required) shift in sea quark mass of about 0.008. Since this results from varying both light quarks together, it should be divided by two for the single strange quark in the simulation. This is about a one percent downward shift in the mass, which is smaller than the statistical errors, as shown in the next section, so we ignore it.

## VI. LATTICE SCALE, QUARK MASSES AND DECAY CONSTANTS USING SU(2) CHPT

### A. SU(2) $\times$ SU(2) Chiral Fits

In this subsection we present a brief overview of the techniques we use to perform the chiral extrapolations for pseudoscalar masses and decay constants. For our simulations with 2+1 flavors of dynamical fermions, the traditional approach would be to use the SU(3) chiral perturbation theory to guide the extrapolations. However, as we shall see in Section VII A, NLO SU(3) ChPT does not describe our data for the pseudoscalar mesons which contain a quark as heavy as the strange quark. In order to extrapolate our results reliably to the physical quark masses (and in particular to the physical strange quark mass) we therefore use a different approach and impose only SU(2) chiral symmetry in the light quark sector, as has been discussed in Section II. We divide our discussion into two parts. In Section VI A 1 we discuss the chiral extrapolations in the pion sector and in Section VI A 2 we extend the discussion to kaons. We present physical results for the quark masses and pseudoscalar decay constants using the SU(2) chiral fits in Section VI B below.

#### 1. The Pion Sector

In the pion sector, the chiral dynamics of SU(2)<sub>L</sub>  $\times$  SU(2)<sub>R</sub> symmetry is sufficient to describe the physics we are interested in. The effects of the dynamical strange quark are fully contained in the

low-energy constants of  $SU(2)_L \times SU(2)_R$  ChPT [12]. There is a caveat. A posteriori we learn that the dynamical strange quark mass used in our simulations is a little larger than the physical one. Ideally, we would need to perform the simulations with several different dynamical strange quark masses and interpolate the results to the physical strange quark mass. In the absence of such simulations, the dynamical strange quark mass is fixed to  $m_h = 0.04$ , and we need to be aware that the corresponding LECs will have a corresponding small systematic error (see Sec. VI C 3).

The next-to-leading order partially quenched  $SU(2)$  formulae for the squared masses,  $m_{xy}^2$ , and decay constants,  $f_{xy}$ , of the light pseudoscalar mesons composed of two valence quarks with masses  $m_x$  and  $m_y$  can be derived from [46], as has been done, for instance, in [47]. For reference, we summarize these formulae in Appendix B 2. As discussed in Section II, for domain wall fermions the effective quark mass is the sum of the input quark parameters  $m_{x,y,l,h}$  and the residual mass, which we denote as  $\tilde{m}_{x,y,l,h} \equiv m_{x,y,l,h} + m_{\text{res}}$  (here  $l$  and  $h$  denote the light and heavy sea quarks respectively). To next-to-leading order, this is the only correction to the continuum chiral formulae. Since  $f_{xy}$  and  $m_{xy}^2$  share two unknown low energy constants  $B$  and  $f$ , we perform combined fits to both of them, using the two ensembles with dynamical light quark masses of  $m_l = 0.005$  and  $0.01$ . Such combined fits with valence quark masses  $m_x, m_y = 0.001, 0.005$ , and  $0.01$  (which therefore satisfy the cut  $m_{\text{avg}} \equiv (m_x + m_y)/2 \leq 0.01$ ) are shown in Fig. 10. The values of the fit parameters are given in Table X, where we quote the scale-dependent low energy constants at two commonly used renormalization scales  $\Lambda_\chi = 770$  MeV and  $1.0$  GeV. These partially quenched LECs (of  $SU(4|2)$  PQChPT) can be related to those in the physical unitary theory ( $SU(2)$ ),  $l_3^r$  and  $l_4^r$ , by Eqs. (B35) and (B39). In Table X we also quote the values of  $\bar{l}_3$  and  $\bar{l}_4$ , which are conventionally defined at the scale of the pion mass, see Eq. (B44).

Using partially quenched NLO  $SU(2)$  chiral perturbation theory we are able to describe the data with the mass cut  $m_{\text{avg}} \equiv (m_x + m_y)/2 \leq m_{\text{cut}} = 0.01$ . It is not possible however, to extend the range of masses significantly. For example, the quality of the fit degrades significantly if instead we impose a mass cut of  $m_{\text{avg}} \leq 0.02$ : the  $\chi^2/\text{d.o.f}$  increases from  $0.3$  ( $m_{\text{cut}} = 0.01$ ) to  $1.2$  ( $m_{\text{cut}} = 0.015$ ) and even  $3.6$  for  $m_{\text{cut}} = 0.02$ . (We only report the uncorrelated  $\chi^2/\text{d.o.f}$  since we could not reliably determine the correlations, so these numbers most likely underestimate the “true” deviation from the fit.) This suggests that higher orders of chiral perturbation theory (NNLO or even more) are needed in this mass range. (See also the discussion in Sec. VI C 1 regarding the inclusion of analytic NNLO terms.)

## 2. The Kaon Sector

In order to incorporate the valence strange quark mass in the chiral extrapolations, we need to extend the SU(2) ChPT to the kaon sector. As has been discussed in Section II, this can be done by considering the kaon as a heavy meson under the assumption that  $\tilde{m}_l \ll \tilde{m}_s$ , in analogy to the heavy-light meson (or heavy baryon) chiral perturbation theory [32, 48]. In this framework the chiral expansions are ordered in powers of  $\tilde{m}_l/\tilde{m}_h$  or equivalently  $m_\pi^2/m_K^2$ , as well as  $m_\pi^2/\Lambda_\chi^2$ . We present the NLO chiral formulae for  $m_{xy}^2$  and  $f_{xy}$ , the masses and decay constants of pseudoscalar mesons composed of a light valence quark with mass  $m_x$  and a heavy valence quark with mass  $m_y$  in Eqs. (66) and (67) (see also App. B 3 for the complete set of formulae at NLO).

For kaons a new set of low-energy constants  $f^{(K)}$ ,  $B^{(K)}$  and  $\lambda_{1,2,3,4}$  are introduced. These LECs depend on the valence and dynamical strange quark masses and we have made this explicit by assigning a functional dependence, writing for instance,  $f^{(K)}(m_h)$ . Here  $m_h$  represents both the masses of the heavy (strange) dynamical and valence quarks. The parameters  $B$  and  $f$  are the usual LECs in the (pionic) SU(2) theory, and their values are determined from the quantities in the pion sector, *i.e.*, their values are fixed to the ones given in Table X.

The strange quark mass dependence in the formulae for the meson masses and decay constants, Eqs. (66) and (67) are contained in the low energy constants. Since it is not possible to tune the dynamical heavy quark mass  $m_h$  perfectly to the mass  $m_s$  of the physical strange quark, in principle we would wish to perform the calculations at several values of  $m_h$  and interpolate the results to  $m_s$ . Since we only have results at a single value of  $m_h$  ( $m_h = 0.04$ ) we rely as far as possible on using the behaviour of our results with the valence strange quark masses,  $m_y$ , to extrapolate to the physical kaon.

Finally, we briefly summarise our fitting procedure. We start by fitting the mass dependence of  $m_{xy}^2$  and  $f_{xy}$  using Eqs.(66) and (67) for  $m_x \in [0.001, 0.01]$  and  $m_y = 0.04$ , with  $B$  and  $f$  fixed to the values in Table X. Since these two formulae do not have any unknown parameters in common, the fits can be done independently. We then extrapolate to the physical value of the light quark mass to obtain  $m_K(m_y = 0.04)$  and  $f_K(m_y = 0.04)$ . (The physical light quark mass  $m_{ud}$  is determined from the SU(2) pion sector fits, see VIB 1 for a detailed description.) This step is shown in Fig. 11, where the circles give the extrapolated values  $m_K(m_y = 0.04)$  (right) and  $f_K(m_y = 0.04)$  (left). Then similar fits are performed with  $m_y = 0.03$ , giving values for  $m_K(m_y = 0.03)$  and  $f_K(m_y = 0.03)$ . Eventually, we take the results at  $m_y = 0.03$  and  $0.04$  and interpolate linearly between them.

As discussed in Sec. VI B, we define the physical strange quark mass from the interpolation of  $m_{xy}^2$  to the physical value of  $m_K^2$ . Having determined the physical value of the strange quark mass, we extract the kaon decay constant from the interpolation of  $f_{xy}$  to this mass. The linear fits are shown in Fig. 12. In the same figure we also include the points obtained with  $m_y = 0.02$ . Although at such a low mass the use of SU(2) chiral perturbation theory is questionable, we see that nevertheless the points lie very close to the line obtained from the interpolation between  $m_y = 0.04$  and  $m_y = 0.03$ , suggesting that the higher-order corrections of  $O(\tilde{m}_l/\tilde{m}_h)^2$  may be small.

## B. Lattice Scale, Physical Quark Masses and Decay Constants

Having established the procedure for the chiral extrapolations, we now turn to obtaining the physical results. In this subsection we start by explaining how the lattice scale and physical bare quark masses were determined. We then use the renormalization constant for the quark masses which was determined non-perturbatively in [21] to obtain the physical quark masses in the  $\overline{\text{MS}}$  scheme at  $\mu = 2 \text{ GeV}$ . Finally we present the results for  $f_\pi$ ,  $f_K$  and the CKM matrix element  $|V_{us}|$  determined from our measured ratio  $f_K/f_\pi$  together with experimental inputs.

### 1. Determination of $m_{ud}$ , $m_s$ and $a^{-1}$

In order to determine the quark masses  $m_{ud}$ ,  $m_s$  and the lattice spacing  $a$ , we need to compare our lattice results for three quantities to their physical values. We take the pseudoscalar masses  $m_\pi$  and  $m_K$  as two of these. Natural choices for the third would be the  $\rho$  mass or the Sommer scale. However, since the  $\rho$  meson is a resonance with a finite width and there is an uncertainty of order 10% in the value of the Sommer scale, we choose instead to use the mass of the  $\Omega$  baryon. This is a state composed of three valence strange quarks. One advantage of using this baryon mass, is that up to NLO in  $\chi$ PT it is free of logarithms containing the light quark masses [43, 44]. Therefore the extrapolation of the measured masses to the light physical mass can be readily performed using a linear ansatz without an uncertainty due to chiral logarithms.

The physical quark masses were obtained from the SU(2)  $\times$  SU(2) fits described in Section VI A. For the average light quark mass,  $m_{ud} \equiv (m_u + m_d)/2$ , we solved for a pion mass of  $m_\pi = 135.0 \text{ MeV}$ , corresponding to the physical neutral pion mass, while for the strange quark mass  $m_s$  the fit to the kaon mass was solved at  $m_K = 495.7 \text{ MeV}$ , which is the quadratically averaged

neutral and charged kaon mass.

The determination of the three parameters is a coupled problem. The lattice scale is needed to convert masses between lattice units and physical ones, whereas the quark masses are needed for the extrapolation and interpolation in the light and strange quark masses to obtain the mass of the  $\Omega$  baryon. We performed the determination iteratively, starting with an initial “guess” for the quark masses, fixing the lattice spacing by requiring that  $m_\Omega$  takes its physical value, then using this value of  $a$  to adjust the quark masses by requiring that  $m_\pi$  and  $m_K$  take their physical values and so on until no further changes in the parameters were observed. The final values for  $1/a$ ,  $a$ ,  $m_{ud}$ ,  $m_s$  can be found in Table XI, with only the statistical errors shown. (We will discuss the systematic errors in Sec. VI C.) We also find the quark mass ratio to be  $\tilde{m}_{ud} : \tilde{m}_s = 1 : 28.8(4)$ .

An independent check of the lattice scale has been done from the spectrum of heavy-heavy and heavy-strange quark states using the non-perturbatively determined relativistic heavy quark action [49, 50]. The preliminary analysis [51] gave  $1/a = 1.749(14)$  GeV, where the error is statistical only. The agreement of this result with that obtained from the  $m_{\Omega^-}$  shown in Table XI suggests that the associated systematic errors are small.

## 2. Quark Masses in $\overline{\text{MS}}$ Scheme

In this section we present the results for the quark masses in the  $\overline{\text{MS}}$  renormalization scheme. The renormalization factor  $Z_m = 1/Z_S$  (where  $S$  represents the scalar density) needed to convert the bare quark masses to the commonly used  $\overline{\text{MS}}$  scheme at a scale of 2 GeV has been calculated with the same action on a  $16^3 \times 32 \times 16$  lattice [21]. (For details about this ensemble of configurations, see [34].) We first matched the bare lattice operators to the RI-MOM scheme using the non-perturbative Rome-Southampton technique [52], and then performed a perturbative matching to the  $\overline{\text{MS}}$  scheme. The relation between the renormalized and bare quark masses is given by

$$m_X^{\overline{\text{MS}}}(2 \text{ GeV}) = Z_m^{\overline{\text{MS}}}(2 \text{ GeV}) a^{-1} (a\tilde{m}_X), \quad (95)$$

where  $X = ud, s$  and for clarity we made explicit the factors of the lattice spacing  $a$ . In Ref. [21] it was found that  $Z_m^{\overline{\text{MS}}}(2 \text{ GeV}) = 1.656(48)(150)$ , where the first error is statistical, while the second is the combined systematic uncertainty due to residual chiral symmetry breaking, the use of a three-loop matching factor between the RI-MOM and  $\overline{\text{MS}}$  schemes and mass effects. With this renormalization constant, the results for the average light quark mass and the strange quark mass



are determined to be

$$m_{ud}^{\overline{\text{MS}}}(2\text{ GeV}) = 3.72(16)(33)\text{ MeV}, \quad (96)$$

$$m_s^{\overline{\text{MS}}}(2\text{ GeV}) = 107.3(4.4)(9.7)\text{ MeV}, \quad (97)$$

where the first error is the combined statistical error from the bare lattice quark masses, the lattice spacing and  $Z_m^{\overline{\text{MS}}}$  and the second error is the systematic error in  $Z_m^{\overline{\text{MS}}}$ .

Related to the renormalization of the quark masses is the renormalization of the lowest order LEC  $B$ , which is proportional to the quark condensate and therefore is renormalized by  $Z_S = 1/Z_m$ , ensuring that the product of  $B$  and a quark mass does not depend on the renormalization scheme or scale. We have

$$B^{\overline{\text{MS}}}(2\text{ GeV}) = \left(Z_m^{\overline{\text{MS}}}(2\text{ GeV})\right)^{-1} \cdot (1/a) \cdot aB \quad (98)$$

$$= 2.52(11)(23)\text{ GeV}, \quad (99)$$

where the first error is statistical and the second is the systematic uncertainty from renormalization. The renormalized value for the chiral condensate,  $\Sigma = f^2 B/2$ , reads

$$\Sigma^{\overline{\text{MS}}}(2\text{ GeV}) = \left(255(8)(8)\text{ MeV}\right)^3. \quad (100)$$

### 3. $f_\pi$ , $f_K$ and $|V_{us}|$

The chiral fits described in Section VIA also allow us to determine the decay constants  $f_\pi$  and  $f_K$ . Extrapolation to the physical light quark mass  $m_{ud}$  using the  $\text{SU}(2) \times \text{SU}(2)$  fits in the pion sector gives  $f_\pi = 124.1(3.6)\text{ MeV}$ , while interpolation to the physical strange quark mass  $m_s$ , as described in Section VIA, gives  $f_K = 149.6(3.6)\text{ MeV}$ . In both cases only the statistical errors are given. Systematic errors will be discussed in Section VIC. These results can be compared to the physical values [53],  $f_\pi = 130.7(0.1)(0.36)$  and  $f_K = 159.8(1.4)(0.44)\text{ MeV}$ . For the ratio of the decay constants we find  $f_K/f_\pi = 1.205(18)$  compared to the experimental value of 1.223(12). See [102] for possible implications of an updated result for the measured value of the CKM matrix element  $V_{ud}$  [54].

An important application of the result for  $f_K/f_\pi$  is the determination of the CKM matrix element  $|V_{us}|$ , as has been pointed out in [55]. Using the experimentally determined branching ratios  $\Gamma(K \rightarrow \mu\nu(\gamma))$  and  $\Gamma(\pi \rightarrow \mu\nu(\gamma))$ , together with the radiative electroweak corrections from [53],

we obtain:

$$|V_{us}|/|V_{ud}| = 0.2292(034)_{\text{stat}}(118)_{\text{syst}}(005)_{\text{other}}, \quad (101)$$

where the first two errors are statistical and systematic (as discussed in Sec. VIC below), while the third error is the combined uncertainty from the measurement of the branching ratios and the radiative electroweak corrections [53]. Taking  $|V_{ud}| = 0.97377(27)$  from super-allowed nuclear  $\beta$ -decays [53], we obtain

$$|V_{us}| = 0.2232(033)_{\text{stat}}(115)_{\text{syst}}(005)_{\text{other}} \quad (102)$$

(The third error now also contains the uncertainty in  $|V_{ud}|$ ). This implies

$$|V_{us}|^2 + |V_{ud}|^2 = 0.9980(15)_{\text{stat}}(51)_{\text{syst}}(06)_{\text{other}} \equiv 0.9980(54)_{\text{total}}. \quad (103)$$

Since  $|V_{ub}|$  is negligible, our result implies that the unitarity relation is satisfied within the uncertainties, constraining the possible breaking of quark-lepton universality in models of new physics. For completeness we now present the corresponding results obtained using the recently published value  $|V_{ud}| = 0.97418(26)$  [54] (instead of the PDG value of  $|V_{ud}| = 0.97377(27)$  which was used in obtaining the results in Eq. (102) and Eq. (103) above):

$$|V_{us}| = 0.2232(033)_{\text{stat}}(115)_{\text{syst}}(005)_{\text{other}}, \quad (104)$$

$$|V_{us}|^2 + |V_{ud}|^2 = 0.9989(15)_{\text{stat}}(51)_{\text{syst}}(06)_{\text{other}} \equiv 0.9989(54)_{\text{total}}. \quad (105)$$

We have also determined  $V_{us}$  (with a smaller error) from the experimentally measured rates of semileptonic  $K_{\ell 3}$  decays, by computing the form factor  $f^+(q^2 = 0)$ , where  $q$  is the momentum transfer. The results (in particular  $|V_{us}| = 0.2249(14)$ ) and an outline of the calculation are presented in [18].

### C. Systematic Errors

In this section we will discuss the systematic errors resulting from various sources: 1. chiral extrapolations; 2. finite volume effects; 3. the unphysical dynamical strange quark mass and 4. scaling errors.

### 1. Errors arising from the chiral extrapolations

As explained above, we obtain our results by using NLO chiral perturbation theory to fit the measured values of the meson masses and decay constants in the range of valence quark masses satisfying  $m_{\text{avg}} \leq 0.01$  and with  $m_l = 0.005$  and  $0.01$ . We do not have enough data to extend the analysis fully to NNLO where the chiral logarithms depend on the Gasser-Leutwyler coefficients and there are too many parameters to make the fits meaningful. In order to estimate the effects of the (neglected) higher order terms in the chiral expansion we have therefore extended the range of quark masses to  $m_{\text{avg}} \leq 0.02$  but included only the analytic NNLO-terms in the fit functions. In the pion sector, the analytic terms at NNLO are quadratic in the  $\chi$ 's and symmetric under  $\chi_x \leftrightarrow \chi_y$ ; there are four such terms:

$$(\chi_x + \chi_y)^2, (\chi_x - \chi_y)^2, (\chi_x + \chi_y)\chi_l \quad \text{and} \quad \chi_l^2. \quad (106)$$

We therefore have four new parameters for the behaviour of the mass of the pseudoscalar mesons and four for the decay constants. Unfortunately, with only two values for the dynamical sea quark mass (which is proportional to  $\chi_l$ ), we were not able to resolve the complete sea quark mass dependence up to NNLO in our fits. We therefore dropped the term proportional to  $\chi_l^2$  and were then able to obtain stable fits with a good  $\chi^2/\text{d.o.f.}$  (about 0.1). We stress that the NNLO analytic terms are necessary in order to obtain good fits; NLO chiral perturbation theory does not represent our data in the extended range of masses  $m_{\text{avg}} \leq 0.02$ . With the NNLO analytic terms included, not only do we obtain good fits to our data but the behaviour of the chiral expansion is sensible, *i.e.* the relative importance of successive terms in the series is as expected. We illustrate this point in Fig. 14, where, in the top two graphs, we plot the size of LO, NLO, and NNLO contributions (normalized such that the LO contribution equals one) for the masses-squared and decay constants of mesons with  $m_x = m_y = m_l$  (*i.e.* for mesons in the unitary theory). Up to a quark mass of 0.01 (the 3rd vertical dashed line in the plots, counting from the left) the NLO-contributions are much larger than the NNLO terms, which are negligible in this region. As expected, the NNLO corrections become more important for larger quark masses and in particular, for masses close to 0.02 (rightmost vertical dashed line) they represent a significant fraction of the decay constant. This study is reassuring, but, since we have neglected the chiral logarithms at NNLO terms, it is only a phenomenological estimate of the likely contributions from higher order terms in the chiral expansion.

As our final estimate of the errors due to the chiral extrapolation we take *twice* the difference

between the results from our standard NLO SU(2)-ChPT fit in the mass range  $m_{\text{avg}} \leq 0.01$  and those from including the analytic NNLO terms in the range  $m_{\text{avg}} \leq 0.02$ . The factor of 2 was included, rather cautiously, because of the phenomenological nature of the NNLO analysis, and in particular because we were unable to study the sea-quark mass dependence. The systematic error is reported in Table XII.

The systematic error due to the extrapolation in the mass of the light quark in the kaon quantities,  $m_s$  and  $f_K$ , was also estimated as twice the difference between our standard results and those obtained using kaon SU(2) PQChPT in the mass range  $m_x \leq 0.02$  with the values of  $f$  and  $B$  obtained from the NNLO fit described above. The errors are also tabulated in Table XII. For this case we get a good description of our data up to  $m_x = 0.02$  without the necessity of adding NNLO analytic terms ( $\chi_x^2$ ,  $\chi_l^2$ , and  $\chi_x\chi_l$ ). Therefore one expects those terms to have a negligible effect even in the mass range  $m_x \leq 0.02$ . The lower panels in Fig. 14 show the LO and NLO contributions, normalized so that the LO contribution equals one, to  $m_{lh}^2$  and  $f_{lh}$ . The horizontal axis is  $\chi_l$ , which is proportional to the total light sea quark mass. We see that the size of the NLO contributions are at most 35% for the range of masses where we have data.

## 2. Finite volume effects

In this section we estimate the errors due to the fact that the simulations are performed on a finite volume,  $(aL)^3 \approx (2.74\text{fm})^3$ . We do this by following the procedure proposed by Gasser and Leutwyler [56, 57, 58] in which one compares results obtained in ChPT using meson propagators in finite volume,  $G^{(L)}(x)$ , to those obtained with the infinite-volume propagators,  $G(x)$ . The finite-volume and infinite-volume propagators are related by

$$G^{(L)}(x) = G(x) + \sum_{\vec{n} \neq 0} G(x + L\vec{n}), \quad (107)$$

with the 3-vector  $\vec{n} \in \mathbb{Z}^3$ . This allows one to calculate the corrections in the PQChPT formulae for the meson masses and decay constants directly. We list the expressions in Appendix C, where details of the numerical implementation can also be found. (See also refs. [59, 60, 61] for the analogous discussion with staggered PQChPT.) We now repeat the chiral fits using PQChPT with the finite-volume propagators and obtain a new set of fit parameters. For each physical quantity, we assign the difference between the results obtained using the finite-volume and infinite-volume formulae as the systematic error and tabulate these finite-volume errors in Table XII for both the

pion and the kaon sectors. In the latter case we find that the finite-volume corrections in  $m_s$  and  $f_K$  are actually negligible. In Fig. 13 we plot the correction factor for the decay constants and squared masses,  $(1 - \Delta_{xy}^{Lf})$  and  $(1 - \Delta_{xy}^{Lm^2})$  (cf. App. C for their definition), respectively, for our two values of the dynamical light quark mass ( $m_l = 0.01$  and  $0.005$ ). Since the volume is reasonably large, these corrections are found to be below 1 percent, except for the very light valence masses.

We now compare our results for the finite-volume corrections obtained using ChPT (as described above) to the theoretical predictions by Colangelo et al. [62], who use a resummed Lüscher formula. The results in ref. [62] are presented for the unitary theory ( $m_x = m_y = m_l$  in our notation) and so we restrict the comparison to this case. We take the results in Tabs. 3 and 4 of [62] which we interpolate to the volume and pion masses used in our simulation. In Table XIII we present the finite-volume corrections for the pion mass and decay constant estimated using 3 methods, SU(2) and SU(3) ChPT and that of Ref. [62]. The quantities  $R_m$  and  $R_f$  are defined by

$$R_m = \frac{m_{ll}(L) - m_{ll}(\infty)}{m_{ll}(\infty)} = \frac{1}{2} \Delta_{ll}^{Lm^2}, \quad R_f = \frac{f_{ll}(L) - f_{ll}(\infty)}{f_{ll}(\infty)} = \Delta_{ll}^{Lf}, \quad (108)$$

Within the uncertainties, we see a reasonable agreement between the estimates obtained with the different methods.

In an earlier publication [34], we presented results for the masses and decay constants obtained with the same action and coupling as in this paper, but on a smaller volume, about  $(1.83 \text{ fm})^3$  compared to  $(2.74 \text{ fm})^3$  used here. (In [34] a different method was used to extract the lattice scale. Since the gauge action and coupling are identical, for consistency we quote here the volume obtained with the value for  $a^{-1}$  used throughout this work.).

Specifically the lattice in [34] has 16 points in each spatial direction as compared to 24 in this paper. We are therefore able to compare the theoretical estimates of the finite-volume corrections described above, with the difference of our results on the two lattices with different volumes. We compare the measured pion mass and decay constant at the common unitary point at  $m_x = m_y = m_l = 0.01$ ,  $m_h = 0.04$  for which the pion mass is  $\approx 427 \text{ MeV}$  (this is the smallest mass for which we have results on both lattices). On the smaller volume, both finite-volume corrected fits (SU(2) and SU(3)) give results for the correction factors comparable to those interpolated from Colangelo et al.. To obtain these correction factors, we used the parameters obtained from the fits to the  $24^3$  data and evaluated the finite-volume corrections for  $L = 16$  (instead of the original  $L = 24$ ). The SU(2) fits resulted in  $R_m^{(16c)} = 0.42(04)\%$  and  $R_f^{(16c)} = 1.66(14)\%$ , where the superscript is meant to indicate that this is the finite-volume correction for a spatial volume of  $L^3 = 16^3$ . In Table XIV

we list the measured values of the meson masses and decay constants on the  $24^3$  and  $16^3$  lattices and compare their ratios to the prediction from finite volume ChPT and the resummed Lüscher formula (interpolated from [62]). We obtain this prediction from the ratio of the finite-volume correction factor for the  $16^3$  spatial volume and that for the  $24^3$  spatial volume,

$$\frac{m_\pi^{(16c)}}{m_\pi^{(24c)}} \stackrel{?}{=} \frac{1 - R_m^{(16c)}}{1 - R_m^{(24c)}}, \quad \frac{f_\pi^{(16c)}}{f_\pi^{(24c)}} \stackrel{?}{=} \frac{1 - R_f^{(16c)}}{1 - R_f^{(24c)}}. \quad (109)$$

The superscripts in Eq.(109) indicate the spatial volumes on which the results for  $m_\pi$  and  $f_\pi$  were obtained or for which the finite-volume corrections  $R_m$  and  $R_f$  were evaluated. The question mark reminds us that we are checking whether the measured values of the ratios are equal to the theoretical predictions for the finite-volume effects. Whereas (within the errors) the observed  $(2.0 \pm 1.2)\%$  effect for the pion mass is somewhat better reproduced by the FV ChPT predictions than the  $(3.7 \pm 1.1)\%$  for the decay constant, in both cases all three methods tend to underestimate the observed FV effects. We make the following two comments. First, the precision of FV ChPT at NLO and the resummed Lüscher predictions for the finite-volume corrections are expected to improve with increasing volume. A possible reason for underestimating the difference between the results from the  $16^3$  and  $24^3$  lattices may be that the smaller volume is already borderline for the methods used here. Whereas the values for  $m_\pi L$  would appear to be sufficient in both cases; on the  $16^3$  lattice  $m_\pi L \approx 4.0$  compared to  $\approx 5.8$  on the  $24^3$  lattice, it may be that the smaller lattice does not satisfy the relation  $L \gg (\sqrt{2}f_\pi)^{-1} \sim 1$  fm sufficiently. The second comment is that, as has already been pointed out in Sec. IV, the errors on the measured quantities on the smaller volume in general, and on the decay constants in particular, may be underestimated due to shorter plateaus. Furthermore, in this present paper we have obtained the decay constants using an improved ansatz (see also Sec. IV). For these reasons, we believe that the finite volume effects on the larger lattice are well described by our approach and give a reliable estimate for the systematic error.

### 3. Effects of the unphysical dynamical strange quark mass

In this subsection we estimate the systematic error due to the fact that the mass of the dynamical heavy quark ( $m_h$ ) turns out, a posteriori, to be about 15% larger than that of the physical strange quark ( $m_s$ ). To perform this estimate we exploit the fact that the LECs of SU(3) ChPT are independent of the quark masses, and use the NLO conversion formulae relating SU(3) and SU(2) LECs [13] given in Eqs. (B40–B43), together with the results for the SU(3) LECs presented in Sec. VII A. In

this way we obtain the shifts in the SU(2) LECs:

$$B(m_s) - B(m_h) = B_0 \left\{ \frac{16}{f_0^2} (2L_6^{(3)} - L_4^{(3)}) (\chi_s - \chi_h) - \frac{1}{72\pi^2 f_0^2} \left( \chi_s \log \frac{2\chi_s}{3\Lambda_\chi^2} - \chi_h \log \frac{2\chi_h}{3\Lambda_\chi^2} \right) \right\}, \quad (110)$$

$$f(m_s) - f(m_h) = f_0 \left\{ \frac{8}{f_0^2} L_4^{(3)} (\chi_s - \chi_h) - \frac{1}{32\pi^2 f_0^2} \left( \chi_s \log \frac{\chi_s}{2\Lambda_\chi^2} - \chi_h \log \frac{\chi_h}{2\Lambda_\chi^2} \right) \right\}, \quad (111)$$

$$l_3^r(m_s) - l_3^r(m_h) = \frac{1}{576\pi^2} \log \frac{\chi_h}{\chi_s}, \quad (112)$$

$$l_4^r(m_s) - l_4^r(m_h) = \frac{1}{64\pi^2} \log \frac{\chi_h}{\chi_s}. \quad (113)$$

(Note: here one has to use  $B_0$  to determine  $\chi_X$ .) We use the shifted values of the SU(2) LECs to determine  $m_{ud}$  and  $f_\pi$  and again use the shift in those two quantities as the estimate of the corresponding systematic uncertainties. All these uncertainties are presented in Table XII and are small compared to the total errors. (We did not quantify the systematic error on the separate  $L_i^{(2)}$ , just on the  $\bar{l}_{3,4}$  since these are the phenomenologically relevant observables.)

For the kaon sector the shift due to changing the dynamical heavy quark mass to its physical value can be obtained from Eqs. (B49–B54). We perform the conversion for fixed  $m_y$  at  $m_y = 0.03$  and  $0.04$  separately and then in the same way as before linearly interpolate the heavy valence quark mass  $m_y$  to  $m_s$  to determine the shift in the kaon mass and the kaon decay constant. A shifted value for the physical strange quark mass is obtained by solving the following system. Find a value of  $m_s$  such that the interpolation in  $m_y$  to  $m_y = m_s$  between  $m_{ud}^2(m_s, m_y)$  between  $m_y = 0.03$  and  $0.04$  gives the squared physical kaon mass. Here  $m_{ud}^2(m_s, m_y)$  was obtained from the unitary extrapolation in the light quark mass to  $m_{ud}$  using shifted LECs. The shifted LECs are found by starting from their values at the dynamical heavy quark mass used in the simulation and changing to their values at the new value of  $m_s$  (at fixed  $m_y$ ). By this method, we observe a 2% shift in  $\tilde{m}_s$  and less than 0.5% shift in  $f_K$ . Therefore, conservatively we will quote the systematic error from  $m_h \neq m_s$  to be 2% and 1% for  $\tilde{m}_s$  and  $f_K$ , respectively.

#### 4. Scaling errors

At present we only have data at a single value for the lattice spacing ( $a = 0.11$  fm) and so cannot perform a scaling study to extrapolate our results to the continuum limit. (We are currently generating an ensemble of configurations on a finer lattice and so will soon be able to study the discretization errors directly.) We therefore take our central values and assign to them a systematic

uncertainty of 4% due to the missing continuum extrapolation. The 4% is simply an estimate of  $(a\Lambda_{\text{QCD}})^2$  with our value of  $a^{-1} = 1.73 \text{ GeV}$ , but we stress that it is only when we will have results at more than one value of the lattice spacing that we will be able to quantify this error reliably.

Table XII contains the 4% estimate for scaling error for the measured quantities. Again, we did not calculate this uncertainty for the (phenomenologically uninteresting) LECs  $L_i^{(2)}$ , but only for  $\bar{l}_{3,4}$ . Here one has to keep in mind, that a relative error affects the universal low energy scales

$$\Lambda_{3,4} = \Lambda_\chi \cdot \exp\left(\frac{16\pi^2}{\gamma_{3,4}} l_{3,4}^r\right) = (139 \text{ MeV}) \cdot \exp(\bar{l}_{3,4}/2), \quad (114)$$

meaning that a 4% uncertainty translates into an *absolute* error of 0.08 for  $\bar{l}_{3,4}$ .

#### D. Comparison of our results with other recent determinations.

In this subsection we compare our results for the SU(2) LECs to those obtained in the continuum [63, 64] and in other lattice simulations with either  $N_f = 2 + 1$  [65, 66] or  $N_f = 2$  [67, 68] dynamical fermions. We also compare the values we obtain for the quark masses with those from other recent simulations [66, 69, 70, 71, 72, 73].

Our value for the decay constant in the SU(2) chiral limit,  $f = 114.8(4.1)_{\text{stat}}(8.1)_{\text{syst}}$  MeV, is consistent, within our uncertainties, with the phenomenological estimates of 122.3(0.5) [63] or 121.9(0.7) [74]. For the ratio  $f_\pi/f$  we obtain 1.080(08) (with only the statistical error quoted, since the numerator and denominator are likely to be highly correlated), which agrees very well with the phenomenological results 1.069(04) [63] and 1.072(07) [74]. Previous lattice simulations give, e.g., 1.052(2)  $^{(+6)}_{(-3)}$  [66] or 1.075 [68] for the ratio and for  $f$  the results read  $f = 124.2 \text{ MeV}$  [66] and 121.6 MeV [68], respectively, where in Ref. [68] no estimate of the error was provided.

From MILC's results for  $f$  and the chiral condensate,  $(\Sigma^{\overline{\text{MS}}}(2 \text{ GeV}))^{1/3} = 278(1)_{\text{stat}}(5)_{\text{ren}}^{(+2)}_{(-3)}_{\text{syst}}$  MeV [66] (compare to 255(8)  $_{\text{stat}}(8)_{\text{ren}}(13)_{\text{syst}}$  MeV obtained in this paper), one can via  $\Sigma = f^2 B/2$  deduce their result for the LO-LEC  $B^{\overline{\text{MS}}}(2 \text{ GeV}) = 2.79 \text{ GeV}$  (no estimate for the error). Comparing this number with our value of 2.52(.11)  $_{\text{stat}}(.23)_{\text{ren}}(.12)_{\text{syst}}$  GeV shows approximately the same relative deviation as  $f$  for the decay constant in the chiral limit,  $f$ .

In Table XV we compare the values for the NLO LECs  $\bar{l}_{3,4}$  (we also include the values obtained by converting the SU(3) LECs, see Sec. VII C). Within the quoted uncertainties all these numbers agree, except the result for  $\bar{l}_3$  as quoted in [75], which used the MILC SU(3)-LECs as input obtained from a ‘‘NLO plus analytic NNLO and beyond’’ fit. A recent update of the MILC results



finds a more consistent value for  $\bar{l}_3$  obtained from a pure NLO fit. The two results in the table for  $\bar{l}_4$  from the CERN Collaboration, where one was obtained by including NNLO analytic terms, not only agree with our result for the central value, but also suggest a comparable magnitude for the systematic error (as estimated from the difference between the NLO and partial NNLO fits).

Quark masses are computed in lattice simulations using a variety of actions. We end this section by making the observation that results obtained using non-perturbative renormalization (such as those in this paper) appear to be generally higher than those obtained by renormalizing the mass perturbatively (mostly using 2-loops). Whether or not this is significant or merely a coincidence is still to be investigated. We illustrate this point by tabulating recent results obtained using non-perturbative renormalization [69, 70, 71] and perturbative renormalization [66, 72, 73] in Table XVI. Note that for the simulations in this table, both different fermion actions and different numbers of dynamical fermions were used. The ratios  $m_s/m_{ud}$  are also tabulated and agree better across the different computations.

## VII. FITTING MASSES AND DECAY CONSTANTS TO NLO SU(3) CHPT

In the previous section, we have fit our lattice data to NLO SU(2) ChPT formulae and found good agreement. Additionally, for quark masses where we have data, we find that for  $m_{ll}^2$ , the NLO terms are at most a 10% correction, while for  $f_{ll}$  they are less than 30%, as shown in Fig. 14. Our estimates for NNLO effects in this range are appropriately small,  $< 5\%$ , leading to the conclusion that SU(2) ChPT converges reasonably well here. This implies that our range of light quark masses is small enough that NLO SU(2) ChPT provides more than just a useful, smooth phenomenological function to fit our data to, rather it represents the theoretically correct description of our data.

We now turn to fitting our data to SU(3) ChPT, with the following two points in mind: 1) we want to determine how well our data is fit by the NLO SU(3) ChPT formulae and 2) if the fits agree with our data, how convincing is the convergence of the (now known) SU(3) ChPT series for the quark masses where we have data. We will see that the answer to the first point is *yes*, if we only include observables involving light quarks, and is *no* for observables including the strange quark. For the second point, even in the light quark case, we find the convergence of the series to be poor.

### A. $SU(3) \times SU(3)$ Chiral Fits

At NLO, the 2+1 flavor, partially quenched chiral formulae [46] for the squared masses,  $m_{xy}^2$ , and decay constants,  $f_{xy}$ , of the light pseudoscalar mesons composed of two non-degenerate quarks with masses  $m_x$  and  $m_y$  involve six unknown low energy constants (LECs), which we denote as  $B_0$ ,  $f_0$  and  $L_{4,5,6,8}^{(3)}$ . (The complete formulae used in our chiral fits are summarized in Appendix B 1.) As  $f_{xy}$  and  $m_{xy}^2$  share the unknown low energy constants  $B_0$  and  $f_0$ , we performed combined fits to both of them, using the two ensembles with dynamical light quark masses of  $m_l = 0.005$  and  $0.01$ . A reasonable  $\chi^2/\text{d.o.f.}$  of 0.7 (uncorrelated) could only be achieved by imposing a cut in the average valence quark mass of  $m_{\text{avg}} \equiv (m_x + m_y)/2 \leq 0.01$ , corresponding to partially quenched pion masses in the range of about 250 MeV to 420 MeV. The chiral fits with such a cut are shown in Fig. 15, and the fit parameters are given in Table XVII, where, for convenience, we quote the scale-dependent LECs at two commonly used chiral scales of  $\Lambda_\chi = 770$  MeV and 1 GeV. Only statistical errors are quoted in this table, as discussed in more detail below. In these fits, the valence quark masses are all in a region where NLO  $SU(3)$  ChPT might be expected to be reasonably reliable (corresponding to masses below 420 MeV for pseudoscalar mesons made of such valence quarks), but we point out that the dynamical heavy quark mass, which is approximately 15% higher than the physical strange quark mass, lies outside of our fit region ( $m_{\text{avg}} \leq 0.01$ ). Even the combination of our lightest valence quark mass of 0.001 with the dynamical heavy quark mass leads to a pseudoscalar mass of  $\approx 554$  MeV.

Extending the fit range to valence quarks satisfying  $m_{\text{avg}} \equiv (m_x + m_y)/2 \leq 0.03$ , or a partially quenched valence pseudoscalar mass of up to 660 MeV, we find that the fit curves miss almost all of the data points, resulting in a poor  $\chi^2/\text{d.o.f.}$  of 5.7. This is shown in Fig.16. Similar behavior is seen for a lower mass cut of  $m_{\text{avg}} \equiv (m_x + m_y)/2 \leq 0.02$ , which allows the largest valence pseudoscalar masses to be just above the kaon mass, and gives an uncorrelated  $\chi^2/\text{d.o.f.}$  of about 3. From these fits, we conclude that we cannot use  $SU(3)$  ChPT at NLO to obtain physical results for kaon observables, such as  $f_K$  or the physical strange quark mass from  $m_K$ , with well-controlled interpolation or extrapolation errors. For these important quantities, we have used kaon  $SU(2)$  ChPT as described in previous sections.

## B. Systematic Errors

For the SU(3) PQChPT results, we have to consider the same sources of systematic uncertainties (chiral extrapolation errors, finite volume effects and scaling errors) as in the SU(2) case, except that, in principle, the SU(3) approach allows one to directly extrapolate the dynamical heavy quark mass to the value of the physical strange quark mass.

For the chiral extrapolations, we first investigate the systematic error from the convergence of NLO ChPT. We have already seen that we cannot use NLO SU(3) ChPT for valence quarks near the physical strange quark mass, since the fits do not agree well with our data. Focusing on the results from fits to the light quark region ( $m_{\text{avg}} \equiv (m_x + m_y)/2 \leq 0.01$ ), where our data is well represented by the NLO formula, in Fig. 17 we plot the LO and NLO contributions to the pseudoscalar decay constant  $f_{ll}$  in the unitary case. The values of  $f_{ll}$  are plotted as functions of the light quark mass parameter ( $\chi_l \propto \tilde{m}_l$ ) and the heavy quark mass parameter ( $\chi_h \propto \tilde{m}_h$ ) using our results from the SU(3) fit with the mass cut  $m_{\text{avg}} \leq 0.01$ . We see that the corrections are generally large, even for relatively small light-quark masses. For example, the top left-hand panel shows that for  $m_h = 0.04$  and for pseudoscalar masses in the 250–400MeV range, i.e. in the region where we have data, the NLO correction is as large as 70% of the LO term.

In the preceding paragraph we found that, for the unitary case with  $m_\pi \approx 400$  MeV, the SU(3) ChPT expansion for the decay constant is approximately of the form  $f_0(1 + 0.7 + O(p^4))$ , which leads one to expect the  $O(p^4)$  term to be about  $(0.7)^2 \approx 0.5$ . This would be a 30% correction to the sum of LO plus NLO terms. However, the NLO fits agree with our data quite well, certainly excluding corrections beyond the few percent level. From this we conclude that the agreement between our data and the SU(3) ChPT formula is not indicative of NLO SU(3) ChPT working well for these quark masses, since this would imply anomalously small  $O(p^4)$  corrections. It seems that the SU(3) ChPT formula are serving as smooth fitting functions with sufficient flexibility in the parameters to absorb the effects of higher order terms and to match our data. We would need more data to investigate this hypothesis fully and, in particular, this data should come from ensembles with more than the single  $m_h$  we currently have. This will be done in the future and if our hypothesis is correct then, as discussed in the following section, part of the reason for the small value of  $f_0$  is due to the fact that it absorbs some of the NNLO corrections. We now briefly discuss our limited attempts to use our current data to obtain additional information but stress that a complete analysis of the range of validity and precision of SU(3) ChPT will have to wait until

we have data at more values of quark masses.

One can also try to extend the range of validity of  $\chi$ PT by going from NLO to NNLO. The complete continuum NNLO formulae are available in the literature [76] and we have done some preliminary fits of our data, augmented with results from an ensemble with  $m_l = 0.02$  [77], to these formulae. Many more LECs are needed at NNLO ( $L_i^{(3)}$  for  $i = 0$  to 9 and 12 linear combinations of  $K_i$ ) and it is not currently clear how stable such fits will be. We defer a discussion of these fits pending completion of the ongoing analysis.

To further probe the convergence of the series, we have dropped the additional logarithm terms that appear at NNLO and fitted to the analytic terms, as we did for our SU(2) fits in Section VI A. The analytic terms for the meson masses and decay constants for SU(3) are

$$(\chi_x + \chi_y)^2, (\chi_x - \chi_y)^2, (\chi_x + \chi_y)\bar{\chi}, \bar{\chi}^2, \overline{\chi^2} = (2\chi_l^2 + \chi_s^2)/3. \quad (115)$$

With our present data, limited to a single value of  $\chi_h$  and to a small set of  $\chi_l$ 's, we were not able to include the last two terms in our NNLO phenomenological fits. The fits led, *e.g.*, to an approximate 10% increase in the value of  $f_0$  (for this particular case a fit range of  $m_{\text{avg}} \leq 0.01$  has been used) and to even more significant changes in some of the NLO LECs. This supports our conjecture that SU(3) ChPT shows a slow convergence and NNLO terms are indeed important. On the other hand, since NNLO-terms are not negligible, taking into account only (some of) the analytic NNLO terms and neglecting the logarithmic terms is not sufficient to determine the chiral behaviour of observables quantitatively. It is for this reason that we choose to use SU(2) ChPT to determine our physical results and at this time we do not quote any estimates for systematic errors for quantities from our fits with SU(3) ChPT.

In spite of our reservations about the convergence of SU(3) ChPT, we have used the corresponding formulae in finite volumes to estimate finite volume effects (see Appendix C), as we had done previously for the SU(2) case. We find similar results for the correction factors. Table XIII also contains the corrections obtained in the SU(3) case for the unitary pions; for more details see the discussion in Sec. VI C 2.

### C. Comparing SU(3) $\times$ SU(3) and SU(2) $\times$ SU(2) Chiral Fits

In this section, we compare the results of our SU(3) ChPT fits with other results and also compare them with the results of our SU(2) fits. This serves to further probe the behavior of ChPT in the

region of quark masses we are studying. We stress however, that we believe that the convergence of the SU(3) series is relatively poor and therefore at this stage any quantitative conclusions will be limited.

To compare the SU(3) fit results with the previous ones obtained in SU(2) PQChPT (Sec. VI A), we use Eqs. (B40)–(B43) (cf. also [13, 26]) to match the three flavor ChPT to the two flavor case at NLO. The results for  $B_0$ ,  $f_0$  and the low energy constants  $\bar{l}_{3,4}$  (for a definition of the latter see Eq. (B44) and [13]) are shown in Table XVIII. Indeed, having a fixed dynamical heavy quark mass in the SU(3)  $\times$  SU(3) theory is equivalent to the SU(2)  $\times$  SU(2) theory, up to terms of  $O((m_l/m_s)^2)$ . The remarkable agreement between the LECs obtained directly from the fit to the chiral behaviour using SU(2) ChPT and those obtained by converting the SU(3) LECs using Eqs. (B40)–(B43) (see Table XVIII) is evidence that these terms of  $O((m_l/m_s)^2)$  are small. Although reassuring, we stress that this in itself is insufficient to demonstrate fully the validity of the SU(3) ChPT at NLO. For example, if the  $m_s^2$  term in the expansion for the decay constant were large, this would appear in our NLO fits as a shift in  $f_0$  but the behaviour with  $m_l$  would be equivalent to that in SU(2) ChPT (up to corrections of  $O((m_l/m_s)^2)$  of course). We suspect that this is the case and use SU(2) ChPT to obtain physical results nevertheless, for the remainder of this section, we take our SU(3) results at face value and compare them to previous determinations of the LECs.

We first consider the ratio of the decay constants in the two and three flavor chiral limit. From our fits to SU(2) and SU(3) ChPT we obtain  $f/f_0 = 1.229(59)$  (here we quote only the statistical error), showing the influence of the strange quark loops. An important observation is that the value of  $f_0$ , the pion decay constant in the SU(3) chiral limit, is much smaller than the measured pseudoscalar decay constant  $f_{ll}$  at, say,  $m_l = 0.01$  and also much smaller than  $f_\pi$ . This is due to the large NLO correction shown in Fig. 17. The small value of  $f_0$  may be a contributor to poor convergence, since the chiral logarithms come in with a factor of  $1/f_0^2$ . Of course, one can rearrange the series and expand in  $m_{xy}^2/f_\pi^2$  consistently to NLO and possibly improve the convergence. We are exploring these options, but if such a rearrangement, which only effects the series at NNLO, markedly changes the convergence properties, one is still lead to the conclusion that the series is not well controlled.

If we compare our result for  $f_0$  to phenomenological estimates by Bijnens [78], our value of  $f_0 = 93.5(7.3)\text{MeV}$  (statistical error only) turns out to be substantially lower than the preferred value from Bijnens, which is 124.0 MeV (NNLO, alternative fits also published there give values of

114.7 (NLO), 99.6 (NNLO), and 113.7 (NNLO) MeV). His ratio  $f_\pi/f_0$  is also different from ours (in contrast to the SU(2) case, where for the ratio  $f_\pi/f$  a better agreement has been achieved): we obtain a value of 1.33(07) (statistical error only), whereas Bijmens' preferred fit suggests  $f_\pi/f_0 = 1.05$ . Interestingly, the  $N_f = 2 + 1$  lattice simulation by MILC [65, 66] also observed a higher ratio of  $f_\pi/f_0 = 1.21(5)^{(+13)}_{(-3)}$ , which translates into a central value for  $f_0 = 106.0$  MeV (using their value for  $f_\pi = 128.3(0.5)^{(+2.4)}_{(-3.5)}$ , we do not quote an error for this number, since we do not know the correlation between  $f_\pi$  and  $f_\pi/f_0$ .)

For the ratio  $B/B_0$  we obtain  $B/B_0 = 1.03(05)$ . The very small deviation from 1 is perhaps surprising, and indicates good agreement with the predictions of the large  $N_c$  approximation and only small Zweig rule violations in this case. A comparison of the LO-LEC  $B_0$  is not directly possible, since this number depends on the renormalization scheme (see Sec. VI B 2). Instead, Bijmens quotes a number for the renormalization scheme independent and dimensionless ratio  $2B_0 m_{ud}/m_\pi^2$  of 0.736 (from the preferred NNLO-fit; alternative fits give: 0.991 (NLO), 1.129 (NNLO), 0.958 (NNLO)). From our SU(3) fit we obtain 0.995(41) (statistical error only), which agrees better with the alternative phenomenological fits than the preferred one.

The ratio of  $\Sigma = f^2 B/2$ , the chiral condensate in the two-flavor theory, and  $\Sigma_0 = f_0^2 B_0/2$  in the three-flavor theory, can also be compared directly. We obtain  $\Sigma/\Sigma_0 = 1.55(21)$ , whereas MILC quotes a value of  $1.52(17)^{(+38)}_{(-15)}$ . It should be noted however, that we obtain slightly different values for  $f/f_0$  and for  $B/B_0$  than the MILC collaboration.

In Table XIX we compare the NLO-LECs to phenomenological NLO and NNLO fits [78] and the results of MILC's  $N_f = 2 + 1$  dynamical lattice simulations [65, 66] (all LECs in that table are quoted at the scale  $\Lambda_\chi = 770$  MeV). In the fits by Bijmens,  $L_4^{(3)}$  and  $L_6^{(3)}$  were set to zero (at  $\Lambda_\chi = 770$  MeV  $\approx m_\rho$ ) as motivated by Zweig-rule and large  $N_c$  arguments. Whereas for the latter our result agrees with this assumption within the statistical uncertainty, for  $L_4^{(3)}$  we observe some discrepancy (without taking systematic errors into account). Interestingly, our NLO results for  $L_5^{(3)}$  and  $L_8^{(3)}$  agree very well with Bijmens' numbers from the NNLO fit, but not for his NLO fit (for which no systematic error is given however). Within the reported uncertainties, our NLO LECs agree nicely with the set of values quoted by the MILC Collaboration.

In Fig. 18 we summarize some of the results presented in this section. Here we plot our measured values for the decay constant, converted to physical units, versus the degenerate valence pseudoscalar mass squared, along with the results of fits to SU(2) and SU(3) ChPT. The data for degenerate quarks is denoted by filled symbols and for non-degenerate quarks, open symbols are

used. The graph shows that we see small effects for non-degenerate quarks. The results of SU(2) and SU(3) partially quenched ChPT fits to our data are shown, and both fits agree well with the data. From the (now determined) fit functions, we plot the unitary SU(2) chiral extrapolation. Two of our data points lie on this curve, but one sees that our measured decay constant for a pseudoscalar mass of 420 MeV is about 30% above the chiral limit value,  $f$ . We also plot the SU(3) chiral limit curve. For this curve, the horizontal axis is the unitary meson mass in the theory where all quarks are degenerate. Therefore, none of our measured values must lie on this line. Figure 18 shows graphically the large difference between  $f_0$  and our measurements. This is graphical evidence of the poor convergence of NLO SU(3) ChPT, with LECs as determined from our data. In summary, we have found that we can fit our data well using NLO SU(3) ChPT for average valence quark masses  $< 0.01$ , corresponding to pseudoscalar masses below 420 MeV. The SU(3) LECs we determine are generally in reasonable agreement with continuum phenomenology and other lattice results (note however, the small value of  $f_0$  which we find). We see that the LECs from our SU(3) and SU(2) fits agree well when a conversion is performed from SU(3) to SU(2). However, since we find large corrections at NLO we would expect significant ones also at NNLO. We are therefore not at all confident that the systematic errors in the SU(3) LECs are currently under control. In addition, the fits do not agree with our data when we extend the NLO SU(3) ChPT theory to the kaon mass scale. It is possible that with more data it will become feasible to perform NNLO SU(3) fits and to control the systematic uncertainties with sufficient precision. We will investigate this in the future but we stress that whether or not this proves to be the case, we can happily use SU(2) PQChPT to obtain predictions for physical results (including quantities in kaon physics as explained in section II B). This is what we do in this paper.

## VIII. $B_K$

### A. Pseudoscalar Bag Parameter on the Lattice

The kaon bag parameter is defined as the ratio of the neutral kaon mixing matrix element and its expectation value from the vacuum saturation approach,

$$B_K = \frac{\langle \bar{K}^0 | \mathcal{O}_{LL}^{\Delta S=2} | K^0 \rangle}{\frac{8}{3} f_K^2 m_K^2}, \quad (116)$$

where  $m_K$  is the neutral kaon mass,  $f_K$  the kaon decay constant, and

$$\mathcal{O}_{LL}^{\Delta S=2} = \left( \bar{s}(1 - \gamma_5)\gamma_\mu d \right) \left( \bar{s}(1 - \gamma_5)\gamma_\mu d \right) \quad (117)$$

is the local, effective four quark operator, which couples to the left-handed quarks and induces a change in strangeness by  $\Delta S = 2$ . In our simulations, we define the corresponding pseudoscalar bag parameter for a meson made from either valence or sea quarks with masses  $m_x$  and  $m_y$ , which we measure by fitting the ratio

$$B_{xy}(t) = \frac{3}{8} \frac{\mathcal{C}_{P\mathcal{O}P}^{WLW}(t_{\text{src}}, t, t_{\text{snk}})}{\mathcal{C}_{PA}^{WL}(t_{\text{src}}, t) \mathcal{C}_{AP}^{LW}(t, t_{\text{snk}})} \quad (118)$$

to a constant  $B_{xy}$  over some range in time  $t$ . Here,  $t$  denotes the time coordinate at which we insert the four quark operator,  $t_{\text{src}}$  and  $t_{\text{snk}}$  are the temporal coordinates at which we insert Coulomb gauge fixed (spatial) walls of anti-kaon and kaon interpolating operators, respectively. The correlators using wall source and local sinks, which we construct from the WL-propagators obtained with quark masses  $m_x$  and  $m_y$ , are defined as

$$\mathcal{C}_{P\mathcal{O}P}^{WLW}(t_{\text{src}}, t, t_{\text{snk}}) = \frac{1}{V} \sum_{y \in V} \langle q_w(t_{\text{src}}) P \bar{q}_w(t_{\text{src}}) \mathcal{O}_{LL}^{\Delta S=2}(y, t) q_w(t_{\text{snk}}) P \bar{q}_w(t_{\text{snk}}) \rangle, \quad (119)$$

$$\mathcal{C}_{PA}^{WL}(t_{\text{src}}, t) = \frac{1}{V} \sum_{y \in V} \langle q_w(t_{\text{src}}) P \bar{q}_w(t_{\text{src}}) q(y, t) A \bar{q}(y, t) \rangle, \quad (120)$$

$$\mathcal{C}_{AP}^{LW}(t, t_{\text{snk}}) = \frac{1}{V} \sum_{y \in V} \langle q(y, t) A \bar{q}(y, t) q_w(t_{\text{snk}}) P \bar{q}_w(t_{\text{snk}}) \rangle, \quad (121)$$

where  $q_w(t)$  and  $q(y, t)$  denote a Coulomb gauge fixed (spatial) wall smeared quark field and a local quark field, respectively. A summation over all spatial points for the local operators is performed, and a balancing volume factor  $V = L^3$  included giving a spatial volume average that is statistically efficient. In addition, we average over propagators obtained with periodic and anti-periodic boundary conditions in the time direction, which results in a doubled time extent available for the plateau fit.

The values measured on the  $24^3 \times 64$ ,  $L_s = 16$  lattices are given in Table XX. There, the fit to the plateau was performed over the range  $t \in [12, 52]$  using an uncorrelated fit, since, due to the large time extent, correlated fits became unstable. Previously, our collaboration also obtained the pseudoscalar bag parameter on smaller  $16^3 \times 32$ ,  $L_s = 16$  lattices with dynamical light quark masses  $m_l \in \{0.01, 0.02, 0.03\}$  and  $m_s = 0.04$  at the same gauge coupling [19, 34, 79, 80]. For comparison we quote those values in Table XXI. In this case the plateau was fitted over a range  $t \in [12, 22]$ .



We will have to extrapolate our measured values to the physical light and strange quark masses for which PQChPT in the  $SU(2) \times SU(2)$  formulation will be used. These fits are discussed in the next part of this section; the result obtained for  $B_K$  was already published in [19], but here we provide some more details on the chiral fitting procedure. In the remainder of this section, we employ  $SU(3) \times SU(3)$  PQChPT to extract the bag parameter in the chiral limit and briefly discuss the data from the  $16^3$  lattices.

### B. $SU(2) \times SU(2)$ Chiral Fitting Procedure

For the chiral extrapolation of  $B_K$ , we use  $SU(2) \times SU(2)$  ChPT for the kaon sector, as introduced in Sec. II and applied to the kaon masses and decay constants in Sec. VI A. Specifically we use Eq. (B48) to extrapolate to the physical average light quark mass  $m_{ud}$  determined in Sec. VI B 1. Here we consider the data from the  $24^3$  lattices at values of  $m_y = 0.03$  and  $0.04$  for the heavier quark mass approximating the strange quark mass. Of these two values only the latter describes a truly unquenched quark and we account for possible effects of a partially quenched strange quark treatment in our discussion of systematic errors. The fits using  $SU(2) \times SU(2)$  ChPT for the kaon sector are shown in Fig. 19, whereas the fitted parameters are given in Table XXII. The parameters  $B$  and  $f$  have been fixed to their values obtained in the combined  $SU(2) \times SU(2)$  ChPT fits for the pseudoscalar masses and decay constants, cf. Sec. VI. We applied a cut in the light valence quark mass of  $m_x \leq 0.01$ . The low energy constant  $b_1(m_y)$  multiplying the dynamical light quark mass in Eq. (B48) shows almost no dependence on the heavy quark mass, whereas  $b_2(m_y)$  and  $B_{\text{PS}}^{(K)}(m_y)$  vary by 12% and 4%, respectively, when going from  $m_y = 0.03$  to  $0.04$ . Also the value of the kaon bag parameter extrapolated to the physical average light quark mass,  $B_{udy}$ , increases by approximately 4% due to this change in  $m_y$ .

The interpolation to the physical value of the strange quark mass (obtained from the kaon mass, cf. Sec. VI B 1) is done linearly as shown in Fig. 20. Included in the plot (and also in Table XXII) is a point at  $m_y = 0.02$  for information only. It was not included in the linear fit and interpolation because this supposedly heavy quark mass is likely too light to be sufficiently separated from the simulated light quark masses to enable convergent effective treatment. However, the linear interpolation does not seem to deviate much even at this point, giving us confidence that non-linear effects in the strange quark mass region at least do not show up at the level of the numerical precision achieved. Finally, we quote for the unrenormalized physical value of the kaon bag

parameter  $B_K^{\text{lat}} = 0.565(10)$ . We will now discuss the renormalization of  $\mathcal{O}_{LL}^{\Delta S=2}$  and estimate all significant contributions to the systematic error.

### 1. Renormalization

The renormalization of  $\mathcal{O}_{LL}^{\Delta S=2}$  has been treated in [21] using the RI-MOM non-perturbative renormalization technique. Couplings to wrong chirality four quark operators are in principle admitted by the presence of a non-zero residual mass. It has been demonstrated in that paper that they are highly suppressed and small, using non-exceptional momenta to remove the spontaneous chiral symmetry breaking effects that might obscure this fact at the modest, accessible lattice momenta. Thus we only need to consider a simple, multiplicative renormalization. Here we quote the renormalization factors for the regularization independent (RI) and the modified minimal subtraction ( $\overline{\text{MS}}$ ) schemes both at  $\mu = 2 \text{ GeV}$  as well as the renormalization group invariant (RGI) result:

$$Z_{B_K}^{\text{RI}}(2 \text{ GeV}) = 0.910(05)_{\text{stat}}(13)_{\text{syst}}, \quad B_K^{\text{RI}}(2 \text{ GeV}) = 0.514(10)_{\text{stat}}(07)_{\text{ren}}, \quad (122)$$

$$Z_{B_K}^{\overline{\text{MS}}}(2 \text{ GeV}) = 0.928(05)_{\text{stat}}(23)_{\text{syst}}, \quad B_K^{\overline{\text{MS}}}(2 \text{ GeV}) = 0.524(10)_{\text{stat}}(13)_{\text{ren}}, \quad (123)$$

$$Z_{B_K}^{\text{RGI}} = 1.275(10)_{\text{stat}}(25)_{\text{syst}}, \quad \hat{B}_K = 0.720(13)_{\text{stat}}(14)_{\text{ren}}, \quad (124)$$

where the first error is the (combined) statistical error and the second error the systematic error from the renormalization.

### 2. Systematic Errors

*a. Finite Volume Effects* The spatial volume in our simulation is approximately  $(2.7 \text{ fm})^3$ , therefore, from [81] it follows that the difference between the  $B_{xy}$  measured on the finite lattice volume and the result in infinite volume is negligible for all points except the lightest ones (both valence quarks at a mass of 0.001), where the difference may be as large as 2%. Excluding the point  $m_l = 0.01$ ,  $m_x = m_y = 0.001$  from the fit, the final result for  $B_K^{\text{lat}}$  remains almost unchanged. Comparing points with  $m_l = 0.01$  from the smaller volume simulation ( $16^3$  lattice,  $\approx (1.8 \text{ fm})^3$  spatial volume) from Table XXI with the corresponding ones from the  $24^3$  simulation (Table XX), statistically marginal differences of up to 1% are observed, see Sec. VIII D for a more detailed discussion. Conservatively, we adopt this as an estimate for finite volume effects affecting our final number for  $B_K$ . (Note, that for the lightest point in the  $16^3$  ensemble ( $m_x = m_y = m_l$ ) we

have  $m_\pi L \approx 4.0$ , whereas for our lightest valence pion in both  $24^3$  ensembles ( $m_x = m_y = 0.001$ ,  $m_l = 0.005$  or  $0.01$ ) we still have  $m_\pi L \approx 3.4$ , so it is reasonable to assume the finite volume effects in those points to be comparable to the observed effect from comparing  $16^3$  and  $24^3$  lattices.)

*b. Scaling Effects* Having only data at a single value for the lattice spacing does not allow to quantify the scaling effects affecting our data. The CP-PACS Collaboration calculated  $B_K$  in a quenched calculation using the Iwasaki gauge action with Domain Wall valence quarks at two different lattice scales, namely  $1/a = 1.81(4)$  and  $2.81(6)$  GeV (determined from the  $\rho$ -meson mass) keeping the physical volume approximately fixed [82]. Extrapolating their observed scaling violation to our coarser lattice spacing, we would expect a 3.5% scaling effect. We assume a 4% systematic error, which is in agreement with the scaling violations discussed in conjunction with the meson masses and decay constants in Sec. VIC 4.

*c. Interpolation to the Physical Strange Quark Mass* Currently only ensembles with a fixed value for the dynamical heavy quark mass are available. We estimate the effect of this 15% too high sea quark mass from the measurements done at the  $16^3$  lattices. There dynamical light quark masses of  $m_l = 0.02$  and  $0.03$  have been simulated, which are closer to the physical value of the strange quark mass than the dynamical light quark masses available from the  $24^3$  data. Comparing  $B_{xy}$  for  $m_x = 0.01$ ,  $m_y = 0.04$  (lightest valence quark mass and dynamical strange quark mass) at the two aforementioned light sea quark masses, an increase of 3% is observed (Table XXI). In that case, *two* dynamical quark flavors were changed by  $\Delta m = 0.01$ , whereas the *single* strange quark mass only has to be changed by  $0.0057$ . Accordingly, the systematic error has to be scaled down by 2 (from number of flavors) times  $\approx 1.8$  (from scaling  $\Delta m$ ), resulting in an 1% effect. (This is an exclusive sea quark effect and should not be confused with the 4% difference discussed above, when changing the valence  $m_y$  from  $0.03$  to  $0.04$  in the kaon itself.)

*d. Extrapolation in the Light Quark Mass* Including terms up to NLO in our chiral fit functions, we have to assign a systematic error to our extrapolation resulting from neglecting NNLO and higher order terms. The linear fit to the  $16^3$  data gives a 6% higher value for  $B_K$ , see Sec. VIII D. Assigning this difference to the (here included) NLO terms, the size of NNLO contribution can be estimated to be 2% by scaling the observed 6% difference by  $\tilde{m}_l/\tilde{m}_s \approx 0.4$  taken at the lightest value for quark mass in the linear fit,  $m_l = 0.01$ , and the strange quark mass at the physical point  $m_s$ .

### 3. Final Result

Combining the 1% finite volume, 4% scaling, 1% heavy quark mass interpolation, and 2% ChPT extrapolation systematic errors with the one from the NPR (except for  $B_K^{\text{lat}}$ , of course), our final result in the different renormalization schemes considered reads:

$$B_K^{\text{lat}} = 0.565(10)_{\text{stat}}(27)_{\text{syst}}, \quad (125)$$

$$B_K^{\text{RI}}(2 \text{ GeV}) = 0.514(10)_{\text{stat}}(07)_{\text{ren}}(24)_{\text{syst}} = 0.514(10)_{\text{stat}}(25)_{\text{comb}}, \quad (126)$$

$$B_K^{\overline{\text{MS}}}(2 \text{ GeV}) = 0.524(10)_{\text{stat}}(13)_{\text{ren}}(25)_{\text{syst}} = 0.524(10)_{\text{stat}}(28)_{\text{comb}}, \quad (127)$$

$$\hat{B}_K = 0.720(13)_{\text{stat}}(14)_{\text{ren}}(34)_{\text{syst}} = 0.720(13)_{\text{stat}}(37)_{\text{comb}}, \quad (128)$$

where “stat” denotes the statistical error, “syst” the systematic error as discussed above and “ren” the error due to renormalization, “comb” is the combined systematic error from the latter two.

#### C. Fits to $SU(3) \times SU(3)$ PQChPT

Here we apply Eq. (B22) from  $SU(3) \times SU(3)$  PQChPT to fit our data. That means, we now also try to describe the dependence on the heavier (valence) quark mass by (PQ)ChPT. As discussed in Sec. II B 5, if Eq. (B22) were applied for a fixed value of the heavier valence quark mass (also fixing the heavy sea quark mass), it would naturally revert to the kaon  $SU(2) \times SU(2)$  form. If we were able to describe the valence mass dependence with the  $SU(3) \times SU(3)$  PQChPT form up to the strange quark mass, this form would be applicable to a determination of  $B_K^{\text{lat}}$ . However, it is also possible that this form can be used to describe only light valence masses  $m_x, m_y$  to obtain the  $SU(3) \times SU(3)$  low energy constant  $B_{\text{PS}}^Z$  representing the pseudoscalar bag parameter in the three flavor theory in the limit of all three masses being zero, which is of phenomenological interest [83]. The only remnant terms involving a large mass in such a fit of the  $SU(3) \times SU(3)$  PQChPT arise from the fixed dynamical heavy quark mass  $m_h$ , and we will estimate a systematic error from this.

We observe the same behaviour as for the meson masses and decay constants: a reliable fit including quark masses up to the strange quark mass is not possible with only terms of NLO included in the fit formula. In Fig. 21 fits to the  $24^3$  data are shown with two different ranges for the mass cut  $m_{\text{avg}}$ . While the fit with  $m_{\text{avg}} \leq 0.01$  describes the data inside the fit range but badly fails at the heavier points, going to  $m_{\text{avg}} \leq 0.02$  already fails to describe the data at the lowest masses.

The fitted parameters are given in Table XXIII. Here we fixed  $B_0$  to its value obtained from the  $SU(3) \times SU(3)$  fit for the meson masses and decay constants ( $m_{\text{avg}} \leq 0.01$ ), cf. Sec. VII. Due to the failure to describe the data with one quark mass as heavy as the strange quark, a determination of  $B_K^{\text{lat}}$  is not meaningful using this ansatz. However, limiting the fit range to small masses, we will estimate the  $SU(3) \times SU(3)$  LEC  $B_{\text{PS}}^\chi$ . In Fig. 22 the dependence of  $B_{\text{PS}}^\chi$  on the applied mass cut is shown. From that we conclude that at least within the statistical error the result is stable, therefore we quote (from a fit using  $m_{\text{avg}} \leq 0.01$ ):

$$B_{\text{PS}}^{\chi\text{lat}} = 0.266(26)_{\text{stat}}, \quad (129)$$

$$B_{\text{PS}}^{\chi\text{RI}}(2\text{ GeV}) = 0.242(24)_{\text{stat}}(03)_{\text{ren}}, \quad (130)$$

$$B_{\text{PS}}^{\chi\overline{\text{MS}}}(2\text{ GeV}) = 0.247(24)_{\text{stat}}(06)_{\text{ren}}, \quad (131)$$

$$\hat{B}_{\text{PS}}^\chi = 0.339(33)_{\text{stat}}(07)_{\text{ren}}, \quad (132)$$

using the same renormalization factors as in Eqs. (122–124) (first error statistical, second error systematics from renormalization). One has to keep in mind that this result was obtained by extrapolating  $\tilde{m}_h$  from its value used in the simulation to zero (*i.e.*, extrapolating  $m_h \rightarrow -m_{\text{res}}$ ). Considering Eq. (B22) which was used to fit the data, one sees that—except for the analytic terms in  $I_{\text{disc}}$  where it enters via  $\chi_\eta$ —the heavy quark mass only enters via  $\tilde{\chi}$ , which multiplies the LEC  $d$ . By only using one dynamical heavy quark mass value, this LEC is exclusively determined by the dependence of  $B_{xy}$  on the light dynamical quark mass, a very mild dependence as can be seen by comparing the columns for  $m_l = 0.005$  and  $0.01$  in Table XX. Two problems might arise. Firstly, the slope with respect to variations of  $m_h$  may differ from the slope with respect to variations of  $m_l$  due to higher order corrections. Secondly, with our fit procedure we might not be able to reliably determine this parameter. We assign the full size of this NLO estimate of the contribution,

$$\left| B_{\text{PS}}^\chi \frac{\chi_h}{3(4\pi f_0)^2} d \right| = \left| B_{\text{PS}}^\chi \frac{2B_0 \tilde{m}_h}{48\pi^2 f_0^2} d \right| \quad (133)$$

to be the systematic error of our chiral extrapolation in the heavy quark mass, which is a 10% effect for the chosen cut-off,  $m_{\text{cut}} = 0.01$ . (Going to higher values in  $m_{\text{cut}}$  the contribution increases to as much as 28% for  $m_{\text{cut}} = 0.02$ .) The NLO-contribution of the extrapolation in the light quark mass, which should be well under control by our fit procedure, we get from the difference of linearly extrapolating the measured  $B_{xy}$  values at the dynamical points with  $m_l = m_x = m_y = 0.01$  and  $0.005$  to  $m_l = m_x = m_y = -m_{\text{res}}$  (*i.e.*  $\tilde{m}_l = \tilde{m}_x = \tilde{m}_y = 0$ ) and the chiral extrapolation to this point

( $m_h = 0.04$  is fixed in this procedure). By multiplying the resulting difference of

$$\Delta = B_{ll}^{\text{linear}}(\tilde{m}_l = 0, m_h = 0.04) - B_{ll}^{\chi\text{PT}}(\tilde{m}_l = 0, m_h = 0.04) \approx 0.154 \quad (134)$$

by  $\chi_l/(4\pi f_0)^2$ , we determine the uncertainty due to neglected NNLO contribution to be 8%.

For the systematic errors due to finite volume and scaling, the same applies as for the  $SU(2) \times SU(2)$  analysis of  $B_K$ , so we assume them to be 1% and 4%, respectively. Eventually, with the 10% strange and 8% NNLO light quark mass extrapolation, the 1% finite volume, 4% scaling and NPR systematic error, we obtain (first error statistical, second combined systematic error):

$$B_{\text{PS}}^{\chi\text{lat}} = 0.266(26)_{\text{stat}}(36)_{\text{comb}}, \quad (135)$$

$$B_{\text{PS}}^{\chi\text{RI}}(2\text{ GeV}) = 0.242(24)_{\text{stat}}(03)_{\text{ren}}(33)_{\text{syst}} = 0.242(24)_{\text{stat}}(33)_{\text{comb}}, \quad (136)$$

$$B_{\text{PS}}^{\chi\overline{\text{MS}}}(2\text{ GeV}) = 0.247(24)_{\text{stat}}(06)_{\text{ren}}(33)_{\text{syst}} = 0.247(24)_{\text{stat}}(34)_{\text{comb}}, \quad (137)$$

$$\hat{B}_{\text{PS}}^{\chi} = 0.339(33)_{\text{stat}}(07)_{\text{ren}}(46)_{\text{syst}} = 0.339(33)_{\text{stat}}(47)_{\text{comb}}. \quad (138)$$

Our final number for  $\hat{B}_{\text{PS}}^{\chi}$  is in agreement with the phenomenological estimates from (i) the large  $N_c$  approximation,  $\hat{B}_{\text{PS}}^{\chi} = 0.38 \pm 0.15$  [83] ( $\hat{B}_K^{\chi}$  in their notation), and (ii)  $\hat{B}_{\text{PS}}^{\chi} = 0.39 \pm 0.10$  [84] using the QCD-hadronic duality approach (which is close to the chiral limit value, see remark in [83]).

#### D. Results from Simulations on a Smaller Volume

As mentioned in the beginning of this section, our collaboration first performed a study of the pseudoscalar bag parameter at a smaller volume of  $(1.8\text{ fm})^3$  with higher dynamical masses  $m_l \in \{0.01, 0.02, 0.03\}$ , see Table XXI. It turned out, that these masses were not light enough to probe the regime of ChPT, as was revealed by comparing a simple linear fit in the light quark mass with a fit to (PQ)ChPT. The extrapolations from these fits gave similar results within the numerical uncertainty, suggesting that the chiral logarithms occurring in NLO were not represented correctly, or—in other words—the influence of the linear terms in the PQ $\chi$ PT formula was overestimated. Here, we just quote the result of extrapolating the three unitary points ( $m_x = m_l \in \{0.01, 0.02, 0.03\}$ ,  $m_y = m_h = 0.04$ ) by a linear fit to the light quark mass at the physical point  $m_{ud}$

$$B_{udh}^{16^3, \text{linear}}(m_h = 0.04) = 0.611(08), \quad (139)$$

which gives the value of the kaon bag parameter at a slightly too high strange quark mass. This has to be compared with  $B_{udy} = 0.5789(97)$  at  $m_y = 0.04$  from Table XXII, yielding a 6% difference between these two approaches. (More details on the fits to the  $16^3$  data have already been published in [80].)

Also this data enables us to check for possible finite volume effects. The spatial volume increases by a factor  $1.5^3 = 3.375$  when going to the  $24^3$  lattices. Fig. 23 shows a comparison of the measured  $B_{xy}$  values at  $m_l = 0.01$  for the two different volumes, revealing only small changes in the range of valence quark masses  $0.01 \leq m_x, m_y \leq 0.04$ , where data is available from both simulations, see also Table XXIV. The maximal deviation of 0.8% is observed for the lightest points  $(m_x, m_y) = (0.01, 0.02)$  and  $(0.02, 0.02)$  and decreases down to 0.4% for the heaviest point  $(0.04, 0.04)$ . (Accidentally,  $(0.01, 0.01)$  shows almost no, *i.e.*,  $\leq 0.1\%$  deviation in the central value.)

## IX. VECTOR MESON COUPLINGS

In this section we discuss the couplings of the light vector mesons  $V$  to vector and tensor currents. These couplings  $f_V$  and  $f_V^T$  are defined through the matrix elements:

$$\langle 0 | \bar{q}_2(0) \gamma^\mu q_1(0) | V(p; \lambda) \rangle = f_V m_V \varepsilon_\lambda^\mu \quad (140)$$

$$\langle 0 | \bar{q}_2(0) \sigma^{\mu\nu} q_1(0) | V(p; \lambda) \rangle = i f_V^T(\mu) (\varepsilon_\lambda^\mu p^\nu - \varepsilon_\lambda^\nu p^\mu), \quad (141)$$

where  $p$  and  $\lambda$  are the momentum and polarization state of the vector meson  $V(p; \lambda)$  and  $\varepsilon_\lambda$  is the corresponding polarization vector. The tensor bilinear operator  $\bar{q}_2 \sigma^{\mu\nu} q_1$  (and hence  $f_V^T(\mu)$ ) depends on the renormalization scheme and scale  $\mu$ . The final results will be quoted in the  $\overline{\text{MS}}$  scheme at  $\mu = 2 \text{ GeV}$ . We have presented preliminary results for the ratios  $f_V^T/f_V$  in Ref. [85].

### A. Experimental Determination of $f_V$

The decay constants  $f_V$  can be determined experimentally. For the charged  $\rho$  and  $K^*$  mesons, one can use  $\tau$  decays to deduce  $f_\rho$  and  $f_{K^*}$  as illustrated by the diagram in Fig. 24, where the curly line represents the  $W$ -boson. From the measured branching ratios one obtains the following values for the decay constants [86]:

$$\text{Br}(\tau^- \rightarrow \rho^- \nu_\tau) = (25.0 \pm 0.3)\% \Rightarrow f_{\rho^-} \simeq 208 \text{ MeV} \quad (142)$$

$$\text{Br}(\tau^- \rightarrow K^{*-} \nu_\tau) = (1.29 \pm 0.03)\% \Rightarrow f_{K^{*-}} \simeq 217 \text{ MeV}. \quad (143)$$

One can also determine  $f_{\rho^0}$  from the width of the decay of the  $\rho^0$  into  $e^+e^-$  which gives  $f_{\rho^0} = 216(5)$  MeV. Similarly from the width of the decay  $\phi \rightarrow e^+e^-$  one deduces  $f_\phi \simeq 233$  MeV.

The couplings  $f_V^T$  are not known directly from experiment but are used as inputs in sum-rule calculations (see, for example, refs. [87, 88]) and other phenomenological applications to  $B$ -decays (see, for example, refs. [89, 90, 91, 92]). Previous lattice results for the vector meson couplings are recalled below; determinations obtained using QCD sum-rules are nicely reviewed in [87]. We now present our calculation and results for  $f_V^T/f_V$ , which can then be combined with the experimental values of  $f_V$  to obtain  $f_V^T$ . For the  $\phi$  we neglect the Zweig suppressed disconnected contribution.

### B. Lattice Calculation of $f_V^T/f_V$

In order to determine  $f_V^T/f_V$  it is sufficient to calculate the following zero-momentum correlation functions for large values of the Euclidean time  $t$ :

$$C_{VV}^{s_1 s_2}(t) \equiv \sum_{\vec{x}, i} \langle 0 | V_i^{s_1}(t, \vec{x}) V_i^{s_2}(0) | 0 \rangle = 3 f_V^{s_1} f_V^{s_2} m_V e^{-m_V T/2} \cosh(m_V (T/2 - t)) \quad (144)$$

$$C_{TV}^{s_1 s_2}(t) \equiv \sum_{\vec{x}, i} \langle 0 | T_{4i}^{s_1}(t, \vec{x}) V_i^{s_2}(0) | 0 \rangle = 3 f_V^{T s_1} f_V^{s_2} m_V e^{-m_V T/2} \sinh(m_V (T/2 - t)), \quad (145)$$

where  $V_i$  and  $T_{4i}$  represent the vector and tensor currents and  $i = 1, 2, 3$  is a spatial index.  $s_1$  and  $s_2$  label the smearing at the sink and at the source, respectively. From the ratio

$$R(t) = \frac{C_{TV}^{L s_2}}{C_{VV}^{L s_2}} = \frac{f_V^T}{f_V} \tanh(m_V (T/2 - t)) \quad (146)$$

we readily obtain the ratio of (bare) couplings.

### C. Results

In Table XXV we summarize our results for the vector meson masses from fits to (144) on the DEG data set (cf. Table II) and from fits to (144) and (145) on the UNI data set. In the latter case we average over various choices of the source smearing function (cf. Table IV) while always using a point sink. We restrict our study to the unitary case in which the sea and valence quarks have the same masses. The bare strange quark mass is always fixed at 0.04. On the UNI data set, again averaging over the same choices for the source and the sink, we also evaluate the ratios  $f_V^T/f_V$ . In each case Eq. (146) exhibits well pronounced plateaus which we fit to a constant.



In Table XXVI we present the bare values of  $f_V^T/f_V$ . It can be seen that the measured results are obtained with excellent precision. We have also compared our results with those obtained on a  $16^3 \times 32 \times 16$  lattice for  $m_l = 0.01, 0.02$  and  $0.03$  [85] (the properties of the ensembles on the  $16^3$  lattice have been presented in ref. [34]). No significant finite volume effects were found.

From Fig. 25 it can be seen that the dependence of the bare  $f_V^T/f_V$  on the masses of the light quarks is very mild and so we restrict our chiral extrapolation to linear and quadratic functions in the quark mass as shown in the figure. For the ratio of bare couplings in the chiral limit we obtain:

$$\frac{f_\rho^T}{f_\rho} = 0.619(15)(18); \quad \frac{f_{K^*}^T}{f_{K^*}} = 0.6498(62)(60); \quad \frac{f_\phi^T}{f_\phi} = 0.6838(32)(22), \quad (147)$$

where the central value corresponds to the linear extrapolation and the second error is the difference between the results from the linear and quadratic extrapolations.

The bare results in Eq. (147) were obtained with the notional strange quark mass of  $m_h = 0.04$  rather than the physical value of  $m_s = 0.0343$  (see Table XI). The values of the ratios in Eq. (147) are very similar for the  $\rho$ ,  $K^*$  and  $\phi$  mesons and we correct for the change in  $m_s$  by linear interpolation in the valence quark mass ( $m_h$  is fixed at 0.04). Thus, for example, for the  $K^*$  meson we interpolate between the  $K^*$  and the  $\rho$ :

$$\frac{f_{K^*}^T}{f_{K^*}}(m_s = 0.0343) = \frac{f_{K^*}^T}{f_{K^*}}(m_h = 0.04) + \frac{\Delta}{(0.04 + m_{\text{res}})}(0.0343 - 0.04), \quad (148)$$

where  $\Delta = f_{K^*}^T/f_{K^*}(m_h = 0.04) - f_\rho^T/f_\rho$ . After carrying out a similar extrapolation for  $f_\phi^T/f_\phi$  the corrected bare values are then

$$\frac{f_\rho^T}{f_\rho} = 0.619(15)(18); \quad \frac{f_{K^*}^T}{f_{K^*}} = 0.6457(62)(60); \quad \frac{f_\phi^T}{f_\phi} = 0.6753(32)(22). \quad (149)$$

We determine the renormalization constants non-perturbatively using the Rome-Southampton method and run the results to 2 GeV. The results for the renormalization constants of the tensor and (local) vector currents were presented individually in ref. [21] and for the ratio we find  $Z_T/Z_A = Z_T/Z_V = 1.1101(92) \simeq 1.11(1)$ , where  $Z_A$  is the renormalization constant of the local axial current. The relation between the ratios of bare and renormalized matrix elements is then:

$$\frac{f_V^T(2\text{GeV})}{f_V} = \frac{Z_T(2\text{GeV}a)}{Z_V} \frac{f_V^{\text{bare}}(a)}{f_V^{\text{bare}}} = 1.11(1) \frac{f_V^{\text{bare}}(a)}{f_V^{\text{bare}}}. \quad (150)$$

In the  $\overline{\text{MS}}$  scheme with  $\mu = 2\text{ GeV}$  we finally obtain:

$$\frac{f_\rho^T}{f_\rho} = 0.687(27); \quad \frac{f_{K^*}^T}{f_{K^*}} = 0.717(12); \quad \frac{f_\phi^T}{f_\phi} = 0.750(8). \quad (151)$$

These results can be compared with previous quenched lattice results which we summarize in Table XXVII. The QCDSF/UKQCD collaboration has also presented the result  $f_\rho^T = 168(3)$  MeV using an  $N_f = 2$   $O(a)$  improved clover action with a range of lattice spacings ( $0.07 < a < 0.11$  fm) [93]. Combining our result for the ratio from Eq. (151) together with the experimental value for  $f_\rho$  we obtain a smaller value  $f_\rho^T = 143(6)$  MeV.

## X. CONCLUSIONS

This paper reports the results of simulations of 2+1 flavor QCD with domain wall fermions at a single lattice spacing, with a larger volume than has been achieved previously. The ensembles we have generated have a length of  $\approx 4,000$  molecular dynamics time units, and we have seen a good distribution of global topological charge, indicative of our algorithm's ability to sample phase space. With our  $(2.74 \text{ fm})^3$  spatial volume, and improvements in the RHMC algorithm, our lightest pion made of dynamical quarks has  $m_\pi = 331$  MeV and our lightest valence pion has a mass of  $m_\pi = 242$  MeV. For these two cases, we have  $m_\pi L = 4.60$  and  $3.36$ , respectively.

Because of the good chiral properties of domain wall fermions at non-zero lattice spacing, the only correction to continuum chiral perturbation theory at NLO order is the inclusion of the residual mass,  $m_{\text{res}}$ , in the quark mass appearing in the ChPT formula. This means we have the same number of ChPT LECs to fit as for continuum physics, although the LECs we determine can differ from the continuum values by  $O(a^2)$  terms. The small number of free parameters in our fits is a powerful advantage of working with a fermion formulation with good chiral and flavor symmetries. To have good control over our chiral extrapolations, we have developed SU(2) ChPT for kaon physics, which does not assume the kaon mass is small. We have fit our data to both SU(2) and SU(3) ChPT, at NLO, and find both approaches give good fits to our data. However, for SU(3) ChPT, the NLO corrections are very large - as much as 50% of the size of the LO term for the pseudoscalar decay constants in the range of quark masses where we have data. This poor convergence of the series does not seem to be due to a single term, such as having the dynamical heavy quark mass close to the physical strange quark mass. Our fits have used pseudoscalar particles with mass  $\lesssim 400$  MeV, where SU(3) ChPT might be expected to be more accurate than we have found it to be. We are investigating this further, making use of the full continuum NNLO expressions of [76]. For our most reliable extrapolations to the physical values for the light quark masses, we turn to SU(2) ChPT for kaons. Here we have found good fits, with the NLO corrections no larger than

35% of the LO terms for the light quark mass values we used in our simulations. This is still a somewhat large NLO contribution, but makes the dropping of NNLO terms more sensible. We have tried to estimate our systematic errors by including possible analytic NNLO terms in the fits. For our central results, we use  $m_\Omega$ ,  $m_\pi$  and  $m_K$  to set the scale and determine  $\tilde{m}_{ud}$  and  $\tilde{m}_s$ . For  $m_\Omega$ , there are no light quark chiral logarithms and for  $\tilde{m}_{ud}$  and  $\tilde{m}_s$  we use the SU(2) ChPT formula to perform the extrapolation. We can then predict the decay constants,  $f_\pi$ ,  $f_K$  and their ratio. The fits also give values for the LECs of SU(2) ChPT.

We have estimated our systematics through several methods. For the systematic errors from our chiral fits, we have tried varying the fit ranges and also including analytic NNLO terms, to see the effects of these changes on our results. Finite volume effects are also estimated through ChPT, as are the errors due to the heavy quark in our simulations being 15% heavier than the physical value. For finite lattice spacing effects, we expect them to be  $O(a\Lambda_{\text{QCD}})^2$  or about 4%. Scaling errors no larger than this have been seen in the quenched case [94], and, since dynamical quark loop effects change the scaling at a higher order in  $\alpha_s$ , similar scaling is expected for the full QCD case studied here. The size of this scaling error also agrees well with the deviation of our central value of  $f_\pi$  from the experimental results, so we have adopted a uniform 4%  $O(a^2)$  error for all of our results. (Simulations are underway at a smaller lattice spacing, so that we will soon have better control over the  $a \rightarrow 0$  extrapolation.)

For  $B_K$ , which has already been published [19], we have given more details about our use of SU(2) ChPT to extrapolate to the light quark limit. We have also measured the vector meson couplings for light vector mesons.

Our major results come from using SU(2) ChPT fits and are summarized below:

$$f = 114.8(4.1)_{\text{stat}}(8.1)_{\text{syst}} \text{ MeV}, \quad (152)$$

$$B^{\overline{\text{MS}}}(2 \text{ GeV}) = 2.52(0.11)_{\text{stat}}(0.23)_{\text{ren}}(0.12)_{\text{syst}} \text{ GeV}, \quad (153)$$

$$\Sigma^{\overline{\text{MS}}}(2 \text{ GeV}) = \left(255(8)_{\text{stat}}(8)_{\text{ren}}(13)_{\text{syst}} \text{ MeV} \right)^3, \quad (154)$$

$$\bar{l}_3 = 3.13(0.33)_{\text{stat}}(0.24)_{\text{syst}}, \quad (155)$$

$$\bar{l}_4 = 4.43(0.14)_{\text{stat}}(0.77)_{\text{syst}}, \quad (156)$$

$$\Lambda_3 = 666(110)_{\text{stat}}(80)_{\text{syst}} \text{ MeV}, \quad (157)$$

$$\Lambda_4 = 1,274(92)_{\text{stat}}(490)_{\text{syst}} \text{ MeV}, \quad (158)$$

$$m_{ud}^{\overline{\text{MS}}}(2 \text{ GeV}) = 3.72(0.16)_{\text{stat}}(0.33)_{\text{ren}}(0.18)_{\text{syst}} \text{ MeV}, \quad (159)$$

$$m_s^{\overline{\text{MS}}}(2 \text{ GeV}) = 107.3(4.4)_{\text{stat}}(9.7)_{\text{ren}}(4.9)_{\text{syst}} \text{ MeV}, \quad (160)$$

$$\tilde{m}_{ud} : \tilde{m}_s = 1 : 28.8(0.4)_{\text{stat}}(1.6)_{\text{syst}}, \quad (161)$$

$$f_\pi = 124.1(3.6)_{\text{stat}}(6.9)_{\text{syst}} \text{ MeV}, \quad (162)$$

$$f_K = 149.6(3.6)_{\text{stat}}(6.3)_{\text{syst}} \text{ MeV}, \quad (163)$$

$$f_K/f_\pi = 1.205(0.018)_{\text{stat}}(0.062)_{\text{syst}}, \quad (164)$$

$$B_K^{\overline{\text{MS}}}(2 \text{ GeV}) = 0.524(0.010)_{\text{stat}}(0.013)_{\text{ren}}(0.025)_{\text{syst}}. \quad (165)$$

These results have total errors for the decay constants of about 6% and for the  $\overline{\text{MS}}$  quark masses of about 10%. The systematic error due to  $O(a^2)$  errors will be reduced by the lattices we are generating at a smaller lattice spacing ( $1/a \approx 2.3 \text{ GeV}$ ) and lighter quark masses on a similar physical volume. The errors on the quark masses are largely due to renormalization and should improve as better renormalization conditions are chosen [21].

With the expected increases in computer power over the next few years, we should be able to push to much lighter quark masses and minimize our reliance on chiral perturbation theory in the extrapolation to physical results. This is possible for domain wall fermions, since the chiral limit is decoupled from the continuum limit. With lighter quark masses, we should be able to check the convergence of the chiral perturbation theory expansion and achieve better control over the low energy constants. Finally, the ensembles that we are generating in these basic studies of the low energy properties of QCD are useful for a wide variety of other measurements, including heavy quark systems and hadronic weak interaction matrix elements.

### Acknowledgments

The calculations reported here were done on the QCDOC computers [95, 96, 97] at Columbia University, Edinburgh University, and at Brookhaven National Laboratory (BNL). At BNL, the QCDOC computers of the RIKEN-BNL Research Center and the USQCD Collaboration were used. The software used includes: the CPS QCD codes [http://qcdoc.phys.columbia.edu/chulwoo\\_index.html](http://qcdoc.phys.columbia.edu/chulwoo_index.html), supported in part by the USDOE SciDAC program; the BAGEL <http://www.ph.ed.ac.uk/~paboyle/bagel/Bagel.html> assembler kernel generator for many of the high-performance optimized kernels; and the UKHadron codes.

The authors would like to acknowledge useful discussions with Heinrich Leutwyler, Jürg Gasser, Johan Bijnens and Steve Sharpe.

T.B. and T.Y. (University of Connecticut) were partially supported by the U.S. DOE under contract DE-FG02-92ER40716. N.C., S.C, M.L, S.L, M.F.L., and R.M. (Columbia University) were partially supported by the U.S. DOE under contract DE-FG02-92ER40699. C.J., E.S and A.S. (BNL) were partially supported by the U.S. DOE under contract DE-AC02-98CH10886. S.S (University of Tokyo) was partially supported in part by a JSPS Grant-In-Aid for Scientific Research (C) (No.19540265). M.D., J.F., A.J., and C.S (University of Southampton) were partially supported by UK STFC Grant PP/D000211/1 and by EU contract MRTN-CT-2006-035482 (Flavianet). The work of the Edinburgh authors was supported by PPARC grants PP/D000238/1 and PP/C503154/1. The former directly supported CMM, JW and JMZ. PAB acknowledges support from RCUK and AH acknowledges support from the Royal Society. The Edinburgh QCDOC system was funded by PPARC JIF grant PPA/J/S/1998/00756 and operated through support from the Universities of Edinburgh, Southampton and Wales Swansea, and from STFC grant PP/E006965/1.

Computations for this work were carried out in part on facilities of the USQCD Collaboration, which are funded by the Office of Science of the U.S. Department of Energy. We thank RIKEN, BNL and the U.S. DOE for providing the facilities essential for the completion of this work.

## APPENDIX A: NOTATION, CONVENTIONS

### 1. Quark Masses

Here we discuss our notation for quark masses. In Section II B, where we discuss Kaon ChPT, continuum notation is used and  $m$  represents the total quark mass. Throughout the rest of the paper, we need to distinguish between the input bare quark mass in the domain wall fermion formulation and the total quark mass, which includes the additive contribution to the quark mass from finite  $L_s$ .

Input (sometimes also called bare) quark masses for domain wall fermions will be denoted by the symbol  $m_X$ , where the index  $X \in \{l, h, x, y, ud, s\}$  distinguishes between different types of quarks:

- $m_l$ : dynamical light input quark mass (two degenerate flavors),
- $m_h$ : dynamical heavy input quark mass (one flavor),
- $m_x, m_y$ : valence input quark masses,
- $m_{ud}$ : average light input quark mass at the physical point, *i.e.*, a meson made of two quarks of mass  $m_{ud}$  acquires the experimentally measured mass of the neutral pion (this is related to the input quark masses of the up- and down-quarks via:  $m_{ud} = (m_u + m_d)/2$ ),
- $m_s$ : heavy input quark mass at the physical point (strange quark mass), *i.e.*, a meson made of one quark of mass  $m_{ud}$  and one of mass  $m_s$  acquires the quadratically averaged experimentally measured mass of the neutral kaons.

The total quark mass, which has the residual mass  $m_{\text{res}}$  added, will be denoted by  $\tilde{m}$ ,

$$\tilde{m}_X = m_X + m_{\text{res}}. \quad (\text{A1})$$

The total renormalized quark masses at the physical point carry a superscript indicating the renormalization scheme used. For example, physical masses in the  $\overline{\text{MS}}$  scheme renormalized at a scale  $\mu = 2 \text{ GeV}$  read

$$m_{ud}^{\overline{\text{MS}}}(2 \text{ GeV}) = Z_m^{\overline{\text{MS}}}(2 \text{ GeV}) \cdot (m_{ud} + m_{\text{res}}) = Z_m^{\overline{\text{MS}}}(2 \text{ GeV}) \tilde{m}_{ud}, \quad (\text{A2})$$

$$m_s^{\overline{\text{MS}}}(2 \text{ GeV}) = Z_m^{\overline{\text{MS}}}(2 \text{ GeV}) \cdot (m_s + m_{\text{res}}) = Z_m^{\overline{\text{MS}}}(2 \text{ GeV}) \tilde{m}_s, \quad (\text{A3})$$

where  $Z_m^{\overline{\text{MS}}}(2 \text{ GeV})$  is the mass renormalization constant.

## 2. Pseudoscalar Quantities

The pseudoscalar quantities considered in this work (masses, decay constants, and bag parameters) will carry two indices, denoting the quark content. For example the mass of a pseudoscalar made from two valence quarks with mass  $m_x$  and  $m_y$  will be labeled  $m_{xy}$ , the decay constant of a meson with one valence quark and one dynamical heavy quark is  $f_{xh}$  and the pseudoscalar bag parameter of a meson with one quark at the physical average light quark mass and one valence quark is  $B_{udy}$ . Also we will use the obvious symbols for quantities at the physical point:

$$\begin{aligned} m_\pi &= m_{udud}, & m_K &= m_{uds}, \\ f_\pi &= f_{udud}, & f_K &= f_{uds}, \\ B_K &= B_{uds}. \end{aligned}$$

## 3. Low energy constants in ChPT

The following table lists the LECs we use in the PQChPT formulae:

	LO	NLO
PQ $SU(3) \times SU(3)$	$B_0, f_0,$ $B_{\text{PS}}^\chi$	$L_4^{(3)}, L_5^{(3)}, L_6^{(3)}, L_8^{(3)},$ $b, c, d$
PQ $SU(2) \times SU(2)$	$B, f$	$L_4^{(2)}, L_5^{(2)}, L_6^{(2)}, L_8^{(2)}$
PQ $SU(2) \times SU(2)$ kaon	$B^{(K)}(m_h), f^{(K)}(m_h),$ $B_{\text{PS}}^{(K)}(m_h)$	$\lambda_1(m_h), \lambda_2(m_h), \lambda_3(m_h), \lambda_4(m_h),$ $b_1(m_h), b_2(m_h)$

The renormalization scale dependent NLO LECs are defined at a scale  $\Lambda_\chi$ . For the decay constants, we use the normalization such that the experimentally measured value for the pion decay constant is  $f_\pi \approx 132 \text{ MeV} \approx \sqrt{2} \cdot 93 \text{ MeV}$ .

Further, we will use the following abbreviations for (tree-level) masses in the formulae:

$$\chi_X = 2B_0 \tilde{m}_X, \quad SU(3) \times SU(3), \quad (\text{A4})$$

$$\chi_X = 2B \tilde{m}_X, \quad SU(2) \times SU(2), \quad (\text{A5})$$

where it should be clear from the context, whether the  $SU(3) \times SU(3)$  or  $SU(2) \times SU(2)$  expression is to be used. In addition, we define the average dynamical mass to be

$$\bar{m} = \frac{1}{3}(2m_l + m_h), \quad (\text{A6})$$

and the dynamical  $\eta$ -mass

$$m_\eta = \frac{1}{3}(m_l + 2m_h). \quad (\text{A7})$$

(Note: this is not the tree-level  $\eta$ -mass at the physical point, which would be  $(m_{ud} + 2m_s)/3$ .)

## APPENDIX B: PQCHPT FIT FUNCTIONS

### 1. $SU(3) \times SU(3)$

The following formulae hold for  $N_f = 2 + 1$  sea quark masses and two valence quarks ( $SU(5|3)$ ). The formulae for masses and decay constants were derived from [46], while the ones for the bag parameter  $B_{PS}$  can be found in [98].

#### a. Squared Pseudoscalar Mass

##### a. non-degenerate ( $m_x \neq m_y$ )

- $m_x \neq m_\eta \neq m_y$ :

$$m_{xy}^2 = \frac{\chi_x + \chi_y}{2} \cdot \left\{ 1 + \frac{48}{f_0^2}(2L_6^{(3)} - L_4^{(3)})\bar{\chi} + \frac{8}{f_0^2}(2L_8^{(3)} - L_5^{(3)})(\chi_x + \chi_y) \right. \\ \left. + \frac{1}{24\pi^2 f_0^2} \left[ \frac{(\chi_x - \chi_l)(\chi_x - \chi_h)}{(\chi_x - \chi_y)(\chi_x - \chi_\eta)} \chi_x \log \frac{\chi_x}{\Lambda_\chi^2} + \frac{(\chi_y - \chi_l)(\chi_y - \chi_h)}{(\chi_y - \chi_x)(\chi_y - \chi_\eta)} \chi_y \log \frac{\chi_y}{\Lambda_\chi^2} \right. \right. \\ \left. \left. + \frac{(\chi_\eta - \chi_l)(\chi_\eta - \chi_h)}{(\chi_\eta - \chi_x)(\chi_\eta - \chi_y)} \chi_\eta \log \frac{\chi_\eta}{\Lambda_\chi^2} \right] \right\} \quad (\text{B1})$$

- $m_x \rightarrow m_\eta \neq m_y$ :

$$m_{xy}^2 = \frac{\chi_x + \chi_y}{2} \cdot \left\{ 1 + \frac{48}{f_0^2}(2L_6^{(3)} - L_4^{(3)})\bar{\chi} + \frac{8}{f_0^2}(2L_8^{(3)} - L_5^{(3)})(\chi_x + \chi_y) \right. \\ \left. + \frac{1}{24\pi^2 f_0^2} \left[ \frac{(\chi_y - \chi_l)(\chi_y - \chi_h)}{(\chi_y - \chi_x)^2} \chi_y \log \frac{\chi_y}{\Lambda_\chi^2} \right. \right. \\ \left. \left. + \frac{(\chi_x - \chi_y) \left[ (\chi_x - \chi_h)\chi_x + (\chi_x - \chi_l)(2\chi_x - \chi_h) \right] - (\chi_x - \chi_l)(\chi_x - \chi_h)\chi_x}{(\chi_x - \chi_y)^2} \log \frac{\chi_x}{\Lambda_\chi^2} \right. \right. \\ \left. \left. + \frac{(\chi_x - \chi_l)(\chi_x - \chi_h)}{\chi_x - \chi_y} \right] \right\} \quad (\text{B2})$$



b. *degenerate* ( $m_x = m_y$ )

- $m_x = m_y \neq m_\eta$ :

$$m_{xx}^2 = \chi_x \cdot \left\{ 1 + \frac{48}{f_0^2}(2L_6^{(3)} - L_4^{(3)})\bar{\chi} + \frac{16}{f_0^2}(2L_8^{(3)} - L_5^{(3)})\chi_x \right. \\ \left. + \frac{1}{24\pi^2 f_0^2} \left[ \left( \frac{2\chi_x - \chi_l - \chi_h}{\chi_x - \chi_\eta} - \frac{(\chi_x - \chi_l)(\chi_x - \chi_h)}{(\chi_x - \chi_\eta)^2} \right) \chi_x \log \frac{\chi_x}{\Lambda_\chi^2} \right. \right. \\ \left. \left. + \frac{(\chi_x - \chi_l)(\chi_x - \chi_h)}{\chi_x - \chi_\eta} \left( 1 + \log \frac{\chi_x}{\Lambda_\chi^2} \right) + \frac{(\chi_\eta - \chi_l)(\chi_\eta - \chi_h)}{(\chi_x - \chi_\eta)^2} \chi_\eta \log \frac{\chi_\eta}{\Lambda_\chi^2} \right] \right\} \quad (\text{B3})$$

- $m_x = m_y \rightarrow m_\eta$ :

$$m_{xx}^2 = \chi_x \cdot \left\{ 1 + \frac{48}{f_0^2}(2L_6^{(3)} - L_4^{(3)})\bar{\chi} + \frac{16}{f_0^2}(2L_8^{(3)} - L_5^{(3)})\chi_x \right. \\ \left. + \frac{1}{24\pi^2 f_0^2} \left[ \frac{\chi_l \chi_h}{2\chi_x} + \frac{5\chi_x - 3\chi_l - 3\chi_h}{2} + (3\chi_x - \chi_l - \chi_h) \log \frac{\chi_x}{\Lambda_\chi^2} \right] \right\} \quad (\text{B4})$$

c. *Pion and Kaon masses*  $m_\pi^2$  and  $m_K^2$  From Eq. (B3) we obtain for the degenerate meson mass in unquenched QCD ( $m_x = m_l$ )

$$m_{ll}^2 = \chi_l \cdot \left\{ 1 + \frac{48}{f_0^2}(2L_6^{(3)} - L_4^{(3)})\bar{\chi} + \frac{16}{f_0^2}(2L_8^{(3)} - L_5^{(3)})\chi_l \right. \\ \left. + \frac{1}{24\pi^2 f_0^2} \left[ \frac{3}{2}\chi_l \log \frac{\chi_l}{\Lambda_\chi^2} - \frac{1}{2}\chi_\eta \log \frac{\chi_\eta}{\Lambda_\chi^2} \right] \right\}, \quad (\text{B5})$$

and from Eq. (B1) for the kaon mass ( $m_x = m_l$ ,  $m_y = m_h$ ):

$$m_{lh}^2 = \frac{\chi_l + \chi_h}{2} \cdot \left\{ 1 + \frac{48}{f_0^2}(2L_6^{(3)} - L_4^{(3)})\bar{\chi} + \frac{8}{f_0^2}(2L_8^{(3)} - L_5^{(3)})(\chi_l + \chi_h) \right. \\ \left. + \frac{1}{24\pi^2 f_0^2} \chi_\eta \log \frac{\chi_\eta}{\Lambda_\chi^2} \right\}. \quad (\text{B6})$$

So that for  $m_x = m_l = m_{ud}$  and  $m_y = m_h = m_s$  we get  $m_\pi^2$  and  $m_K^2$ , respectively. These expressions agree with [13].

For a ‘‘kaon’’ made from light sea quark and valence quark ( $m_x \neq m_l$ ), one obtains:

- $m_x \neq m_\eta$ :

$$m_{lx}^2 = \frac{\chi_l + \chi_x}{2} \cdot \left\{ 1 + \frac{48}{f_0^2} (2L_6^{(3)} - L_4^{(3)}) \bar{\chi} + \frac{8}{f_0^2} (2L_8^{(3)} - L_5^{(3)}) (\chi_l + \chi_x) \right. \\ \left. + \frac{1}{24\pi^2 f_0^2} \left[ \frac{\chi_x - \chi_h}{\chi_x - \chi_\eta} \chi_x \log \frac{\chi_x}{\Lambda_\chi^2} + \frac{\chi_\eta - \chi_h}{\chi_\eta - \chi_x} \chi_\eta \log \frac{\chi_\eta}{\Lambda_\chi^2} \right] \right\}, \quad (\text{B7})$$

- $m_x \rightarrow m_\eta$ :

$$m_{lx}^2 = \frac{\chi_l + \chi_x}{2} \cdot \left\{ 1 + \frac{48}{f_0^2} (2L_6^{(3)} - L_4^{(3)}) \bar{\chi} + \frac{8}{f_0^2} (2L_8^{(3)} - L_5^{(3)}) (\chi_l + \chi_x) \right. \\ \left. + \frac{1}{24\pi^2 f_0^2} \left[ \chi_x - \chi_h + (2\chi_x - \chi_h) \log \frac{\chi_x}{\Lambda_\chi^2} \right] \right\}. \quad (\text{B8})$$

Whereas for a ‘‘kaon’’ made from a valence quark ( $m_x \neq m_h$ ) and a heavy sea quark, we have:

- $m_x \neq m_\eta$ :

$$m_{xh}^2 = \frac{\chi_x + \chi_h}{2} \cdot \left\{ 1 + \frac{48}{f_0^2} (2L_6^{(3)} - L_4^{(3)}) \bar{\chi} + \frac{8}{f_0^2} (2L_8^{(3)} - L_5^{(3)}) (\chi_x + \chi_h) \right. \\ \left. + \frac{1}{24\pi^2 f_0^2} \left[ \frac{\chi_x - \chi_l}{\chi_x - \chi_\eta} \chi_x \log \frac{\chi_x}{\Lambda_\chi^2} + \frac{\chi_\eta - \chi_l}{\chi_\eta - \chi_x} \chi_\eta \log \frac{\chi_\eta}{\Lambda_\chi^2} \right] \right\}, \quad (\text{B9})$$

- $m_x \rightarrow m_\eta$

$$m_{xh}^2 = \frac{\chi_x + \chi_h}{2} \cdot \left\{ 1 + \frac{48}{f_0^2} (2L_6^{(3)} - L_4^{(3)}) \bar{\chi} + \frac{8}{f_0^2} (2L_8^{(3)} - L_5^{(3)}) (\chi_x + \chi_h) \right. \\ \left. + \frac{1}{24\pi^2 f_0^2} \left[ (2\chi_x - \chi_l) \log \frac{\chi_x}{\Lambda_\chi^2} + \chi_x - \chi_l \right] \right\}. \quad (\text{B10})$$

### b. Pseudoscalar Decay Constant

#### a. non-degenerate ( $m_x \neq m_y$ )

- $m_x \neq m_\eta \neq m_y$ :

$$\begin{aligned}
f_{xy} = f_0 \cdot & \left\{ 1 + \frac{24}{f_0^2} L_4^{(3)} \bar{\chi} + \frac{4}{f_0^2} L_5^{(3)} (\chi_x + \chi_y) \right. \\
& - \frac{1}{8\pi^2 f_0^2} \left[ \frac{\chi_x + \chi_l}{4} \log \frac{\chi_x + \chi_l}{2\Lambda_\chi^2} + \frac{\chi_y + \chi_l}{4} \log \frac{\chi_y + \chi_l}{2\Lambda_\chi^2} \right. \\
& \left. \left. + \frac{\chi_x + \chi_h}{8} \log \frac{\chi_x + \chi_h}{2\Lambda_\chi^2} + \frac{\chi_y + \chi_h}{8} \log \frac{\chi_y + \chi_h}{2\Lambda_\chi^2} \right] \right. \\
& + \frac{1}{96\pi^2 f_0^2} \left[ \left( \chi_x \frac{(\chi_l - \chi_x)(\chi_h - \chi_x)}{\chi_\eta - \chi_x} + \chi_y \frac{(\chi_l - \chi_y)(\chi_h - \chi_y)}{\chi_\eta - \chi_y} + (\chi_x - \chi_y)^2 \right) \frac{\log \frac{\chi_x}{\chi_y}}{\chi_x - \chi_y} \right. \\
& + \chi_\eta (\chi_y - \chi_x) \frac{(\chi_\eta - \chi_l)(\chi_\eta - \chi_h)}{(\chi_\eta - \chi_x)(\chi_\eta - \chi_y)} \left( \frac{\log \frac{\chi_\eta}{\chi_x}}{\chi_x - \chi_\eta} - \frac{\log \frac{\chi_\eta}{\chi_y}}{\chi_y - \chi_\eta} \right) \\
& \left. \left. - \frac{(\chi_l - \chi_x)(\chi_h - \chi_x)}{\chi_\eta - \chi_x} - \frac{(\chi_l - \chi_y)(\chi_h - \chi_y)}{\chi_\eta - \chi_y} \right] \right\} \quad (\text{B11})
\end{aligned}$$

- $m_x \rightarrow m_\eta \neq m_y$ :

$$\begin{aligned}
f_{xy} = f_0 \cdot & \left\{ 1 + \frac{24}{f_0^2} L_4^{(3)} \bar{\chi} + \frac{4}{f_0^2} L_5^{(3)} (\chi_x + \chi_y) \right. \\
& - \frac{1}{8\pi^2 f_0^2} \left[ \frac{\chi_x + \chi_l}{4} \log \frac{\chi_x + \chi_l}{2\Lambda_\chi^2} + \frac{\chi_y + \chi_l}{4} \log \frac{\chi_y + \chi_l}{2\Lambda_\chi^2} \right. \\
& \left. \left. + \frac{\chi_x + \chi_h}{8} \log \frac{\chi_x + \chi_h}{2\Lambda_\chi^2} + \frac{\chi_y + \chi_h}{8} \log \frac{\chi_y + \chi_h}{2\Lambda_\chi^2} \right] \right. \\
& + \frac{1}{96\pi^2 f_0^2} \left[ \frac{\chi_x^3 + \chi_x^2(\chi_l + \chi_h - 5\chi_y) + \chi_x(5\chi_y(\chi_l + \chi_h) - 5\chi_l\chi_h - 2\chi_y^2) - \chi_y\chi_l\chi_h}{2\chi_x(\chi_x - \chi_y)} \right. \\
& \left. \left. + \frac{\chi_x(3\chi_y^2 + \chi_l\chi_h - 2\chi_y(\chi_l + \chi_h)) + \chi_y(2\chi_l\chi_h - \chi_y(\chi_l + \chi_h))}{(\chi_x - \chi_y)^2} \log \frac{\chi_x}{\chi_y} \right] \right\} \quad (\text{B12})
\end{aligned}$$

- b. *degenerate* ( $m_x = m_y$ )

$$\begin{aligned}
f_{xx} = f_0 \cdot & \left\{ 1 + \frac{24}{f_0^2} L_4^{(3)} \bar{\chi} + \frac{8}{f_0^2} L_5^{(3)} \chi_x \right. \\
& \left. - \frac{1}{16\pi^2 f_0^2} \left[ (\chi_x + \chi_l) \log \frac{\chi_x + \chi_l}{2\Lambda_\chi^2} + \frac{\chi_x + \chi_h}{2} \log \frac{\chi_x + \chi_h}{2\Lambda_\chi^2} \right] \right\} \quad (\text{B13})
\end{aligned}$$

c. *Pion and Kaon decay constants  $f_\pi$  and  $f_K$*  From Eq. (B13) we obtain for the pion decay constant in unquenched QCD ( $m_x = m_l$ )

$$f_{ll} = f_0 \cdot \left\{ 1 + \frac{24}{f_0^2} L_4^{(3)} \bar{\chi} + \frac{8}{f_0^2} L_5^{(3)} \chi_l - \frac{1}{16\pi^2 f_0^2} \left[ \frac{\chi_l + \chi_h}{2} \log \frac{\chi_l + \chi_h}{2\Lambda_\chi^2} + 2\chi_l \log \frac{\chi_l}{\Lambda_\chi^2} \right] \right\}, \quad (\text{B14})$$

and from Eq. (B11) for the kaon decay constant ( $m_x = m_l, m_y = m_h$ ):

$$f_{lh} = f_0 \cdot \left\{ 1 + \frac{24}{f_0^2} L_4^{(3)} \bar{\chi} + \frac{4}{f_0^2} L_5^{(3)} (\chi_l + \chi_h) - \frac{3}{64\pi^2 f_0^2} \left[ 2 \frac{\chi_l + \chi_h}{2} \log \frac{\chi_l + \chi_h}{2\Lambda_\chi^2} + \chi_l \log \frac{\chi_l}{\Lambda_\chi^2} + \chi_\eta \log \frac{\chi_\eta}{\Lambda_\chi^2} \right] \right\}. \quad (\text{B15})$$

Again, for  $m_x = m_l = m_{ud}$  and  $m_y = m_h = m_s$  we get  $f_\pi$  and  $f_K$ , respectively, and these expressions agree with [13].

For a ‘‘kaon’’ made from a light sea quark and valence quark ( $m_x \neq m_l$ ), one obtains:

- $m_x \neq m_\eta$ :

$$f_{lx} = f_0 \cdot \left\{ 1 + \frac{24}{f_0^2} L_4^{(3)} \bar{\chi} + \frac{4}{f_0^2} L_5^{(3)} (\chi_l + \chi_x) + \frac{1}{8\pi^2 f_0^2} \left[ -\frac{3}{8} \chi_l \log \frac{\chi_l}{\Lambda_\chi^2} - \frac{\chi_x + \chi_l}{4} \log \frac{\chi_x + \chi_l}{2\Lambda_\chi^2} - \frac{\chi_l + \chi_h}{8} \log \frac{\chi_l + \chi_h}{2\Lambda_\chi^2} - \frac{\chi_x + \chi_h}{8} \log \frac{\chi_x + \chi_h}{2\Lambda_\chi^2} + \frac{(\chi_x - \chi_l)^2 (\chi_\eta - \chi_h)}{12(\chi_\eta - \chi_x)^2 (\chi_\eta - \chi_l)} \chi_\eta \log \frac{\chi_\eta}{\Lambda_\chi^2} + \frac{\chi_x^2 (\chi_h - \chi_l - \chi_\eta) - \chi_\eta \chi_l (\chi_h - 2\chi_x)}{12(\chi_\eta - \chi_x)^2} \log \frac{\chi_x}{\Lambda_\chi^2} - \frac{(\chi_l - \chi_x)(\chi_h - \chi_x)}{12(\chi_\eta - \chi_x)} \right] \right\}, \quad (\text{B16})$$

- $m_x \rightarrow m_\eta$ :

$$\begin{aligned}
f_{lx} = f_0 \cdot & \left\{ 1 + \frac{24}{f_0^2} L_4^{(3)} \bar{\chi} + \frac{4}{f_0^2} L_5^{(3)} (\chi_l + \chi_x) \right. \\
& + \frac{1}{8\pi^2 f_0^2} \left[ -\frac{3}{8} \chi_l \log \frac{\chi_l}{\Lambda_\chi^2} - \frac{\chi_x + \chi_l}{4} \log \frac{\chi_x + \chi_l}{2\Lambda_\chi^2} \right. \\
& - \frac{\chi_l + \chi_h}{8} \log \frac{\chi_l + \chi_h}{2\Lambda_\chi^2} - \frac{\chi_x + \chi_h}{8} \log \frac{\chi_x + \chi_h}{2\Lambda_\chi^2} \\
& \left. \left. + \frac{\chi_l(\chi_h - 3\chi_x) + \chi_x(\chi_h + \chi_x)}{24\chi_x} + \frac{\chi_l(\chi_h - \chi_l)}{12(\chi_l - \chi_x)} \log \frac{\chi_x}{\Lambda_\chi^2} \right] \right\}. \quad (\text{B17})
\end{aligned}$$

Whereas for a ‘‘kaon’’ made from a valence quark ( $m_x \neq m_h$ ) and a heavy sea quark, we have:

- $m_x \neq m_\eta$

$$\begin{aligned}
f_{xh} = f_0 \cdot & \left\{ 1 + \frac{24}{f_0^2} L_4^{(3)} \bar{\chi} + \frac{4}{f_0^2} L_5^{(3)} (\chi_x + \chi_h) \right. \\
& - \frac{1}{8\pi^2 f_0^2} \left[ \frac{\chi_x + \chi_l}{4} \log \frac{\chi_x + \chi_l}{2\Lambda_\chi^2} + \frac{\chi_h + \chi_l}{4} \log \frac{\chi_h + \chi_l}{2\Lambda_\chi^2} \right. \\
& \left. + \frac{\chi_x + \chi_h}{8} \log \frac{\chi_x + \chi_h}{2\Lambda_\chi^2} + \frac{\chi_h}{4} \log \frac{\chi_h}{\Lambda_\chi^2} \right] \\
& + \frac{1}{96\pi^2 f_0^2} \left[ \left( \chi_x - \chi_h - \chi_x \frac{\chi_l - \chi_x}{\chi_\eta - \chi_x} \right) \log \frac{\chi_x}{\chi_h} \right. \\
& + \chi_\eta (\chi_h - \chi_x) \frac{\chi_\eta - \chi_l}{\chi_\eta - \chi_x} \left( \frac{\log \frac{\chi_\eta}{\chi_x}}{\chi_x - \chi_\eta} - \frac{\log \frac{\chi_\eta}{\chi_h}}{\chi_h - \chi_\eta} \right) \\
& \left. \left. - \frac{(\chi_l - \chi_x)(\chi_h - \chi_x)}{\chi_\eta - \chi_x} \right] \right\}, \quad (\text{B18})
\end{aligned}$$

- $m_x \rightarrow m_\eta$

$$\begin{aligned}
f_{xh} = f_0 \cdot & \left\{ 1 + \frac{24}{f_0^2} L_4^{(3)} \bar{\chi} + \frac{4}{f_0^2} L_5^{(3)} (\chi_x + \chi_h) \right. \\
& - \frac{1}{8\pi^2 f_0^2} \left[ \frac{\chi_x + \chi_l}{4} \log \frac{\chi_x + \chi_l}{2\Lambda_\chi^2} + \frac{\chi_h + \chi_l}{4} \log \frac{\chi_h + \chi_l}{2\Lambda_\chi^2} \right. \\
& \left. + \frac{\chi_x + \chi_h}{8} \log \frac{\chi_x + \chi_h}{2\Lambda_\chi^2} + \frac{\chi_h}{4} \log \frac{\chi_h}{\Lambda_\chi^2} \right] \\
& + \frac{1}{96\pi^2 f_0^2} \left[ \frac{\chi_x^3 + \chi_x^2(\chi_l - 4\chi_h) + 3\chi_x\chi_h^2 - \chi_h^2\chi_l}{2\chi_x(\chi_x - \chi_h)} \right. \\
& \left. \left. + \chi_h \frac{\chi_x(\chi_h - \chi_l) + \chi_h(\chi_l - \chi_h)}{(\chi_x - \chi_h)^2} \log \frac{\chi_x}{\chi_h} \right] \right\}. \quad (\text{B19})
\end{aligned}$$

c. *Scale-dependence of the NLO-LECs*

The NLO-LECs  $L_i^{(3)}(\Lambda_\chi)$  at a renormalization scale  $\Lambda_\chi$  can be converted to a different scale  $\Lambda'_\chi$  using [13]

$$L_i^{(3)}(\Lambda'_\chi) = L_i^{(3)}(\Lambda_\chi) + \frac{\Gamma_i}{16\pi^2} \log \frac{\Lambda_\chi}{\Lambda'_\chi}, \quad (\text{B20})$$

with

$$\Gamma_4 = \frac{1}{8}, \quad \Gamma_5 = \frac{3}{8}, \quad \Gamma_6 = \frac{11}{144}, \quad \Gamma_8 = \frac{5}{48}. \quad (\text{B21})$$

d. *Pseudoscalar Bag Parameter*

Here we follow the notation of [98] for the LEC's relevant for the pseudoscalar bag parameter and denote them by  $b$ ,  $c$ , and  $d$ . Also here we only work in (PQ) SU(3) chiral perturbation theory.

a. *non-degenerate ( $m_x \neq m_y$ )*

$$B_{xy} = B_{\text{PS}}^\chi \left\{ 1 + \frac{1}{24\pi^2 f_0^2} \left[ \frac{I_{\text{conn}} + I_{\text{disc}}}{\chi_x + \chi_y} + \frac{\chi_x + \chi_y}{4} b + \frac{(\chi_x - \chi_y)^2}{\chi_x + \chi_y} c + \frac{3}{2} \bar{\chi} d \right] \right\}, \quad (\text{B22})$$

$$\begin{aligned} I_{\text{conn}} &= \frac{3}{2} (\chi_x + \chi_y)^2 \left( -1 - \log \frac{\chi_x + \chi_y}{2\Lambda_\chi^2} \right) \\ &\quad - \frac{3}{2} (3\chi_x + \chi_y) \chi_x \log \frac{\chi_x}{\Lambda_\chi^2} - \frac{3}{2} (\chi_x + 3\chi_y) \chi_y \log \frac{\chi_y}{\Lambda_\chi^2}, \end{aligned} \quad (\text{B23})$$

$$I_{\text{disc}} = I_x + I_y + I_\eta, \quad (\text{B24})$$

$$\begin{aligned} I_x &= \frac{(3\chi_x + \chi_y)(\chi_l - \chi_x)(\chi_h - \chi_x)}{2(\chi_\eta - \chi_x)} \left( -1 - \log \frac{\chi_x}{\Lambda_\chi^2} \right) \\ &\quad - \left[ \frac{(3\chi_x + \chi_y)(\chi_l - \chi_x)(\chi_h - \chi_x)}{2(\chi_\eta - \chi_x)^2} + \frac{(3\chi_x + \chi_y)(\chi_l - \chi_x)(\chi_h - \chi_x)}{(\chi_y - \chi_x)(\chi_\eta - \chi_x)} \right. \\ &\quad \left. + \frac{2(\chi_l - \chi_x)(\chi_h - \chi_x) - (3\chi_x + \chi_y)(\chi_h - \chi_x) - (3\chi_x + \chi_y)(\chi_l - \chi_x)}{2(\chi_\eta - \chi_x)} \right] \\ &\quad \cdot \chi_x \log \frac{\chi_x}{\Lambda_\chi^2}, \end{aligned} \quad (\text{B25})$$

$$I_y = I_x(x \leftrightarrow y), \quad (\text{B26})$$

$$I_\eta = \frac{(\chi_x - \chi_y)^2 (\chi_x + \chi_y + 2\chi_\eta) (\chi_l - \chi_\eta) (\chi_h - \chi_\eta)}{2(\chi_x - \chi_\eta)^2 (\chi_y - \chi_\eta)^2} \chi_\eta \log \frac{\chi_\eta}{\Lambda_\chi^2}. \quad (\text{B27})$$

For  $m_x \rightarrow m_\eta$ ,  $m_x \neq m_y$ , one obtains from the disconnected diagrams

$$\begin{aligned}
I_{\text{disc}} = & -\chi_l \frac{\chi_\eta^3 + \chi_\eta^2(7\chi_h - 16\chi_y) + \chi_\eta\chi_y(16\chi_h - 9\chi_y) + \chi_h\chi_y^2}{4\chi_\eta(\chi_\eta - \chi_y)} \\
& - \frac{-7\chi_\eta^3 - 9\chi_h\chi_y^2 + 6\chi_y^3 + \chi_\eta\chi_y(-16\chi_h + 7\chi_y) + \chi_\eta^2(\chi_h + 18\chi_y)}{4(\chi_\eta - \chi_y)} \\
& + \frac{1}{2(\chi_\eta - \chi_y)^2} \log \frac{\chi_\eta}{\Lambda_\chi^2} \cdot \\
& \cdot \left[ 2\chi_\eta^4 - 8\chi_\eta^3\chi_y - \chi_y^2(\chi_h\chi_y + \chi_l(\chi_y - 4\chi_h)) \right. \\
& + \chi_\eta\chi_y(\chi_l(7\chi_h - 9\chi_y) + 3\chi_y(\chi_y - 3\chi_h)) \\
& \left. + \chi_\eta^2(\chi_l(\chi_h - 2\chi_y) + \chi_y(15\chi_y - 2\chi_h)) \right] \\
& + \frac{1}{2(\chi_\eta - \chi_y)^2} \log \frac{\chi_y}{\Lambda_\chi^2} \cdot \\
& \cdot \left[ \chi_y(\chi_\eta^2(2\chi_h - 3\chi_y) + \chi_\eta\chi_y(9\chi_h - 11\chi_y) + \chi_y^2(\chi_h + 2\chi_y)) \right. \\
& \left. + \chi_l(-\chi_\eta^2(\chi_h - 2\chi_y) + \chi_y^2(\chi_y - 4\chi_h) + \chi_\eta\chi_y(9\chi_y - 7\chi_h)) \right] \quad (\text{B28})
\end{aligned}$$

b. *degenerate* ( $m_x = m_y$ ) In this case  $I_{\text{disc}} = 0$  and therefore

$$B_{xx} = B_{\text{PS}}^\chi \left\{ 1 + \frac{1}{24\pi^2 f_0^2} \left[ -9\chi_x \log \frac{\chi_x}{\Lambda_\chi^2} + \frac{\chi_x}{2}(b-6) + \frac{3}{2}\bar{\chi}d \right] \right\}, \quad (\text{B29})$$

c. *Kaon bag parameter*  $B_K$  From Eq. (B22) one obtains the full (unquenched) QCD result ( $m_x = m_l, m_y = m_h$ )

$$\begin{aligned}
B_{lh} = & B_{\text{PS}}^\chi \left\{ 1 - \frac{1}{16\pi^2 f_0^2} \left[ (\chi_l + \chi_h) \left( 1 + \log \frac{\chi_l + \chi_h}{2\Lambda_\chi^2} \right) + \frac{3\chi_l + \chi_h}{2(\chi_l + \chi_h)} \chi_l \log \frac{\chi_l}{\Lambda_\chi^2} \right. \right. \\
& \left. \left. + \frac{5\chi_l + 7\chi_h}{2(\chi_l + \chi_h)} \chi_\eta \log \frac{\chi_\eta}{\Lambda_\chi^2} - b \frac{\chi_l + \chi_h}{6} - c \frac{2(\chi_l - \chi_h)^2}{3(\chi_l + \chi_h)} - d\bar{\chi} \right] \right\}, \quad (\text{B30})
\end{aligned}$$

so that at the physical point ( $m_l = m_{ud}, m_h = m_s$ ) we have

$$\begin{aligned}
B_K = & B_{\text{PS}}^\chi \left\{ 1 - \frac{2}{(4\pi f_0)^2} \left[ M_K^2 \left( 1 + \log \frac{M_K^2}{\Lambda_\chi^2} \right) + \frac{M_\pi^2(M_\pi^2 + M_K^2)}{4M_K^2} \log \frac{M_\pi^2}{\Lambda_\chi^2} \right. \right. \\
& \left. \left. + \frac{7M_K^2 - M_\pi^2}{4M_K^2} M_\eta^2 \log \frac{M_\eta^2}{\Lambda_\chi^2} - \frac{b}{6} M_K^2 - \frac{2c}{3} \frac{(M_\pi^2 - M_K^2)^2}{M_K^2} - \frac{d}{6} (M_\pi^2 + 2M_K^2) \right] \right\} \quad (\text{B31})
\end{aligned}$$

Here we expressed everything in terms of meson masses:  $M_\pi^2 = \chi_{ud}$ ,  $M_K^2 = \frac{1}{2}(\chi_{ud} + \chi_s)$ ,  $M_\eta^2 = \chi_\eta|_{m_l=m_{ud}, m_h=m_s}$ . (This agrees for the non-analytic terms with Eq. (12) of [81], analytic terms were not considered in that reference.)

## 2. $SU(2) \times SU(2)$

The following formulae hold for  $N_f = 2$  (degenerate) sea quark masses (mass  $m_l$ ) and two valence quarks. ( $SU(4|2)$ ). The formulae for masses and decay constants were derived from [46], also cf. [99].

### a. Squared Pseudoscalar Mass

#### a. non-degenerate

$$m_{xy}^2 = \frac{\chi_x + \chi_y}{2} \cdot \left\{ 1 + \frac{32}{f^2}(2L_6^{(2)} - L_4^{(2)})\chi_l + \frac{8}{f^2}(2L_8^{(2)} - L_5^{(2)})(\chi_x + \chi_y) + \frac{1}{16\pi^2 f^2} \left[ \frac{\chi_x - \chi_l}{\chi_x - \chi_y} \chi_x \log \frac{\chi_x}{\Lambda_\chi^2} + \frac{\chi_y - \chi_l}{\chi_y - \chi_x} \chi_y \log \frac{\chi_y}{\Lambda_\chi^2} \right] \right\} \quad (\text{B32})$$

#### b. degenerate

$$m_{xx}^2 = \chi_x \cdot \left\{ 1 + \frac{32}{f^2}(2L_6^{(2)} - L_4^{(2)})\chi_l + \frac{16}{f^2}(2L_8^{(2)} - L_5^{(2)})\chi_x + \frac{1}{16\pi^2 f^2} \left[ \chi_x - \chi_l + (2\chi_x - \chi_l) \log \frac{\chi_x}{\Lambda_\chi^2} \right] \right\} \quad (\text{B33})$$

c. Pion mass  $m_\pi^2$  From Eq. (B33) one obtains the degenerate meson mass in full (unquenched) QCD ( $m_x = m_l$ ):

$$m_{ll}^2 = \chi_l \cdot \left\{ 1 + \frac{16}{f^2} \left( (2L_8^{(2)} - L_5^{(2)}) + 2(2L_6^{(2)} - L_4^{(2)}) \right) \chi_l + \frac{1}{16\pi^2 f^2} \chi_l \log \frac{\chi_l}{\Lambda_\chi^2} \right\} \quad (\text{B34})$$

which gives for  $m_x = m_l = m_{ud}$  the pion mass  $m_\pi^2$  and agrees with [12]. Furthermore, we can relate the LECs  $L_{4,5,6,8}^{(2)}$  from PQChPT to  $l'_3$  in ChPT:

$$4 \left( (2L_8^{(2)} - L_5^{(2)}) + 2(2L_6^{(2)} - L_4^{(2)}) \right) = l'_3 \quad (\text{B35})$$



b. *Pseudoscalar Decay Constant*

a. *non-degenerate*

$$f_{xy} = f \cdot \left\{ 1 + \frac{16}{f^2} L_4^{(2)} \chi_l + \frac{4}{f^2} L_5^{(2)} (\chi_x + \chi_y) - \frac{1}{32\pi^2 f^2} \left[ (\chi_x + \chi_l) \log \frac{\chi_x + \chi_l}{2\Lambda_\chi^2} + (\chi_y + \chi_l) \log \frac{\chi_y + \chi_l}{2\Lambda_\chi^2} \right] + \frac{1}{64\pi^2 f^2} \left[ \chi_x + \chi_y - 2\chi_l + \frac{2\chi_x \chi_y - \chi_l (\chi_x + \chi_y)}{\chi_y - \chi_x} \log \frac{\chi_x}{\chi_y} \right] \right\} \quad (\text{B36})$$

b. *degenerate*

$$f_{xx} = f \cdot \left\{ 1 + \frac{16}{f^2} L_4^{(2)} \chi_l + \frac{8}{f^2} L_5^{(2)} \chi_x - \frac{\chi_x + \chi_l}{16\pi^2 f^2} \log \frac{\chi_x + \chi_l}{2\Lambda_\chi^2} \right\} \quad (\text{B37})$$

c. *Pion decay constant  $f_\pi$*

$$f_{ll} = f \cdot \left\{ 1 + \frac{8}{f^2} (2L_4^{(2)} + L_5^{(2)}) \chi_l - \frac{\chi_l}{8\pi^2 f^2} \log \frac{\chi_l}{\Lambda_\chi^2} \right\}. \quad (\text{B38})$$

Again, for  $m_x = m_l = m_{ud}$  this reproduces the pion decay constant  $f_\pi$  and agrees with [12]. Furthermore, we can relate the LECs  $L_{4,5}^{(2)}$  from PQChPT to  $l_4^r$  in ChPT:

$$4(2L_4^{(2)} + L_5^{(2)}) = l_4^r. \quad (\text{B39})$$

c. *Conversion from  $\text{SU}(3) \times \text{SU}(3)$  to  $\text{SU}(2) \times \text{SU}(2)$*

The conversion from the  $\text{SU}(3)$  LEC's to the  $\text{SU}(2)$  ones can be done (incl. terms up to NLO) following [13] (see [26] for NNLO, note the latter organizes the expansion in a slightly different way compared to the former).

$$f = f_0 \left\{ 1 - \frac{\chi_s}{32\pi^2 f_0^2} \log \frac{\chi_s}{2\Lambda_\chi^2} + \frac{8}{f_0^2} L_4^{(3)} \chi_s \right\} \quad (\text{B40})$$

$$B = B_0 \left\{ 1 - \frac{\chi_s}{72\pi^2 f_0^2} \log \frac{2\chi_s}{3\Lambda_\chi^2} + \frac{16}{f_0^2} (2L_6^{(3)} - L_4^{(3)}) \chi_s \right\} \quad (\text{B41})$$

$$l_3^r = 4(2L_8^{(3)} - L_5^{(3)}) + 8(2L_6^{(3)} - L_4^{(3)}) - \frac{1}{576\pi^2} \left( 1 + \log \frac{2\chi_s}{3\Lambda_\chi^2} \right) \quad (\text{B42})$$

$$l_4^r = 8L_4^{(3)} + 4L_5^{(3)} - \frac{1}{64\pi^2} \left( 1 + \log \frac{\chi_s}{2\Lambda_\chi^2} \right) \quad (\text{B43})$$

Where one has to use  $B_0$  to evaluate the  $\chi_X$  on the right hand side. The relation of the SU(2) LECs in PQChPT,  $L_i^{(2)}$  to the unquenched SU(2) LECs  $l_{3,4}^r$  is given by Eqs. (B35, B39). To define them at the scale of the pion mass  $m_\pi$ , one has to use

$$\bar{l}_i = \frac{32\pi^2}{\gamma_i} l_i^r - \log \frac{m_\pi^2}{\Lambda_\chi^2} \quad (\text{B44})$$

$$\gamma_3 = -\frac{1}{2}, \quad \gamma_4 = 2. \quad (\text{B45})$$

### 3. SU(2) $\times$ SU(2) for the kaon sector

Here, we choose to denote by  $m_x$  always a light and by  $m_y$  a heavier valence quark mass. The additional low-energy constants appearing here (LO:  $B^{(K)}(m_h)$ ,  $f^{(K)}(m_h)$ ,  $B_{\text{PS}}^{(K)}(m_h)$ , NLO:  $\lambda_{1,2,3,4}(m_h)$ ,  $b_{1,2}(m_h)$ ) are in general dependent on the dynamical heavy quark mass  $m_h$  and the valence heavy quark mass  $m_y$ . To simplify the notation the argument  $m_h$  has to be viewed as placeholder for both of those. For more details see Sec. II.

#### a. Light-Heavy Squared Pseudoscalar Mass

$$m_{xy}^2 = B^{(K)}(m_h) \tilde{m}_y \left\{ 1 + \frac{\lambda_1(m_h)}{f^2} \chi_l + \frac{\lambda_2(m_h)}{f^2} \chi_x \right\} \quad (\text{B46})$$

#### b. Light-Heavy Pseudoscalar Decay Constant

$$f_{xy} = f^{(K)}(m_h) \left\{ 1 + \frac{\lambda_3(m_h)}{f^2} \chi_l + \frac{\lambda_4(m_h)}{f^2} \chi_x - \frac{1}{(4\pi f)^2} \left[ \frac{\chi_x + \chi_l}{2} \log \frac{\chi_x + \chi_l}{2\Lambda_\chi^2} + \frac{\chi_l - 2\chi_x}{4} \log \frac{\chi_x}{\Lambda_\chi^2} \right] \right\} \quad (\text{B47})$$

#### c. Light-Heavy Pseudoscalar Bag Parameter

$$B_{xy} = B_{\text{PS}}^{(K)}(m_h) \left\{ 1 + \frac{b_1(m_h)}{f^2} \chi_l + \frac{b_2(m_h)}{f^2} \chi_x - \frac{\chi_l}{32\pi^2 f^2} \log \frac{\chi_x}{\Lambda_\chi^2} \right\} \quad (\text{B48})$$

d. Conversion from  $SU(3) \times SU(3)$  to kaon  $SU(2) \times SU(2)$

For the LECs appearing in the kaon mass and decay constant formulae (Eqs. (B46, B47)), we provide the relation to the  $SU(3)$ -LECs as well:

$$f^{(K)}(m_h, m_y) = f_0 \left\{ 1 + \frac{8}{f_0^2} L_4^{(3)} \chi_h + \frac{4}{f_0^2} L_5^{(3)} \chi_y + \frac{1}{32\pi^2 f_0^2} \left[ \frac{\chi_y - \chi_h}{3\chi_y - 2\chi_h} \chi_y \right. \right. \\ \left. \left. - \frac{\chi_h}{2} \log \frac{\chi_h}{2\Lambda_\chi^2} - \chi_y \log \frac{\chi_y}{2\Lambda_\chi^2} + \frac{\chi_h \chi_y^2}{(3\chi_y - 2\chi_h)^2} \log \frac{\chi_y}{\Lambda_\chi^2} \right. \right. \\ \left. \left. - \frac{\chi_h \chi_y^2}{(3\chi_y - 2\chi_h)^2} \log \frac{2\chi_h}{3\Lambda_\chi^2} - \frac{\chi_h + \chi_y}{2} \log \frac{\chi_h + \chi_y}{2\Lambda_\chi^2} \right] \right\}, \quad (\text{B49})$$

$$B^{(K)}(m_h, m_y) = B_0 \left\{ 1 + \frac{\chi_h}{f_0^2} 16(2L_6^{(3)} - L_4^{(3)}) + \frac{\chi_y}{f_0^2} 8(2L_8^{(3)} - L_5^{(3)}) \right. \\ \left. + \frac{1}{72\pi^2 f_0^2} \left[ 9 \frac{\chi_y - \chi_h}{3\chi_y - 2\chi_h} \chi_y \log \frac{\chi_y}{\Lambda_\chi^2} + 2 \frac{\chi_h^2}{3\chi_y - 2\chi_h} \log \frac{2\chi_h}{3\Lambda_\chi^2} \right] \right\}, \quad (\text{B50})$$

$$\lambda_1(m_h, m_y) = 32(2L_6^{(3)} - L_4^{(3)}) + \frac{1}{72\pi^2} \left[ -\frac{18(\chi_y - \chi_h)^2}{(3\chi_y - 2\chi_h)^2} \log \frac{\chi_y}{\Lambda_\chi^2} \right. \\ \left. + 2 \frac{5\chi_h - 6\chi_y}{(3\chi_y - 2\chi_h)^2} \chi_h \log \frac{2\chi_h}{3\Lambda_\chi^2} + \frac{\chi_h}{3\chi_y - 2\chi_h} \right], \quad (\text{B51})$$

$$\lambda_2(m_h, m_y) = \frac{f_0^2}{\chi_y} + 8(2L_8^{(3)} - L_5^{(3)}) + 16 \frac{\chi_h}{\chi_y} (L_4^{(3)} - (2L_6^{(3)} - L_4^{(3)})) \\ + \frac{1}{4\pi^2} \left[ \frac{\chi_y - \chi_h}{2(3\chi_y - 2\chi_h)} \log \frac{\chi_y}{\Lambda_\chi^2} - \frac{\chi_h}{4\chi_y} \log \frac{\chi_h}{2\Lambda_\chi^2} + \frac{\chi_h(3\chi_y - \chi_h)}{9\chi_y(3\chi_y - 2\chi_h)} \log \frac{2\chi_h}{3\Lambda_\chi^2} \right], \quad (\text{B52})$$

$$\lambda_3(m_h, m_y) = 16L_4^{(3)} + \frac{1}{16\pi^2} \left[ -\frac{1}{2} \log \frac{\chi_y}{2\Lambda_\chi^2} - \frac{4\chi_h^2 - 11\chi_h\chi_y + 8\chi_y^2}{(3\chi_y - 2\chi_h)^2} \right. \\ \left. + \frac{15\chi_y - 14\chi_h}{4(3\chi_y - 2\chi_h)^3} \chi_y^2 \log \frac{2\chi_h}{3\Lambda_\chi^2} + \frac{(3\chi_y - \chi_h)(\chi_y - \chi_h)(\chi_y - 2\chi_h)}{(3\chi_y - 2\chi_h)^3} \log \frac{\chi_y}{\Lambda_\chi^2} \right], \quad (\text{B53})$$

$$\lambda_4(m_h, m_y) = 4L_5^{(3)} + \frac{1}{16\pi^2} \left[ -\frac{1}{4} \log \frac{\chi_h}{2\Lambda_\chi^2} + \frac{\chi_y - \chi_h}{3\chi_y - 2\chi_h} \log \frac{\chi_y}{\Lambda_\chi^2} - \frac{\chi_y}{2(3\chi_y - 2\chi_h)} \log \frac{2\chi_h}{3\Lambda_\chi^2} \right]. \quad (\text{B54})$$

### APPENDIX C: FINITE VOLUME CORRECTION FOR PSEUDOSCALAR MASSES AND DECAY CONSTANTS

In the following we will provide the finite volume corrections for the meson decay constants and squared meson masses obtained in PQChPT for  $N_f = 2 + 1$  and  $N_f = 2$  sea quarks (cf. [56, 57,

58, 59, 60, 61]). The corrections are labeled  $\Delta_{xy}^{Lf}$  and  $\Delta_{xy}^{Lm^2}$ , respectively, for decay constants and squared masses of mesons made of quarks with masses  $m_x$  and  $m_y$  in a finite (spatial) volume  $L^3$ . Labeling decay constants in finite volume  $f_{xy}^L$  and those in infinite volume  $f_{xy}^{L \rightarrow \infty}$  we have the following relations:

$$f_{xy}^{L \rightarrow \infty} = f_{xy}^L \left( 1 - \Delta_{xy}^{Lf} \right) \quad (\text{C1})$$

$$= f_0 \left( 1 + \chi \text{PT}_{xy}^f \right), \quad (\text{C2})$$

$$f_{xy}^L = f_0 \left( 1 + \chi \text{PT}_{xy}^f \right) \left( 1 + \Delta_{xy}^{Lf} \right) \quad (\text{C3})$$

$$= f_0 \left( 1 + \chi \text{PT}_{xy}^f + \Delta_{xy}^{Lf} \right) \quad (\text{C4})$$

and similar for squared meson masses. Here we summarized the NLO contribution in infinite volume (PQ)ChPT (as given in the previous section) by  $\chi \text{PT}_{xy}^f$ . (These equalities hold up to terms of NLO, higher order terms are neglected. Note further, that in case of  $\text{SU}(2) \times \text{SU}(2)$  the  $f_0$  has to be replaced by  $f$ .)

The Bessel functions of imaginary argument (modified Bessel functions of the 2<sup>nd</sup> kind)  $K_n(x)$  enter the expressions for the finite volume corrections via

$$\delta_1(x) = \frac{4}{x} \sum_{\vec{r} \neq 0} \frac{K_1(rx)}{r}, \quad (\text{C5})$$

$$\delta_3(x) = 2 \sum_{\vec{r} \neq 0} K_0(rx), \quad (\text{C6})$$

$$\delta_5(x) = - \sum_{\vec{r} \neq 0} \frac{r}{x} K_1(rx), \quad (\text{C7})$$

where the argument is typically  $x = \sqrt{\chi} L$ . For the numerical implementation, we made use of the multiplicities  $m(n)$  and rewrite the sum as

$$\sum_{\vec{r} \neq 0} f(r) = \sum_{n > 0} m(n) f(\sqrt{n}), \quad (\text{C8})$$

where sum is evaluated until the relative change is less than the required precision  $\varepsilon$  or a maximum number  $N$  for  $n$  is reached. (Typically, we use  $\varepsilon = 5 \cdot 10^{-4}$  and  $N = 100$ , but checked that going to  $\varepsilon = 5 \cdot 10^{-6}$ ,  $N = 1000$  does not change the result.) The multiplicities for  $n \leq 20$  can, *e.g.*, be

found in [62]. Here we list  $m(n)$  for  $n = 1, \dots, 100$ :

$$\begin{aligned}
& 6, 12, 8, 6, 24, 24, 0, 12, 30, 24, 24, 8, 24, 48, 0, 6, 48, 36, 24, 24, \\
& 48, 24, 0, 24, 30, 72, 32, 0, 72, 48, 0, 12, 48, 48, 48, 30, 24, 72, 0, 24, \\
& 96, 48, 24, 24, 72, 48, 0, 8, 54, 84, 48, 24, 72, 96, 0, 48, 48, 24, 72, 0, \\
& 72, 96, 0, 6, 96, 96, 24, 48, 96, 48, 0, 36, 48, 120, 56, 24, 96, 48, 0, 24, \\
& 102, 48, 72, 48, 48, 120, 0, 24, 144, 120, 48, 0, 48, 96, 0, 24, 48, 108, 72, 30. \quad (C9)
\end{aligned}$$

Note that we have the following relations involving the  $\delta_i$ :

$$\frac{d}{d\chi} \chi \delta_1(\sqrt{\chi}L) = -\delta_3(\sqrt{\chi}L), \quad (C10)$$

$$\frac{d}{d\chi} \delta_3(\sqrt{\chi}L) = L^2 \delta_5(\sqrt{\chi}L). \quad (C11)$$

Furthermore, by doing the substitutions in the finite volume correction part  $\Delta_{xy}^L$

$$\delta_1(\sqrt{\chi_X}L) \rightarrow \log \frac{\chi_X}{\Lambda_X^2}, \quad (C12)$$

$$\delta_3(\sqrt{\chi_X}L) \rightarrow -\left(1 + \log \frac{\chi_X}{\Lambda_X^2}\right), \quad (C13)$$

$$L^2 \delta_5(\sqrt{\chi_X}L) \rightarrow -\frac{1}{\chi_X}, \quad (C14)$$

one obtains at NLO the non-analytic part of the corresponding  $\chi\text{PT}_{xy}$  (*i.e.* without the analytic terms multiplying the LECs).

## 1. $\text{SU}(3) \times \text{SU}(3)$

### *a. FV Correction for the Squared Pseudoscalar Mass*

#### *a. non-degenerate ( $m_x \neq m_y$ )*

- $m_x \neq m_\eta \neq m_y$

$$\begin{aligned}
\Delta_{xy}^{Lm^2} = \frac{1}{24\pi^2 f_0^2} & \left[ \frac{(\chi_\eta - \chi_l)(\chi_\eta - \chi_h)}{(\chi_\eta - \chi_x)(\chi_\eta - \chi_y)} \chi_\eta \delta_1(\sqrt{\chi_\eta}L) \right. \\
& + \frac{(\chi_x - \chi_l)(\chi_x - \chi_h)}{(\chi_x - \chi_y)(\chi_x - \chi_\eta)} \chi_x \delta_1(\sqrt{\chi_x}L) + \left. \frac{(\chi_y - \chi_l)(\chi_y - \chi_h)}{(\chi_y - \chi_x)(\chi_y - \chi_\eta)} \chi_y \delta_1(\sqrt{\chi_y}L) \right] \quad (C15)
\end{aligned}$$

- $m_x \rightarrow m_\eta$  ( $m_y \neq m_\eta$ )

$$\begin{aligned} \Delta_{xy}^{Lm^2} = & \frac{1}{24\pi^2 f_0^2} \left[ -\frac{(\chi_x - \chi_l)(\chi_x - \chi_h)}{\chi_x - \chi_y} \delta_3(\sqrt{\chi_x}L) \right. \\ & + \frac{(2\chi_x - \chi_l - \chi_h)(\chi_x - \chi_y) - (\chi_x - \chi_l)(\chi_x - \chi_h)}{(\chi_x - \chi_y)^2} \chi_x \delta_1(\sqrt{\chi_x}L) \\ & \left. + \frac{(\chi_y - \chi_l)(\chi_y - \chi_h)}{(\chi_x - \chi_y)^2} \chi_y \delta_1(\sqrt{\chi_y}L) \right] \end{aligned} \quad (C16)$$

b. *degenerate*

- $m_x \neq m_\eta$

$$\begin{aligned} \Delta_{xx}^{Lm^2} = & \frac{1}{24\pi^2 f_0^2} \left[ \frac{(\chi_\eta - \chi_l)(\chi_\eta - \chi_h)}{(\chi_\eta - \chi_x)^2} \chi_\eta \delta_1(\sqrt{\chi_\eta}L) \right. \\ & + \frac{(\chi_x - \chi_\eta)(2\chi_x - \chi_h - \chi_l) - (\chi_x - \chi_l)(\chi_x - \chi_h)}{(\chi_x - \chi_\eta)^2} \chi_x \delta_1(\sqrt{\chi_x}L) \\ & \left. - \frac{(\chi_x - \chi_l)(\chi_x - \chi_h)}{\chi_x - \chi_\eta} \delta_3(\sqrt{\chi_x}L) \right] \end{aligned} \quad (C17)$$

- $m_x \rightarrow m_\eta$

$$\begin{aligned} \Delta_{xx}^{Lm^2} = & \frac{1}{24\pi^2 f_0^2} \left[ \chi_x \delta_1(\sqrt{\chi_x}L) - (2\chi_x - \chi_l - \chi_h) \delta_3(\sqrt{\chi_x}L) \right. \\ & \left. - \frac{(\chi_x - \chi_l)(\chi_x - \chi_h)}{2} L^2 \delta_5(\sqrt{\chi_x}L) \right] \end{aligned} \quad (C18)$$

b. *FV Correction for the Pseudoscalar Decay Constant*

a. *non-degenerate  $m_x \neq m_y$*

- $m_x \neq m_\eta \neq m_y$

$$\begin{aligned} \Delta_{xy}^{Lf} = & -\frac{1}{8\pi^2 f_0^2} \left[ \frac{\chi_x + \chi_l}{4} \delta_1 \left( \sqrt{\frac{\chi_x + \chi_l}{2}} L \right) + \frac{\chi_y + \chi_l}{4} \delta_1 \left( \sqrt{\frac{\chi_y + \chi_l}{2}} L \right) \right. \\ & \left. + \frac{\chi_x + \chi_h}{8} \delta_1 \left( \sqrt{\frac{\chi_x + \chi_h}{2}} L \right) + \frac{\chi_y + \chi_h}{8} \delta_1 \left( \sqrt{\frac{\chi_y + \chi_h}{2}} L \right) \right] \\ & + \frac{1}{96\pi^2 f_0^2} \left[ -\frac{(\chi_l - \chi_x)(\chi_h - \chi_x)}{\chi_x - \chi_\eta} \delta_3(\sqrt{\chi_x}L) - \frac{(\chi_l - \chi_y)(\chi_h - \chi_y)}{\chi_y - \chi_\eta} \delta_3(\sqrt{\chi_y}L) \right. \\ & + \left( \frac{(\chi_l - \chi_\eta)(\chi_h - \chi_\eta)}{(\chi_x - \chi_\eta)^2} + \frac{(\chi_l - \chi_\eta)(\chi_h - \chi_\eta)}{(\chi_y - \chi_\eta)^2} - 2 \frac{(\chi_l - \chi_\eta)(\chi_h - \chi_\eta)}{(\chi_x - \chi_\eta)(\chi_y - \chi_\eta)} \right) \chi_\eta \delta_1(\sqrt{\chi_\eta}L) \\ & + \left( \frac{\chi_h + \chi_l - 2\chi_x}{\chi_\eta - \chi_x} - \frac{(\chi_l - \chi_x)(\chi_h - \chi_x)}{(\chi_\eta - \chi_x)^2} - 2 \frac{(\chi_l - \chi_x)(\chi_h - \chi_x)}{(\chi_\eta - \chi_x)(\chi_y - \chi_x)} \right) \chi_x \delta_1(\sqrt{\chi_x}L) \\ & \left. + \left( \frac{\chi_h + \chi_l - 2\chi_y}{\chi_\eta - \chi_y} - \frac{(\chi_l - \chi_y)(\chi_h - \chi_y)}{(\chi_\eta - \chi_y)^2} - 2 \frac{(\chi_l - \chi_y)(\chi_h - \chi_y)}{(\chi_\eta - \chi_y)(\chi_x - \chi_y)} \right) \chi_y \delta_1(\sqrt{\chi_y}L) \right] \end{aligned} \quad (C19)$$

- $m_x \rightarrow m_\eta, m_y \neq m_\eta$

$$\begin{aligned}
\Delta_{xy}^{Lf} = & -\frac{1}{8\pi^2 f_0^2} \left[ \frac{\chi_x + \chi_l}{4} \delta_1 \left( \sqrt{\frac{\chi_x + \chi_l}{2}} L \right) + \frac{\chi_y + \chi_l}{4} \delta_1 \left( \sqrt{\frac{\chi_y + \chi_l}{2}} L \right) \right. \\
& + \frac{\chi_x + \chi_h}{8} \delta_1 \left( \sqrt{\frac{\chi_x + \chi_h}{2}} L \right) + \frac{\chi_y + \chi_h}{8} \delta_1 \left( \sqrt{\frac{\chi_y + \chi_h}{2}} L \right) \left. \right] \\
& + \frac{1}{96\pi^2 f_0^2} \left[ -\frac{1}{2} (\chi_l - \chi_x) (\chi_h - \chi_x) L^2 \delta_5(\sqrt{\chi_x} L) - \frac{(\chi_l - \chi_y) (\chi_h - \chi_y)}{\chi_y - \chi_x} \delta_3(\sqrt{\chi_y} L) \right. \\
& + \left( 1 - 2 \frac{2\chi_x - \chi_l - \chi_h}{\chi_x - \chi_y} + 3 \frac{(\chi_l - \chi_x) (\chi_h - \chi_x)}{(\chi_x - \chi_y)^2} \right) \chi_x \delta_1(\sqrt{\chi_x} L) \\
& - \left( 2\chi_x - \chi_l - \chi_h - 2 \frac{(\chi_l - \chi_x) (\chi_h - \chi_x)}{\chi_x - \chi_y} \right) \delta_3(\sqrt{\chi_x} L) \\
& \left. + \left( \frac{\chi_h + \chi_l - 2\chi_y}{\chi_x - \chi_y} - \frac{(\chi_l - \chi_y) (\chi_h - \chi_y)}{(\chi_x - \chi_y)^2} - 2 \frac{(\chi_l - \chi_y) (\chi_h - \chi_y)}{(\chi_x - \chi_y)^2} \right) \chi_y \delta_1(\sqrt{\chi_y} L) \right] \quad (C20)
\end{aligned}$$

- b. *degenerate,  $m_x = m_y$*

$$\Delta_{xx}^{Lf} = -\frac{1}{8\pi^2 f_0^2} \left[ \frac{\chi_x + \chi_l}{2} \delta_1 \left( \sqrt{\frac{\chi_x + \chi_l}{2}} L \right) + \frac{\chi_x + \chi_h}{4} \delta_1 \left( \sqrt{\frac{\chi_x + \chi_h}{2}} L \right) \right] \quad (C21)$$

## 2. $SU(2) \times SU(2)$

### a. *FV Correction for the Squared Pseudoscalar Mass*

- a. *non-degenerate ( $m_x \neq m_y$ )*

$$\Delta_{xy}^{Lm^2} = \frac{1}{16\pi^2 f^2} \left[ \frac{\chi_x - \chi_l}{\chi_x - \chi_y} \chi_x \delta_1(\sqrt{\chi_x} L) + \frac{\chi_y - \chi_l}{\chi_y - \chi_x} \chi_y \delta_1(\sqrt{\chi_y} L) \right] \quad (C22)$$

- b. *degenerate ( $m_x = m_y$ )*

$$\Delta_{xx}^{Lm^2} = \frac{1}{16\pi^2 f^2} \left[ \chi_x \delta_1(\sqrt{\chi_x} L) - (\chi_x - \chi_l) \delta_3(\sqrt{\chi_x} L) \right] \quad (C23)$$

b. *FV Correction for the Pseudoscalar Decay Constant*

a. *non-degenerate* ( $m_x \neq m_y$ )

$$\begin{aligned} \Delta_{xy}^{Lf} = & -\frac{1}{32\pi^2 f^2} \left[ (\chi_x + \chi_l) \delta_1 \left( \sqrt{\frac{\chi_x + \chi_l}{2}} L \right) + (\chi_y + \chi_l) \delta_1 \left( \sqrt{\frac{\chi_y + \chi_l}{2}} L \right) \right] \\ & + \frac{1}{64\pi^2 f^2} \left[ -(\chi_x - \chi_l) \delta_3(\sqrt{\chi_x} L) - (\chi_y - \chi_l) \delta_3(\sqrt{\chi_y} L) \right. \\ & \left. + \frac{\chi_x + \chi_y - 2\chi_l}{\chi_y - \chi_x} \chi_x \delta_1(\sqrt{\chi_x} L) + \frac{\chi_y + \chi_x - 2\chi_l}{\chi_x - \chi_y} \chi_y \delta_1(\sqrt{\chi_y} L) \right] \end{aligned} \quad (C24)$$

b. *degenerate* ( $m_x = m_y$ )

$$\Delta_{xx}^{Lf} = -\frac{1}{16\pi^2 f^2} (\chi_x + \chi_l) \delta_1 \left( \sqrt{\frac{\chi_x + \chi_l}{2}} L \right) \quad (C25)$$

- 
- [1] K. Symanzik, Nucl. Phys. **B226**, 187 (1983).  
[2] M. Bochicchio, L. Maiani, G. Martinelli, G. C. Rossi, and M. Testa, Nucl. Phys. **B262**, 331 (1985).  
[3] R. Sommer (2006), hep-lat/0611020.  
[4] T. Blum *et al.* (RBC), Phys. Rev. **D68**, 114506 (2003), hep-lat/0110075.  
[5] D. B. Kaplan, Phys. Lett. **B288**, 342 (1992), hep-lat/9206013.  
[6] Y. Shamir, Nucl. Phys. **B406**, 90 (1993), hep-lat/9303005.  
[7] V. Furman and Y. Shamir, Nucl. Phys. **B439**, 54 (1995), hep-lat/9405004.  
[8] R. Narayanan and H. Neuberger, Phys. Lett. **B302**, 62 (1993), hep-lat/9212019.  
[9] H. Neuberger, Phys. Lett. **B417**, 141 (1998), hep-lat/9707022.  
[10] P. Hasenfratz, V. Laliena, and F. Niedermayer, Phys. Lett. **B427**, 125 (1998), hep-lat/9801021.  
[11] R. Frezzotti, P. A. Grassi, S. Sint, and P. Weisz (Alpha), JHEP **08**, 058 (2001), hep-lat/0101001.  
[12] J. Gasser and H. Leutwyler, Ann. Phys. **158**, 142 (1984).  
[13] J. Gasser and H. Leutwyler, Nucl. Phys. **B250**, 465 (1985).  
[14] T. Blum, Nucl. Phys. Proc. Suppl. **73**, 167 (1999), hep-lat/9810017.  
[15] Y. Aoki *et al.*, Phys. Rev. **D72**, 114505 (2005), hep-lat/0411006.  
[16] D. J. Antonio *et al.* (RBC and UKQCD), Phys. Rev. **D75**, 114501 (2007), hep-lat/0612005.  
[17] D. J. Antonio *et al.* (RBC and UKQCD) (2007), arXiv:0705.2340 [hep-lat].  
[18] P. A. Boyle *et al.* (2007), arXiv:0710.5136 [hep-lat].



- [19] D. J. Antonio *et al.* (RBC), Phys. Rev. Lett. **100**, 032001 (2008), hep-ph/0702042.
- [20] P. Boyle (RBC) (2007), arXiv:0710.5880 [hep-lat].
- [21] Y. Aoki *et al.* (2007), arXiv:0712.1061 [hep-lat].
- [22] S. R. Sharpe (2007), arXiv:0706.0218 [hep-lat].
- [23] T. Blum *et al.*, Phys. Rev. **D66**, 014504 (2002), hep-lat/0102005.
- [24] T. Blum *et al.*, Phys. Rev. **D69**, 074502 (2004), hep-lat/0007038.
- [25] O. Bar, G. Rupak, and N. Shoresh, Phys. Rev. **D70**, 034508 (2004), hep-lat/0306021.
- [26] J. Gasser, C. Haefeli, M. A. Ivanov, and M. Schmid, Phys. Lett. **B652**, 21 (2007), arXiv:0706.0955 [hep-ph].
- [27] A. Roessl, Nucl. Phys. **B555**, 507 (1999), hep-ph/9904230.
- [28] C. W. Bernard and M. F. L. Golterman, Phys. Rev. **D46**, 853 (1992), hep-lat/9204007.
- [29] C. W. Bernard and M. F. L. Golterman, Phys. Rev. **D49**, 486 (1994), hep-lat/9306005.
- [30] A. Morel, J. Phys. (France) **48**, 1111 (1987).
- [31] S. R. Sharpe (2006), lectures at ILFTN Workshop on Perspectives in Lattice QCD, Nara, Japan, 31 October–11 November, 2005, hep-lat/0607016.
- [32] S. R. Sharpe and Y. Zhang, Phys. Rev. **D53**, 5125 (1996), hep-lat/9510037.
- [33] B. Grinstein, E. E. Jenkins, A. V. Manohar, M. J. Savage, and M. B. Wise, Nucl. Phys. **B380**, 369 (1992), hep-ph/9204207.
- [34] C. Allton *et al.* (RBC and UKQCD), Phys. Rev. **D76**, 014504 (2007), hep-lat/0701013.
- [35] M. A. Clark and A. D. Kennedy, Phys. Rev. Lett. **98**, 051601 (2007), hep-lat/0608015.
- [36] A. D. Kennedy, I. Horvath, and S. Sint, Nucl. Phys. Proc. Suppl. **73**, 834 (1999), hep-lat/9809092.
- [37] C. Urbach, K. Jansen, A. Shindler, and U. Wenger, Comput. Phys. Commun. **174**, 87 (2006), hep-lat/0506011.
- [38] M. Hasenbusch and K. Jansen, Nucl. Phys. **B659**, 299 (2003), hep-lat/0211042.
- [39] M. A. Clark, PoS **LAT2006**, 004 (2006), hep-lat/0610048.
- [40] P. de Forcrand, M. Garcia Perez, and I.-O. Stamatescu, Nucl. Phys. **B499**, 409 (1997), hep-lat/9701012.
- [41] P. Boyle (UKQCD), J. Comput. Phys. **179**, 349 (2002), hep-lat/9903033.
- [42] M. Lin and E. E. Scholz (RBC and UKQCD), PoS **LATTICE2007**, 120 (2007), arXiv:0710.0536 [hep-lat].
- [43] D. Toussaint and C. T. H. Davies, Nucl. Phys. Proc. Suppl. **140**, 234 (2005), hep-lat/0409129.

- [44] B. C. Tiburzi and A. Walker-Loud, Nucl. Phys. **A748**, 513 (2005), hep-lat/0407030.
- [45] K. Sasaki and S. Sasaki, Phys. Rev. **D72**, 034502 (2005), hep-lat/0503026.
- [46] S. R. Sharpe and N. Shoresh, Phys. Rev. **D62**, 094503 (2000), hep-lat/0006017.
- [47] F. Farchioni, C. Gebert, I. Montvay, E. Scholz, and L. Scorzato (qq+q), Phys. Lett. **B561**, 102 (2003), hep-lat/0302011.
- [48] M. J. Booth, Phys. Rev. **D51**, 2338 (1995), hep-ph/9411433.
- [49] H.-W. Lin and N. Christ, Phys. Rev. **D76**, 074506 (2007), hep-lat/0608005.
- [50] N. H. Christ, M. Li, and H.-W. Lin, Phys. Rev. **D76**, 074505 (2007), hep-lat/0608006.
- [51] M. Li and H.-W. Lin (2007), arXiv:0710.0910 [hep-lat].
- [52] G. Martinelli, C. Pittori, C. T. Sachrajda, M. Testa, and A. Vladikas, Nucl. Phys. **B445**, 81 (1995), hep-lat/9411010.
- [53] W. M. Yao *et al.* (Particle Data Group), J. Phys. **G33**, 1 (2006).
- [54] I. S. Towner and J. C. Hardy (2007), arXiv:0710.3181 [nucl-th].
- [55] W. J. Marciano, Phys. Rev. Lett. **93**, 231803 (2004), hep-ph/0402299.
- [56] J. Gasser and H. Leutwyler, Phys. Lett. **B184**, 83 (1987).
- [57] J. Gasser and H. Leutwyler, Phys. Lett. **B188**, 477 (1987).
- [58] J. Gasser and H. Leutwyler, Nucl. Phys. **B307**, 763 (1988).
- [59] C. Bernard (MILC), Phys. Rev. **D65**, 054031 (2002), hep-lat/0111051.
- [60] C. Aubin and C. Bernard, Phys. Rev. **D68**, 034014 (2003), hep-lat/0304014.
- [61] C. Aubin and C. Bernard, Phys. Rev. **D68**, 074011 (2003), hep-lat/0306026.
- [62] G. Colangelo, S. Durr, and C. Haefeli, Nucl. Phys. **B721**, 136 (2005), hep-lat/0503014.
- [63] J. Bijnens, G. Colangelo, and P. Talavera, JHEP **05**, 014 (1998), hep-ph/9805389.
- [64] G. Colangelo, J. Gasser, and H. Leutwyler, Nucl. Phys. **B603**, 125 (2001), hep-ph/0103088.
- [65] C. Aubin *et al.* (MILC), Phys. Rev. **D70**, 114501 (2004), hep-lat/0407028.
- [66] C. Bernard *et al.* (2007), arXiv:0710.1118 [hep-lat].
- [67] L. Del Debbio, L. Giusti, M. Luscher, R. Petronzio, and N. Tantalo, JHEP **02**, 056 (2007), hep-lat/0610059.
- [68] C. Urbach (2007), arXiv:0710.1517 [hep-lat].
- [69] T. Blum, T. Doi, M. Hayakawa, T. Izubuchi, and N. Yamada, Phys. Rev. **D76**, 114508 (2007), arXiv:0708.0484 [hep-lat].
- [70] B. Blossier *et al.* (European Twisted Mass) (2007), arXiv:0709.4574 [hep-lat].

- [71] M. Gockeler *et al.*, Phys. Rev. **D73**, 054508 (2006), hep-lat/0601004.
- [72] N. Ukita *et al.* (PACS-CS) (2007), arXiv:0710.3462 [hep-lat].
- [73] T. Ishikawa *et al.* (JLQCD) (2007), arXiv:0704.1937 [hep-lat].
- [74] G. Colangelo and S. Durr, Eur. Phys. J. **C33**, 543 (2004), hep-lat/0311023.
- [75] H. Leutwyler (2007), arXiv:0706.3138 [hep-ph].
- [76] J. Bijnens, N. Danielsson, and T. A. Lahde, Phys. Rev. **D73**, 074509 (2006), hep-lat/0602003.
- [77] M. Lin, *Hadron physics with 2+1 flavors of domain wall fermions on the lattice*, Ph.D. thesis, Columbia University (2007).
- [78] J. Bijnens (2007), arXiv:0708.1377 [hep-lat].
- [79] S. D. Cohen and J. Noaki (RBC and UKQCD), PoS **LAT2006**, 080 (2006).
- [80] S. D. Cohen and D. J. Antonio (RBC and UKQCD), PoS **LATTICE2007**, 347 (2007).
- [81] D. Becirevic and G. Villadoro, Phys. Rev. **D69**, 054010 (2004), hep-lat/0311028.
- [82] A. Ali Khan *et al.* (CP-PACS), Phys. Rev. **D64**, 114506 (2001), hep-lat/0105020.
- [83] J. Bijnens, E. Gamiz, and J. Prades, JHEP **03**, 048 (2006), hep-ph/0601197.
- [84] J. Prades, C. A. Dominguez, J. A. Penarrocha, A. Pich, and E. de Rafael, Z. Phys. **C51**, 287 (1991).
- [85] M. A. Donnellan *et al.* (2007), arXiv:0710.0869 [hep-lat].
- [86] D. Becirevic, V. Lubicz, F. Mescia, and C. Tarantino, JHEP **05**, 007 (2003), hep-lat/0301020.
- [87] P. Ball, G. W. Jones, and R. Zwicky, Phys. Rev. **D75**, 054004 (2007), hep-ph/0612081.
- [88] P. Ball and R. Zwicky, Phys. Rev. **D71**, 014015 (2005), hep-ph/0406232.
- [89] M. Beneke, T. Feldmann, and D. Seidel, Nucl. Phys. **B612**, 25 (2001), hep-ph/0106067.
- [90] S. W. Bosch and G. Buchalla, Nucl. Phys. **B621**, 459 (2002), hep-ph/0106081.
- [91] A. Ali, B. D. Pecjak, and C. Greub (2007), arXiv:0709.4422 [hep-ph].
- [92] M. Beneke and M. Neubert, Nucl. Phys. **B675**, 333 (2003), hep-ph/0308039.
- [93] M. Gockeler *et al.*, PoS **LAT2005**, 063 (2006), hep-lat/0509196.
- [94] A. A. K. et al (CP-PACS), Phys. Rev. **D64**, 114506 (2001), hep-lat/0105020.
- [95] P. Boyle *et al.*, IBM Journal of Research and Development **49**, number **2/3**, 351 (2005).
- [96] P. A. Boyle, C. Jung, and T. Wettig (QCDOC), ECONF **C0303241**, THIT003 (2003), hep-lat/0306023.
- [97] P. A. Boyle *et al.*, J. Phys. Conf. Ser. **16**, 129 (2005).
- [98] R. S. Van de Water and S. R. Sharpe, Phys. Rev. **D73**, 014003 (2006), hep-lat/0507012.
- [99] S. R. Sharpe, Phys. Rev. **D56**, 7052 (1997), [Erratum-ibid. D **62**, 099901 (2000)], hep-lat/9707018.

- [100] V. M. Braun *et al.*, Phys. Rev. **D68**, 054501 (2003), hep-lat/0306006.
- [101] V. Bernard and E. Passemar (2007), arXiv:0711.3450 [hep-ph].
- [102] In a recent publication [101] an updated measurement of the CKM matrix element  $V_{ud} = 0.97418(26)$  [54] from super-allowed nuclear  $\beta$ -decays has been used to determine  $f_K/f_\pi = 1.192(07)$  and  $f_\pi = 130.5(0.1)$  MeV resulting in  $f_K = 155.6(0.9)$  MeV. (There  $1 = V_{ud}^2 + V_{us}^2$  has been assumed, resulting in  $V_{us} = 0.2258(11)$ .)

TABLE I: Improvements to the RHMC algorithm were implemented as the ensemble generation progressed. The table details the algorithms used for each ensemble and the range, in molecular dynamics (MD) time, where measurements were made.

$m_l$	RHMC	MD range	Measurement range
0.005	II	0-4435	900-4460
	0	0-549	
0.01	I	550-1454	
	II	1455-5020	1460-5020
	0	0-1519	
0.02	I	1520-1884	
	II	1885-3610	1800-3560
	0	0-492	
0.03	I	493-929	
	II	930-3060	1260-3040

TABLE II: Calculation parameters for the three separate datasets FPQ, DEG and UNI. The range and measurement separation  $\Delta$  are specified in molecular dynamics time units.  $N_{\text{meas}}$  is the number of measurements for each source position  $t_{\text{src}}$ . The total number of measurements is therefore  $N_{\text{meas}} \times N_{\text{src}}$ , where  $N_{\text{src}}$  is the number of different values for  $t_{\text{src}}$ .

$m_l$	Dataset	Range	$\Delta$	$N_{\text{meas}}$	$t_{\text{src}}$ locations
0.005	FPQ	900-4460	40	90	5, 59
	DEG	900-4460	40	90	0, 32
	UNI	900-4480	20	180	0, 32, 16
0.01	FPQ	1460-5020	40	90	5, 59
	DEG	1460-5020	40	90	0, 32
	UNI	800-3940	10	315	0, 32
0.02	DEG	1800-3560	40	45	0, 32
	UNI	1800-3580	20	90	0, 32
0.03	DEG	1260-3020	40	45	0, 32
	UNI	1260-3040	20	90	0, 32

TABLE III: Combinations of quark source and sink smearings used for correlation functions for each of the datasets FPQ, DEG and UNI.  $A$  is the time component of the axial current density operator and  $P$  is the pseudoscalar density operator. XY-XY denotes the contraction of two quark propagators with X-type smearing at source and a Y-type smearing at sink. W=wall source, B=box source, H=hydrogen S-wave and L=local.

Operator Type	Dataset		
$\langle \mathcal{O}_{snk} \mathcal{O}_{src} \rangle$	FPQ	DEG	UNI
$\langle A, A \rangle$	WL-WL	BL-BL	HL-HL LL-LL
$\langle P, A \rangle$			HL-HL LL-LL
$\langle A, P \rangle$	WL-WL WW-WW	BL-BL BB-BB	HL-HL LL-LL
$\langle P, P \rangle$	WL-WL WW-WW	BL-BL	HL-HL LL-LL

TABLE IV: The different source and sink contraction of the quark propagators for the UNI dataset.  $V = \gamma_i$  ( $i = 1, 2, 3$ ) is one of the spatial components of the vector current and  $T = \sigma_{4i}$  are the calculated components of the tensor current. XY-XY denotes contraction of two quark propagators with a X-type smearing at source and a Y-type smearing at sink. H=hydrogen S-wave, G=Gaussian wave function (cf. [16]), and L=point.

Contraction	UNI Dataset	
$\langle \mathcal{O}_{snk} \mathcal{O}_{src} \rangle$	m=0.005, 0.02, 0.03	m=0.01
$\langle V, V \rangle$	HL-HL LL-HL HL-LL	GL-GL LL-GL GL-LL
$\langle T, V \rangle$	HL-HL LL-HL HL-LL	GL-GL LL-GL GL-LL

TABLE V: Lattice values for the pseudoscalar meson mass and  $\chi^2/\text{d.o.f.}$  calculated from an *uncorrelated* simultaneous fit to five correlators of the FPQ dataset on  $m_l = 0.005$  and  $m_l = 0.01$  ensembles.

$m_x$	$m_y$	$m_l = 0.005$		$m_l = 0.01$	
		$m_{xy}$	$\chi^2/\text{d.o.f.}$	$m_{xy}$	$\chi^2/\text{d.o.f.}$
0.001	0.001	0.1402(9)	0.36(7)	0.1432(10)	0.18(6)
0.001	0.005	0.1680(8)	0.38(8)	0.1706(9)	0.21(6)
0.005	0.005	0.1915(8)	0.39(9)	0.1938(8)	0.25(6)
0.001	0.010	0.1971(8)	0.38(8)	0.1994(9)	0.26(7)
0.005	0.010	0.2172(8)	0.38(9)	0.2194(8)	0.25(7)
0.010	0.010	0.2400(7)	0.36(9)	0.2421(7)	0.24(7)
0.001	0.020	0.2449(9)	0.36(9)	0.2473(9)	0.30(8)
0.005	0.020	0.2611(8)	0.34(9)	0.2635(8)	0.24(8)
0.010	0.020	0.2802(7)	0.31(8)	0.2825(7)	0.22(7)
0.020	0.020	0.3155(7)	0.26(8)	0.3178(6)	0.23(8)
0.001	0.030	0.2850(10)	0.33(10)	0.2877(10)	0.33(10)
0.005	0.030	0.2990(8)	0.32(9)	0.3016(8)	0.26(9)
0.010	0.030	0.3158(7)	0.28(8)	0.3183(7)	0.24(8)
0.020	0.030	0.3477(6)	0.23(7)	0.3500(6)	0.26(10)
0.030	0.030	0.3775(6)	0.21(8)	0.3797(6)	0.29(11)
0.001	0.040	0.3204(11)	0.34(13)	0.3234(11)	0.36(12)
0.005	0.040	0.3329(8)	0.31(10)	0.3358(8)	0.31(11)
0.010	0.040	0.3482(7)	0.26(8)	0.3508(7)	0.29(11)
0.020	0.040	0.3776(6)	0.22(8)	0.3800(6)	0.30(12)
0.030	0.040	0.4055(6)	0.21(8)	0.4077(5)	0.32(13)
0.040	0.040	0.4320(6)	0.21(9)	0.4341(5)	0.34(13)



TABLE VI: Lattice values for the pseudoscalar decay constant calculated using method described in Eq. (92).

$m_x$	$m_y$	$f_{xy}(m_l = 0.005)$	$f_{xy}(m_l = 0.01)$
0.001	0.001	0.0829(7)	0.0860(7)
0.001	0.005	0.0846(7)	0.0878(6)
0.005	0.005	0.0860(6)	0.0891(6)
0.001	0.010	0.0867(7)	0.0900(6)
0.005	0.010	0.0880(6)	0.0910(6)
0.010	0.010	0.0898(6)	0.0928(6)
0.001	0.020	0.0904(7)	0.0928(7)
0.005	0.020	0.0915(6)	0.0946(6)
0.010	0.020	0.0934(6)	0.0962(6)
0.020	0.020	0.0969(6)	0.0995(5)
0.001	0.030	0.0936(8)	0.0972(8)
0.005	0.030	0.0947(6)	0.0979(6)
0.010	0.030	0.0965(6)	0.0994(6)
0.020	0.030	0.1001(6)	0.1025(5)
0.030	0.030	0.1033(6)	0.1056(5)
0.001	0.040	0.0965(8)	0.1003(8)
0.005	0.040	0.0975(7)	0.1008(7)
0.010	0.040	0.0993(6)	0.1022(6)
0.020	0.040	0.1029(6)	0.1053(5)
0.030	0.040	0.1062(6)	0.1083(5)
0.040	0.040	0.1091(7)	0.1111(5)

TABLE VII: Lattice values for the pseudoscalar meson mass and  $\chi^2/\text{d.o.f.}$  calculated from an *uncorrelated* simultaneous fit to four correlators of the DEG dataset on  $m_l = 0.02$  and  $m_l = 0.03$  ensembles.

$m_x$	$m_l = 0.02$		$m_l = 0.03$	
	$m_{xx}$	$\chi^2/\text{d.o.f.}$	$m_{xx}$	$\chi^2/\text{d.o.f.}$
0.001	0.1493(11)	0.7(4)	-	-
0.005	0.1993(9)	0.5(3)	0.2016(11)	0.4(1)
0.010	0.2471(8)	0.4(2)	0.2500(10)	0.3(1)
0.020	0.3227(7)	0.3(2)	0.3261(9)	0.3(1)
0.030	0.3849(6)	0.4(2)	0.3884(9)	0.2(1)
0.040	0.4396(6)	0.4(2)	0.4429(8)	0.2(1)

TABLE VIII: Lattice values for the pseudoscalar decay constant calculated using method described in Eq. (93).

$m_x$	$f_{xx}(m_l = 0.02)$	$f_{xx}(m_l = 0.03)$
0.001	0.0926(18)	-
0.005	0.0947(15)	0.0961(14)
0.010	0.0969(13)	0.0985(13)
0.020	0.1021(11)	0.1038(12)
0.030	0.1077(10)	0.1092(11)
0.040	0.1133(9)	0.1145(10)

TABLE IX: Decuplet baryon masses for degenerate valence quarks. “traj.” refers to the Monte Carlo trajectories used for measurements. Numbers in ()’s give the total number of measurements, separated by 40 trajectories in each case. To reduce effects of auto-correlations, the measurements were block-averaged into bins of size 80 trajectories before fitting.

$m_l$	$m_x$	traj. (# meas)	$\chi^2/\text{d.o.f.}$	mass
0.005	0.03	900-4460 (90), 920-4480 (90)	0.5(7)	0.9647(65)
0.005	0.04		0.6(8)	1.016(51)
0.01	0.03	1460-5020 (90), 1480-4040 (65)	1.1(1.1)	0.9809(88)
0.01	0.04		1.2(1.2)	1.033(60)
0.02	0.03	1600-3600 (50), 1900-3580 (43)	1.7(1.6)	1.030(11)
0.02	0.04		2.0(1.8)	1.074(10)
0.03	0.03	1020-3060 (52), 1320-3040 (44)	1.4(1.7)	1.040(10)
0.03	0.04		1.8(2.2)	1.082(6)

TABLE X: Low energy constants obtained from  $SU(2) \times SU(2)$  fits with a valence mass cut  $m_{\text{avg}} \leq 0.01$ . For convenience the LECs  $L_i^{(2)}$  are quoted in units of  $10^{-4}$  at two different chiral scales,  $\Lambda_\chi = 770$  MeV and 1 GeV. The definitions of the low energy constants are given in the Appendix. (Only statistical errors are quoted.)

$B$		$f$	$\bar{l}_3$	$\bar{l}_4$
2.414(61)		0.0665(21)	3.13(.33)	4.43(.14)
$\Lambda_\chi$	$L_4^{(2)}$	$L_5^{(2)}$	$(2L_6^{(2)} - L_4^{(2)})$	$(2L_8^{(2)} - L_5^{(2)})$
770 MeV	3.3(1.3)	9.30(.73)	0.32(.62)	0.50(.43)
1 GeV	1.3(1.3)	5.16(.73)	-0.71(.62)	4.64(.43)

TABLE XI: Lattice scale and unrenormalized quark masses in lattice units. Note  $\tilde{m}_X \equiv m_X + m_{\text{res}}$ . Only the statistical errors are given here.

$a^{-1}$ [GeV]	$a$ [fm]	$m_{ud}$	$\tilde{m}_{ud}$	$m_s$	$\tilde{m}_s$	$\tilde{m}_{ud} : \tilde{m}_s$
1.729(28)	0.1141(18)	-0.001847(58)	0.001300(58)	0.0343(16)	0.0375(16)	1:28.8(4)

TABLE XII: Central value and statistical error (stat) for the fit parameters from SU(2) ChPT and systematic error estimates from four sources. These are: finite-volume effects (FV), lattice artefacts ( $a^2$ ), the chiral extrapolation in the light quark masses (ChPT) and the unphysical value of the dynamical strange quark mass ( $m_s$ ). For details we refer to Sec. VIC. The LECs are quoted here only at a scale  $\Lambda_\chi = 1$  GeV, but the absolute value of the error is independent of  $\Lambda_\chi$ . The total systematic error is obtained by adding the separate errors in quadrature, neglecting any possible correlations between them.

	value	stat	systematic errors				total
			FV	$a^2$	ChPT	$m_s$	
$B$	2.414	(.061)	(.049)	(.097)	(.034)	(.017)	(.115)
$f$	0.0665	(21)	(13)	(27)	(36)	(01)	(47)
$(2L_6^{(2)} - L_4^{(2)}) \cdot 10^4$	-0.7	(0.6)	(0.1)	(-)	(1.8)	(-)	(1.8)
$(2L_8^{(2)} - L_5^{(2)}) \cdot 10^4$	4.64	(.43)	(.95)	(-)	(3.20)	(-)	(3.34)
$L_4^{(2)} \cdot 10^4$	1.3	(1.3)	(0.3)	(-)	(1.8)	(-)	(1.8)
$L_5^{(2)} \cdot 10^4$	5.16	(.73)	(.16)	(-)	(8.20)	(-)	(8.20)
$\bar{l}_3$	3.13	(.33)	(.20)	(.08)	(.10)	(.02)	(.24)
$\bar{l}_4$	4.43	(.14)	(.05)	(.08)	(.76)	(.04)	(.77)
$\tilde{m}_{ud}$	0.001300	(58)	(23)	(52)	(22)	(09)	(62)
$\tilde{m}_s$	0.0375	(16)	(00)	(15)	(04)	(08)	(17)
$\tilde{m}_{ud} : \tilde{m}_s$	1:28.8	(0.4)	(0.5)	(1.2)	(0.6)	(0.6)	(1.6)
$f_\pi$ [MeV]	124.1	(3.6)	(1.9)	(5.0)	(4.4)	(0.2)	(6.9)
$f_K$ [MeV]	149.6	(3.6)	(0.4)	(6.0)	(1.0)	(1.5)	(6.3)
$f_K/f_\pi$	1.205	(18)	(14)	(48)	(34)	(12)	(62)

TABLE XIII: Finite volume correction factors obtained from the SU(2) and SU(3) PQChPT fits compared to the prediction by Colangelo, Dürer, and Haefeli (CDH) [62] at the unitary pion masses of 331 MeV ( $m_x = m_y = m_l = 0.005$ ) and 419 MeV ( $m_x = m_y = m_l = 0.01$ ).

$m_\pi$ [MeV]	$R_m$ [%]			$-R_f$ [%]		
	SU(2)	SU(3)	CDH	SU(2)	SU(3)	CDH
331	0.09(.01)	0.14(.04)	0.13(.04)	0.36(.03)	0.56(.16)	0.32(.00)
419	0.03(.00)	0.04(.01)	0.04(.01)	0.10(.01)	0.17(.05)	0.09(.00)

TABLE XIV: The measured pion mass and decay constant at  $m_x = m_y = m_l = 0.01$ ,  $m_h = 0.04$  at two different volumes (for  $16^3$  data see [34]). We compare directly the measured ratio to the predictions from SU(2) and SU(3) ChPT and the value interpolated from Colangelo, Dürri, and Haefeli (CDH) [62]. For explanation see Eq. (109) and text.

	measured			$\frac{1-R^{(16c)}}{1-R^{(24c)}}$		
	$24^3$	$16^3$	ratio	SU(2)	SU(3)	CDH
$m_\pi$	0.24211(75)	0.247(3)	0.980(12)	0.9961(04)	0.9944(15)	0.9942(22)
$f_\pi$	0.0928(6)	0.0895(7)	1.037(11)	1.0155(14)	1.0252(70)	1.0118(03)

TABLE XV: Comparison of the SU(2) NLO-LEC  $\bar{l}_3$  and  $\bar{l}_4$  (defined at a scale of 139 MeV, cf. Eq. (B44)) with results from other  $N_f = 2 + 1$  and  $N_f = 2$  lattice simulations [66, 67, 68] and a phenomenological estimate [64].

	$N_f$	type	$\bar{l}_3$	$\bar{l}_4$
this work, direct SU(2) fit	2+1	DWF	3.13(.33)(.24)	4.43(.14)(.77)
this work, conv. from SU(3)	2+1	DWF	2.87(.28)(-)	4.10(.05)(-)
MILC <sup>a</sup>	2+1	stagg	2.85(.07)(-)	-
MILC <sup>b</sup>	2+1	stagg	0.6(1.2)	3.9(0.5)
ETMC [68]	2	TM-Wilson	3.44(.08)(.35)	4.61(.04)(.11)
CERN [67]	2	impr. Wilson	3.0(0.5)(0.1)	4.1(0.1)(-)
				3.3(0.8)(-) <sup>c</sup>
phenom.[64]			2.9(2.4)	4.4(0.2)

<sup>a</sup>direct SU(2) fit, from [66]

<sup>b</sup>converted from SU(3), see [75]

<sup>c</sup>First number obtained without additional NNLO-term, second number from fit including NNLO-term, see [67] for details.

TABLE XVI: Comparison of light physical quark masses and their ratio obtained from recent lattice simulations using various types of fermion discretizations and different renormalization techniques (non-perturbative and perturbative). (In the cases where no error is given for the quark mass ratio, no error was quoted in the cited work. Since we do not know the correlations, we could not provide the error estimate here.)

	$N_f$	type	$m_{ud}^{\overline{\text{MS}}}(2\text{ GeV})[\text{MeV}]$	$m_s^{\overline{\text{MS}}}(2\text{ GeV})[\text{MeV}]$	$m_s : m_{ud}$
using non-perturbative renormalization					
this work	2+1	DWF	$3.72(0.16)_{\text{stat}}(0.33)_{\text{ren}}(0.18)_{\text{syst}}$	$107.3(4.4)_{\text{stat}}(9.7)_{\text{ren}}(4.9)_{\text{syst}}$	$28.8(0.4)_{\text{stat}}(1.6)_{\text{syst}}$
RBC [69]	2	DWF	$4.25(0.23)_{\text{stat}}(0.26)_{\text{ren}}$	$119.5(5.6)_{\text{stat}}(7.4)_{\text{ren}}$	$28.10(0.38)_{\text{stat}}$
ETMC [70]	2	TM-Wilson	$3.85(0.12)_{\text{stat}}(0.40)_{\text{syst}}$	$105(3)_{\text{stat}}(9)_{\text{syst}}$	$27.3(0.3)_{\text{stat}}(1.2)_{\text{syst}}$
QCDSF [71]	2	impr. Wilson	$4.08(0.23)_{\text{stat}}(0.19)_{\text{syst}}(0.23)_{\text{scale}}$	$111(6)_{\text{stat}}(4)_{\text{syst}}(6)_{\text{scale}}$	$27.2(3.2)$
using perturbative renormalization					
MILC [66]	2+1	stagg.	$3.2(0)_{\text{stat}}(0.1)_{\text{ren}}(0.2)_{\text{EM}}(0)_{\text{cont}}$	$88(0)_{\text{stat}}(3)_{\text{ren}}(4)_{\text{EM}}(0)_{\text{cont}}$	$27.2(0.1)_{\text{stat}}(0.3)_{\text{syst}}$
PACS-CS [72]	2+1	impr. Wilson	$2.3(1.1)$	$69.1(2.5)$	$30(?)$
JLQCD [73]	2+1	impr. Wilson	$3.54(^{+.64}_{-.35})_{\text{total}}$	$91.1(^{+14.6}_{-6.2})_{\text{total}}$	$25.7(?)$

TABLE XVII: Fitted parameters from  $SU(3) \times SU(3)$  fits with a valence mass cut  $m_{\text{avg}} \leq 0.01$ . For convenience the LECs  $L_i^{(3)}$  are quoted in units of  $10^{-4}$  at two different chiral scales,  $\Lambda_\chi = 770$  MeV and 1 GeV. The definitions of the low energy constants are given in the Appendix. (Only statistical errors are quoted here.)

		$B_0 = 2.35(.16)$		$f_0 = 0.0541(40)$	
$\Lambda_\chi$	$L_4^{(3)}$	$L_5^{(3)}$	$(2L_6^{(3)} - L_4^{(3)})$	$(2L_8^{(3)} - L_5^{(3)})$	
770 MeV	1.39(.80)	8.72(.99)	-0.01(.42)	2.43(.45)	
1 GeV	-0.67(.80)	2.51(.99)	-0.47(.42)	5.19(.45)	



TABLE XVIII:  $SU(2) \times SU(2)$  low energy constants obtained directly from the  $SU(2) \times SU(2)$  fits compared to those converted from the  $SU(3) \times SU(3)$  chiral fits with a mass cut of  $m_{\text{avg}} \leq 0.01$ .

	$B$	$f$	$\bar{l}_3$	$\bar{l}_4$
direct $SU(2) \times SU(2)$	2.414(61)	0.0665(21)	3.13(.33)	4.43(.14)
converted $SU(3) \times SU(3)$	2.457(78)	0.0661(18)	2.87(.28)	4.10(.05)

TABLE XIX: Comparison of fitted  $SU(3)$  NLO-LECs  $L_i^{(3)}$  at  $\Lambda_\chi = 770\text{MeV}$  in units of  $10^{-4}$  to phenomenologically obtained values by Bijmans (see Table 2 in [78]) and dynamical  $N_f = 2 + 1$  staggered lattice simulation (MILC), [65] and [66] (there, LECs were quoted at  $\Lambda_\chi = m_\eta$ , conversion was done according to Eq. (B20).)

	$L_4^{(3)}$	$L_5^{(3)}$	$L_6^{(3)}$	$L_8^{(3)}$	$(2L_8^{(3)} - L_5^{(3)})$	$(2L_6^{(3)} - L_4^{(3)})$
this work <sup>a</sup>	1.4(0.8)(-)	8.7(1.0)(-)	0.7(0.6)(-)	5.6(0.4)(-)	2.4(0.4)(-)	0.0(0.4)(-)
Bijmans, NLO	$\equiv 0$	14.6	$\equiv 0$	10.0	5.4	$\equiv 0$
Bijmans, NNLO	$\equiv 0$	9.7(1.1)	$\equiv 0$	6.0(1.8)	2.3 <sup>b</sup>	$\equiv 0$
MILC, 2007	1.3(3.0)( $^{+3.0}_{-1.0}$ )	13.9(2.0)( $^{+2.0}_{-1.0}$ )	2.4(2.0)( $^{+2.0}_{-1.0}$ )	7.8(1.0)(1.0)	2.6(1.0)(1.0)	3.4(1.0)( $^{+2.0}_{-3.0}$ )

<sup>a</sup>For reasons mentioned in Sec. VII B, we do not quote any systematic error for parameters obtained from the  $SU(3)$  fits.

<sup>b</sup>This value was derived from the quoted single values for  $L_5^{(3)}$  and  $L_8^{(3)}$ ; since we do not know the correlation between those two, we cannot provide the error estimate.

TABLE XX: Pseudoscalar B-parameter  $B_{xy}$  for pseudoscalar mesons with valence masses  $m_x, m_y$  for two different values of the light sea quark mass  $m_l$  ( $m_h = 0.04$ ) on  $24^3 \times 64$  lattices, fit range 12–52 (uncorrelated fit)

$m_x$	$m_y$	$B_{xy}$	
		$m_l = 0.005$	$m_l = 0.01$
0.001	0.001	0.4691(83)	0.4698(53)
0.005	0.001	0.4910(66)	0.4953(41)
	0.005	0.5079(46)	0.5119(32)
0.01	0.001	0.5136(57)	0.5209(39)
	0.005	0.5267(37)	0.5312(28)
	0.01	0.5421(29)	0.5459(25)
0.02	0.001	0.5494(52)	0.5593(42)
	0.005	0.5588(31)	0.5629(26)
	0.01	0.5697(25)	0.5727(23)
	0.02	0.5911(23)	0.5935(20)
0.03	0.001	0.5777(55)	0.5886(54)
	0.005	0.5850(32)	0.5884(28)
	0.01	0.5933(26)	0.5957(22)
	0.02	0.6105(23)	0.6126(18)
	0.03	0.6267(22)	0.6287(16)
0.04	0.001	0.6012(64)	0.6131(73)
	0.005	0.6070(38)	0.6105(33)
	0.01	0.6137(30)	0.6160(24)
	0.02	0.6280(23)	0.6299(18)
	0.03	0.6418(21)	0.6435(15)
	0.04	0.6550(19)	0.6565(14)

TABLE XXI: Pseudoscalar B-parameter  $B_{xy}$  for pseudoscalar mesons with valence masses  $m_x, m_y$  for three different values of the light sea quark mass  $m_l$  ( $m_h = 0.04$ ) on  $16^3 \times 32$  lattices, fit range 12–20 (uncorrelated fit)

$m_x$	$m_y$	$B_{xy}$		
		$m_l = 0.01$	$m_l = 0.02$	$m_l = 0.03$
0.01	0.01	0.546(8)	0.539(8)	0.527(7)
0.02	0.01	0.577(6)	0.569(6)	0.556(6)
	0.02	0.598(5)	0.589(5)	0.580(5)
0.03	0.01	0.600(6)	0.594(6)	0.579(5)
	0.02	0.617(4)	0.609(5)	0.600(4)
	0.03	0.633(4)	0.626(4)	0.618(3)
0.04	0.01	0.620(5)	0.616(6)	0.599(5)
	0.02	0.633(4)	0.627(4)	0.618(4)
	0.03	0.647(4)	0.641(4)	0.634(3)
	0.04	0.659(3)	0.655(3)	0.648(3)
0.05	0.01	0.636(5)	0.634(6)	0.616(4)
	0.02	0.648(4)	0.643(4)	0.634(3)
	0.03	0.660(3)	0.655(3)	0.648(3)
	0.04	0.671(3)	0.667(3)	0.661(3)
	0.05	0.682(3)	0.679(3)	0.673(3)

TABLE XXII: Parameters and  $\chi^2/\text{d.o.f.}$  for fits of  $B_{xy}$  to Eq. (B48) as shown in Fig. 19. The parameters  $B = 2.414(61)$  and  $f = 0.0665(21)$  were fixed from combined  $\text{SU}(2) \times \text{SU}(2)$  meson masses and decay constants fits, Sec. VI;  $\Lambda_\chi = 1 \text{ GeV}$ .

$m_y$	$B_{\text{PS}}^{(K)}(m_y)$	$b_1(m_y)/f^2$	$b_2(m_y)/f^2$	$\chi^2/\text{d.o.f.}$	$B_{udy}$
0.02	0.513(10)	-5.2(1.6)	8.18(.65)	0.27	0.5249(86)
0.03	0.544(10)	-5.4(1.5)	6.85(.65)	0.20	0.5550(87)
0.04	0.568(11)	-5.4(1.7)	6.05(.71)	0.14	0.5789(97)

TABLE XXIII: Fit parameters for fits of  $B_{xy}$  to Eq. (B22) as shown in Fig. 21. Values are quoted for different cuts  $m_{\text{cut}}$  in the average valence mass value. The parameters  $B_0 = 2.35(.16)$  and  $f_0 = 0.0541(40)$  were fixed from combined  $SU(3) \times SU(3)$  meson masses and decay constants fits, Sec. VII;  $\Lambda_\chi = 1 \text{ GeV}$ .

$m_{\text{cut}}$	$B_{\text{PS}}^\chi$	$b$	$c$	$d$	$\chi^2/\text{d.o.f.}$	$B_K = B_{uds}$
0.01	0.266(26)	-4.5(1.6)	-0.20(.18)	0.68(.60)	1.8	0.484(15)
0.0125	0.249(24)	-2.5(1.5)	0.87(.13)	0.96(.61)	2.7	0.556(12)
0.015	0.232(22)	0.2(1.5)	0.43(.13)	1.25(.59)	5.4	0.546(11)
0.0175	0.223(22)	1.0(1.5)	0.94(.12)	1.49(.61)	6.1	0.570(12)
0.02	0.205(19)	4.2(1.4)	0.40(.10)	1.89(.58)	10.2	0.553(10)

TABLE XXIV: Finite volume comparison for the pseudoscalar bag parameter measured on  $16^3$  ( $\approx (1.8 \text{ fm})^3$ ) and  $24^3$  ( $\approx (2.7 \text{ fm})^3$ ) for dynamical quark masses  $m_l = 0.01$ ,  $m_h = 0.04$ .

$m_x$	$m_y$	$B_{xy}^{(16^3)}$	$B_{xy}^{(24^3)}$	$\left  B_{xy}^{(16^3)} - B_{xy}^{(24^3)} \right  / B_{xy}^{(24^3)}$
0.01	0.01	0.546(8)	0.5459(25)	0.0(1.5) %
0.02	0.01	0.577(6)	0.5727(23)	0.8(1.1)%
	0.02	0.598(5)	0.5935(20)	0.8(0.9)%
0.03	0.01	0.600(6)	0.5957(22)	0.7(1.1)%
	0.02	0.617(4)	0.6126(18)	0.7(0.7)%
	0.03	0.633(4)	0.6287(16)	0.7(0.7)%
0.04	0.01	0.620(5)	0.6160(24)	0.6(0.9)%
	0.02	0.633(4)	0.6299(18)	0.5(0.7)%
	0.03	0.647(4)	0.6435(15)	0.5(0.7)%
	0.04	0.659(3)	0.6565(14)	0.4(0.5)%

TABLE XXV: Results for the measured vector meson masses (DEG and UNI data sets).

$m_l^{\text{sea}}$	$m_x$	$m_y$	DEG	UNI
0.005	0.005	0.005	0.5053(58)	0.507(19)
	0.005	0.04		0.5591(75)
	0.04	0.04	0.6227(19)	0.6183(48)
0.01	0.01	0.01	0.5288(45)	0.527(17)
	0.01	0.04		0.5887(89)
	0.04	0.04	0.6295(18)	0.6319(48)
0.02	0.02	0.02	0.5789(55)	0.584(16)
	0.02	0.04		0.612(13)
	0.04	0.04	0.6453(33)	0.6453(84)
0.03	0.03	0.03	0.6317(33)	0.6239(76)
	0.03	0.04		0.6447(83)
	0.04	0.04	0.6622(27)	0.6609(69)

TABLE XXVI: Results for the measured of couplings  $f_V^T / f_V$ .

$am_q$	0.03	0.02	0.01	0.005	physical	$\chi^2/\text{d.o.f}$
$f_\rho^T / f_\rho$	0.6806(55)	0.6646(73)	0.645(13)	0.624(21)	0.619(15)	0.17
$f_{K^*}^T / f_{K^*}$	0.6893(55)	0.6781(56)	0.6667(43)	0.6570(68)	0.6498(62)	0.11
$f_\phi^T / f_\phi$	0.6947(36)	0.6933(38)	0.6881(22)	0.6866(32)	0.6838(33)	0.10

TABLE XXVII: Previous quenched lattice results for the ratio of tensor and vector decay constants.

Reference	$\frac{f_\rho^T(2\text{GeV})}{f_\rho}$	$\frac{f_{K^*}^T(2\text{GeV})}{f_{K^*}}$	$\frac{f_\phi^T(2\text{GeV})}{f_\phi}$
Becirevic et al. [86]	0.720(24) $^{(+16)}_{(-00)}$	0.739(17) $^{(+3)}_{(-0)}$	0.759(9)(0)
Braun et al. [100]	0.742(14)	—	0.780(8)

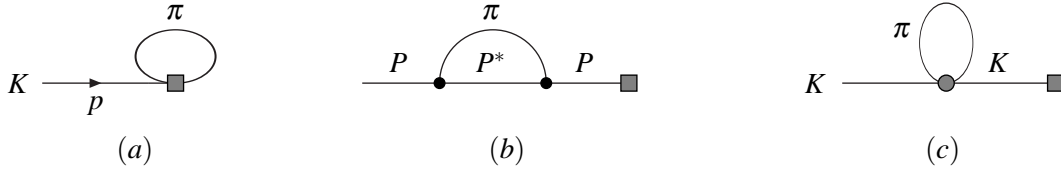


FIG. 1: (a) One loop correction to  $f_K$ ; (b) one-loop wavefunction-like contribution proportional to  $g^2$ ; (c) diagram contributing to the one-loop wavefunction (and mass) renormalization. The grey square denotes a flavor-changing axial-vector current operator, the black bullets in (b) represent the  $PP^*\pi$  vertex and the grey circle in (c) denotes a  $KK\pi\pi$  vertex from  $L_{\pi K}^{(1)}$  in Eq. (22).

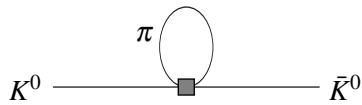


FIG. 2: One-loop contribution to  $B_K$ . The grey box denotes the insertion of the  $KK\pi\pi$  operator  $\mathcal{O}_{22}$  as defined in the text.



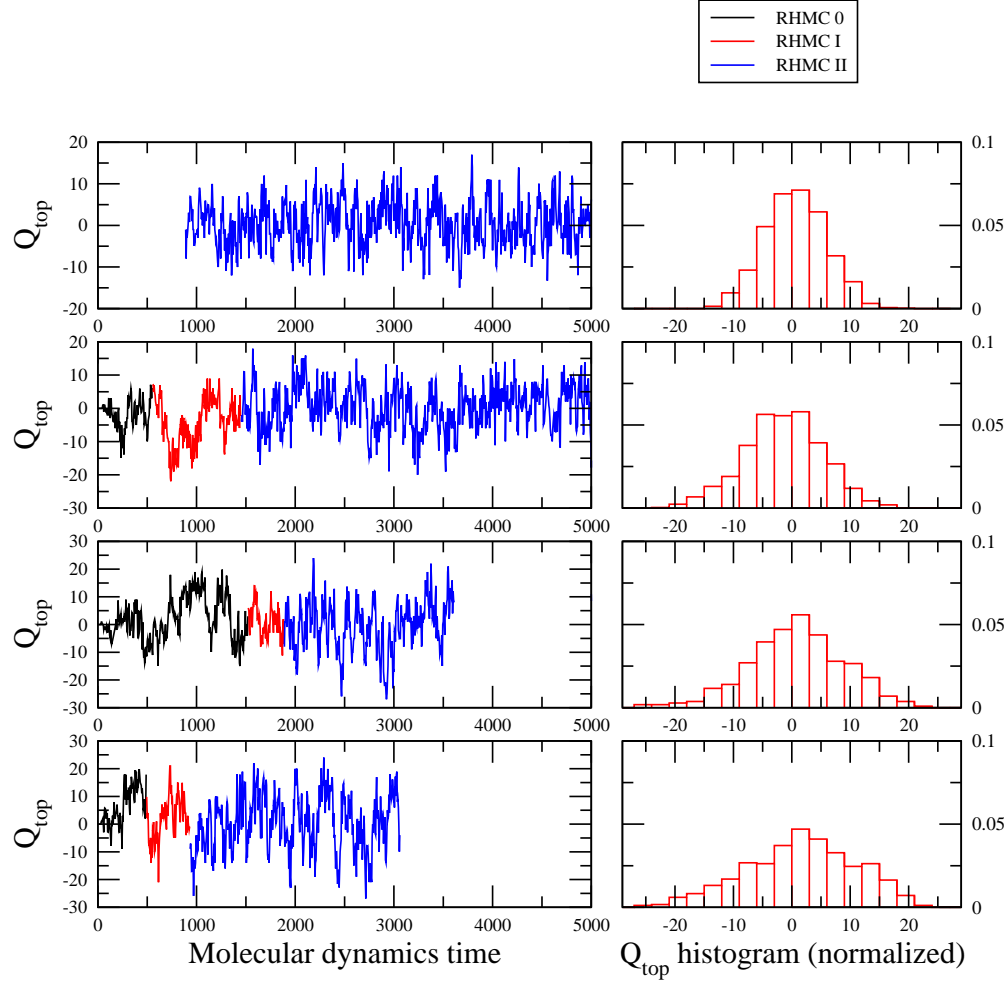


FIG. 3: The left graphs show topological charge, as measured on each ensemble every 5th unit of molecular dynamics time. The right panels show normalised histograms of topological charge. Notice the width of the histograms decreases as the light quark mass is reduced. For both the left and right graphs, the light dynamical quark mass is  $m_l = 0.005, 0.01, 0.02, 0.03$ , from top to bottom.

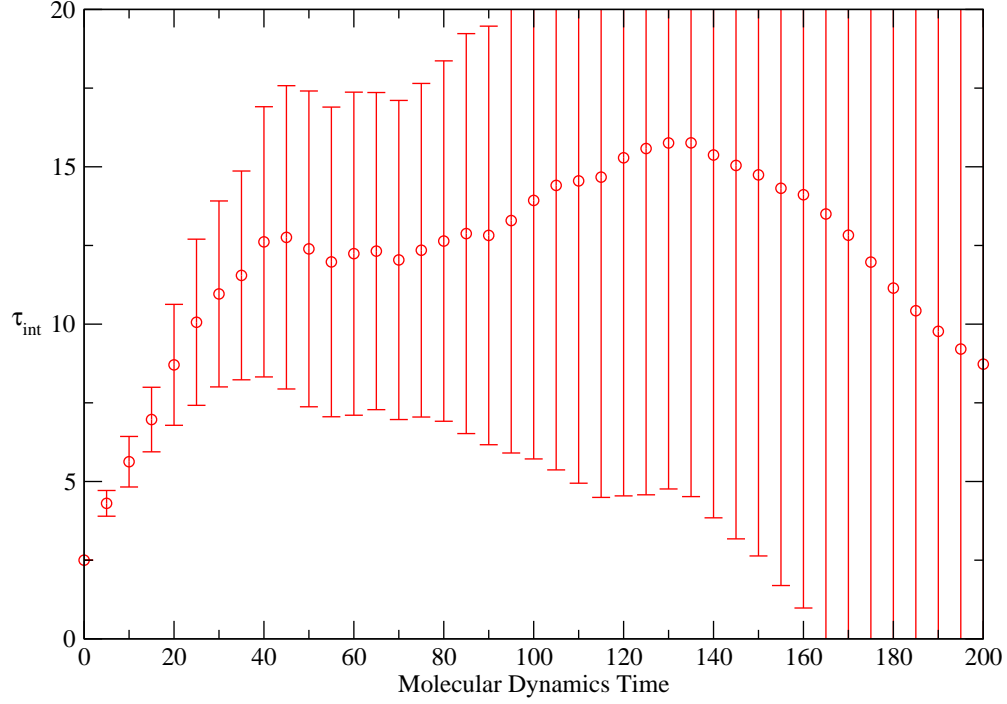


FIG. 4: Integrated autocorrelation time for 12th timeslice of the unitary degenerate pseudoscalar correlator with local sources and sinks,  $\langle P^{LL}, P^{LL} \rangle$ , measured on the  $m_l = 0.005$  ensemble. Measurements were done every fifth trajectory in the range 900-1530 and a bin factor of two was used in the analysis.

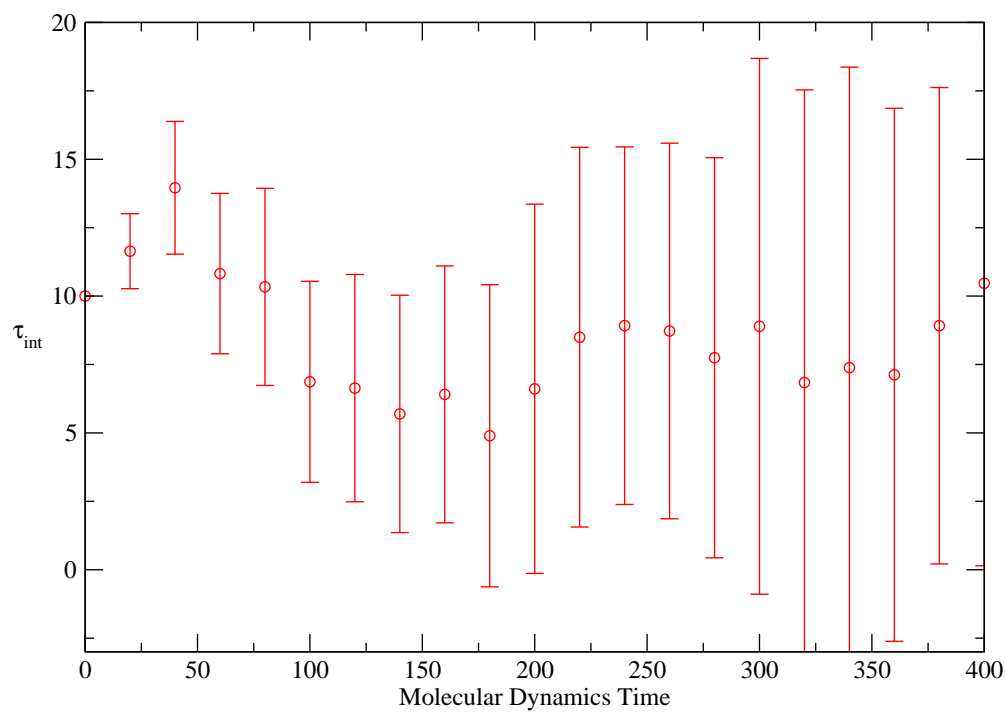


FIG. 5: Integrated autocorrelation time for 12th timeslice of the unitary degenerate pseudoscalar correlator with a local sink and a Gaussian source,  $\langle P^{LL}, P^{HH} \rangle$ , measured on the  $m_l = 0.005$  ensemble. Measurements were done every twentieth trajectory in the range 500-4500 and a bin factor of four was used in the analysis.

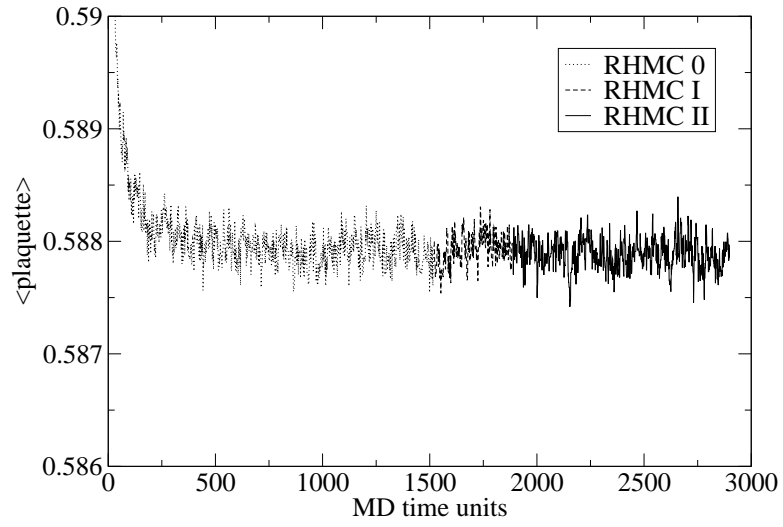


FIG. 6: Evolution history of the plaquette for the ensemble  $m_l = 0.02$

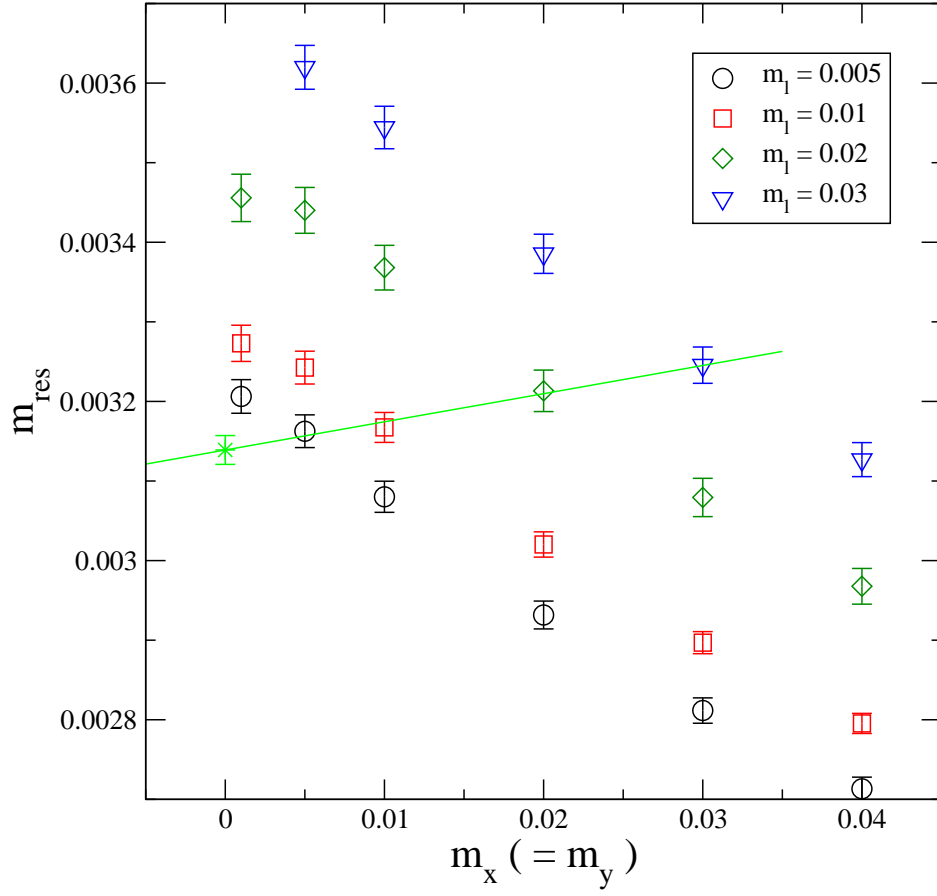


FIG. 7: The residual mass as a function of the valence quark mass. The solid line is a linear fit to the four unitary points with  $m_l = 0.005, 0.01, 0.02$  and  $0.03$ . The star is the extrapolation to  $m_l = 0$ , which we quote as the residual mass in our simulations.

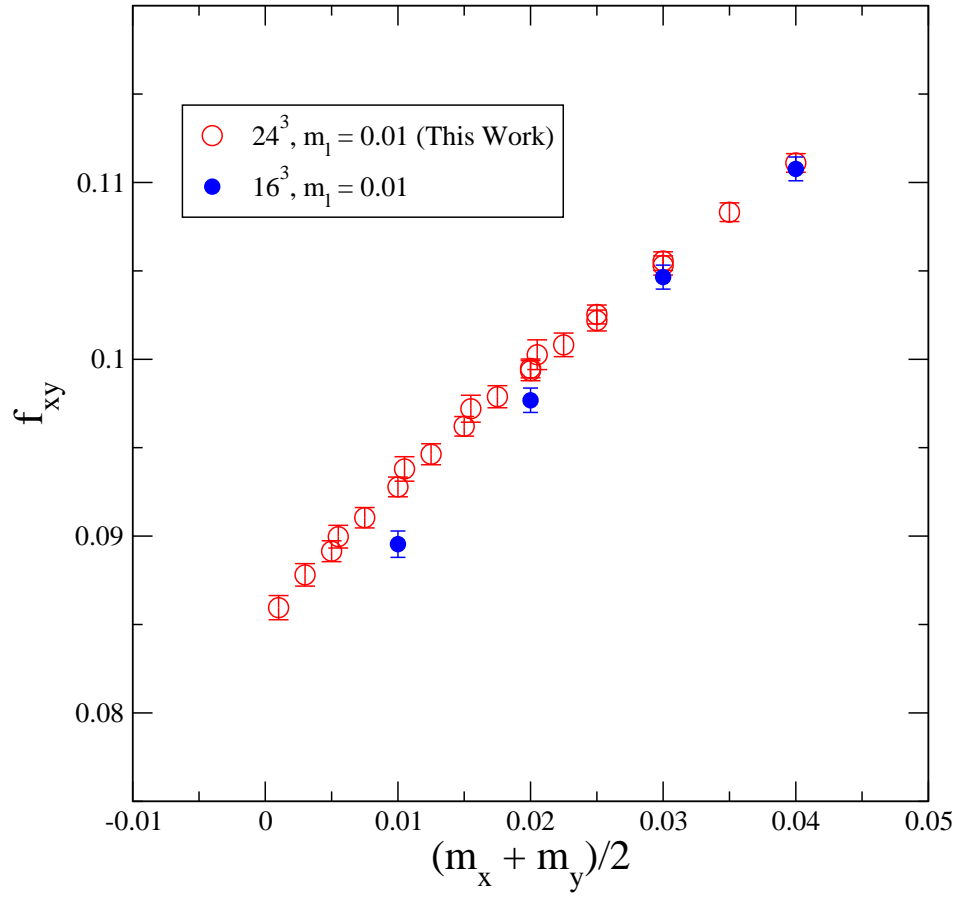


FIG. 8: Comparison of the lattice results for the pseudoscalar decay constants on the  $16^3 \times 32$  and  $24^3 \times 64$  lattices with  $m_l = 0.01$ .

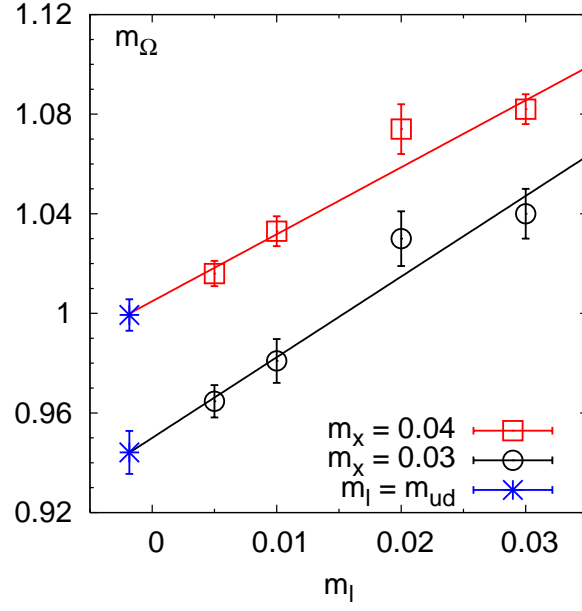


FIG. 9: Sea quark mass dependence of the decuplet baryon masses for degenerate valence quarks  $m_x = 0.03$  (black circles) and 0.04 (red squares). Linear fits are shown by solid lines. Blue asterisks denote masses extrapolated to the physical value of the bare, light sea quark mass  $m_{ud}$ .

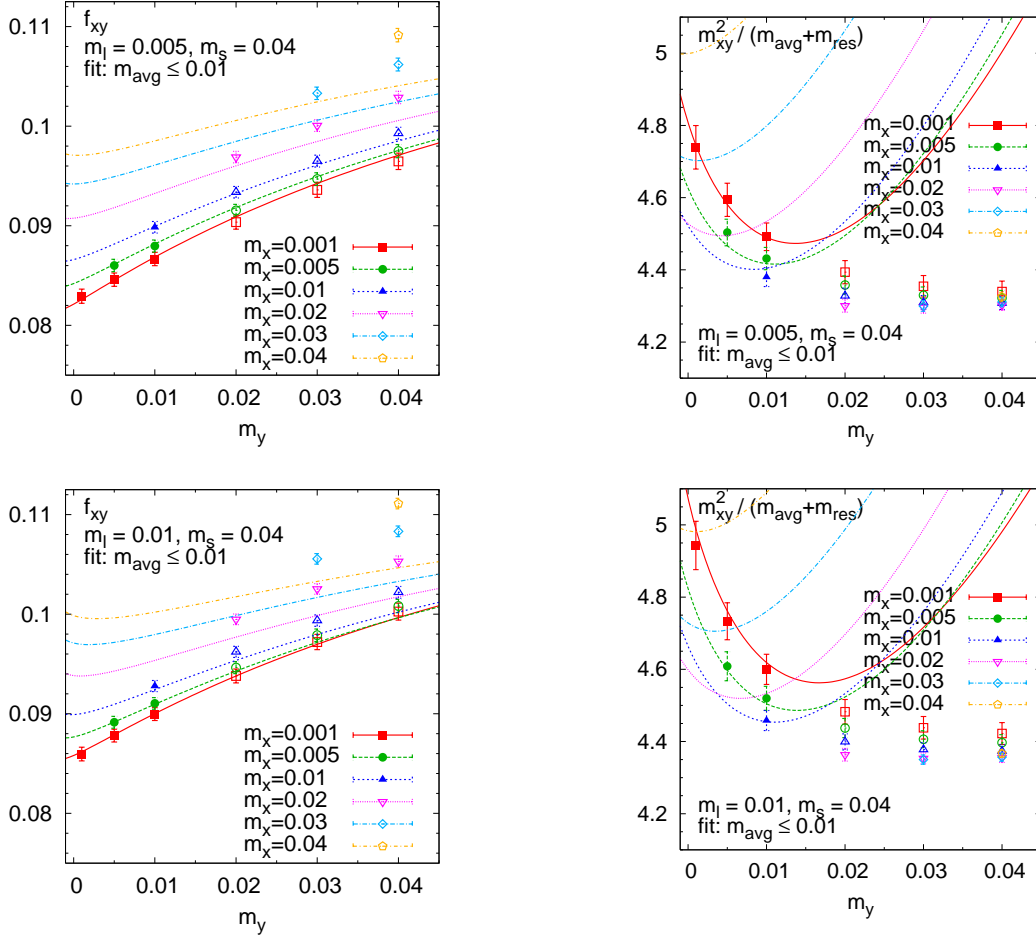


FIG. 10: Combined  $SU(2) \times SU(2)$  fits for the meson decay constants (*left panels*) and masses (*right panels*) at two different values for the light sea quark mass, and with a cut on the valence masses  $m_{\text{avg}} \leq 0.01$ . Points marked by *filled symbols* were included in the fit, while those with *open symbols* were excluded.



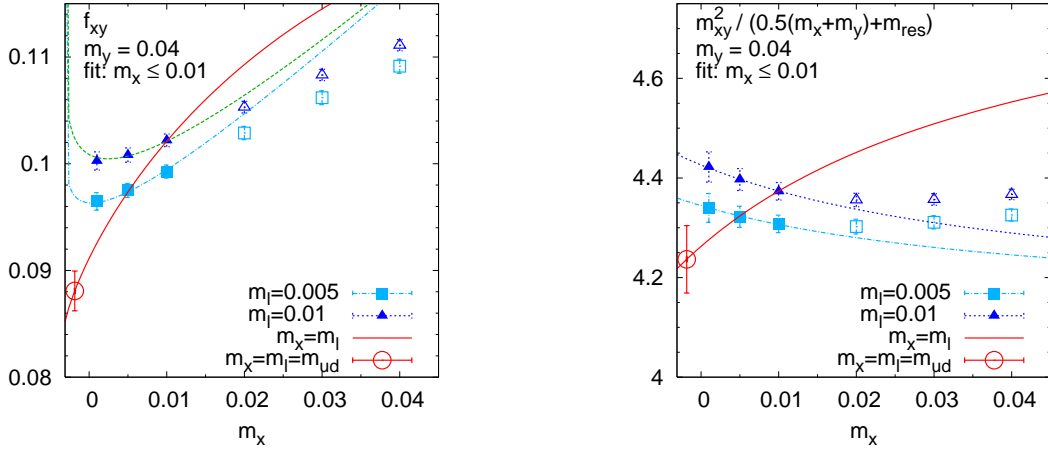


FIG. 11:  $SU(2) \times SU(2)$  fits for the kaon sector. *Left panel:* Kaon decay constant, *right panel:* Kaon mass squared for  $m_s = 0.04$ . Points with *filled symbols* were included in the fit, while those with *open symbols* were excluded.

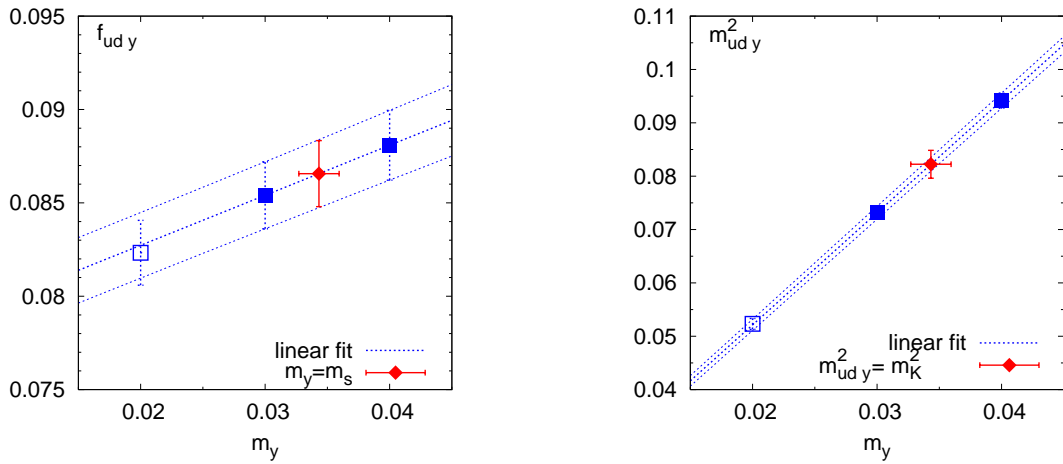


FIG. 12: Interpolation to the physical strange quark mass (*red diamond*) for  $m_K^2$  and  $f_K$ . *Open symbols* are not included in the interpolations. *Left panel:* Kaon decay constant, *right panel:* Squared kaon mass.

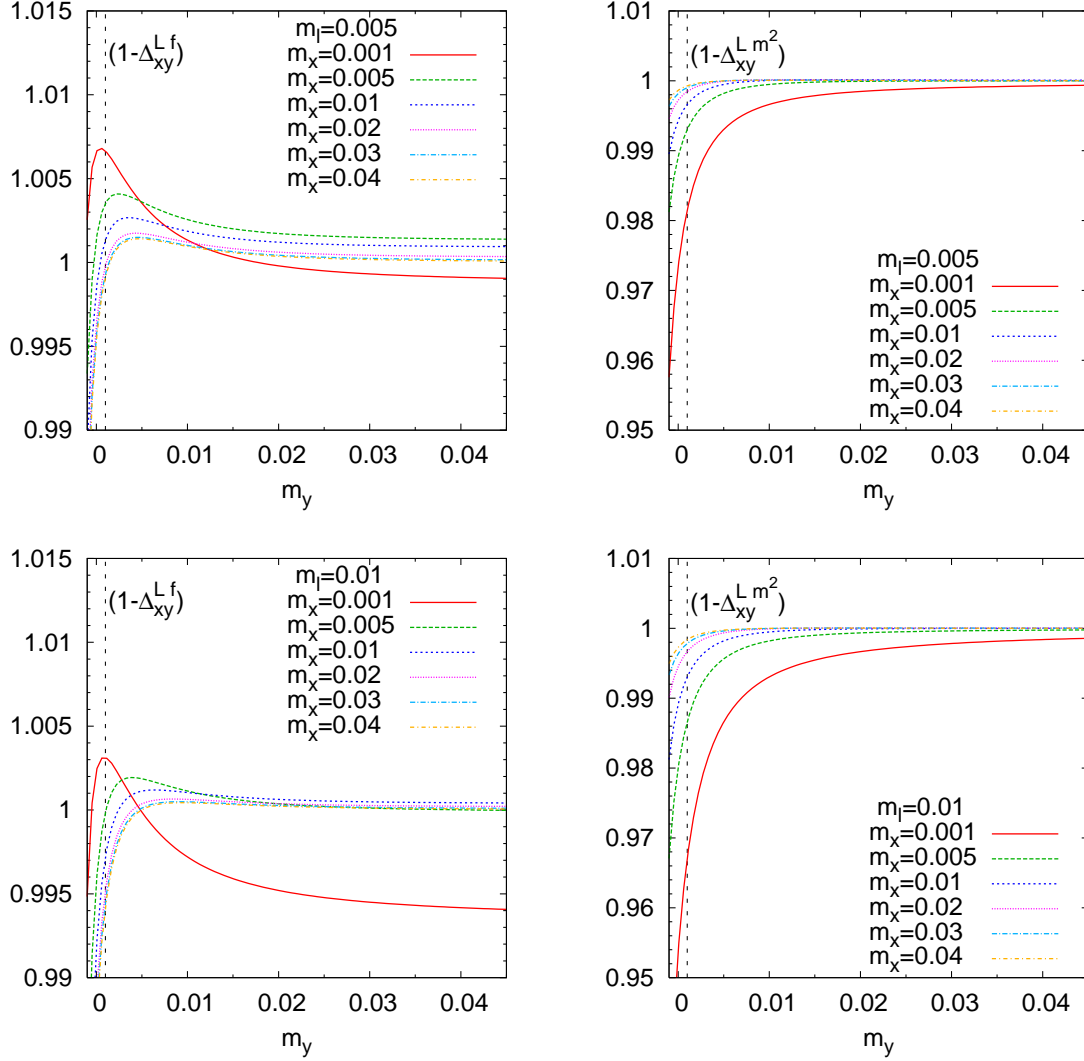


FIG. 13: Finite volume correction factor obtained from the SU(2) fits for the decay constants (*left panels*) and squared meson masses (*right panels*) at sea quark masses  $m_l = 0.005$  (*top panels*) and 0.01 (*bottom panels*). The vertical dashed line denotes the lightest (valence) mass used in this analysis ( $m_y = 0.001$ ).

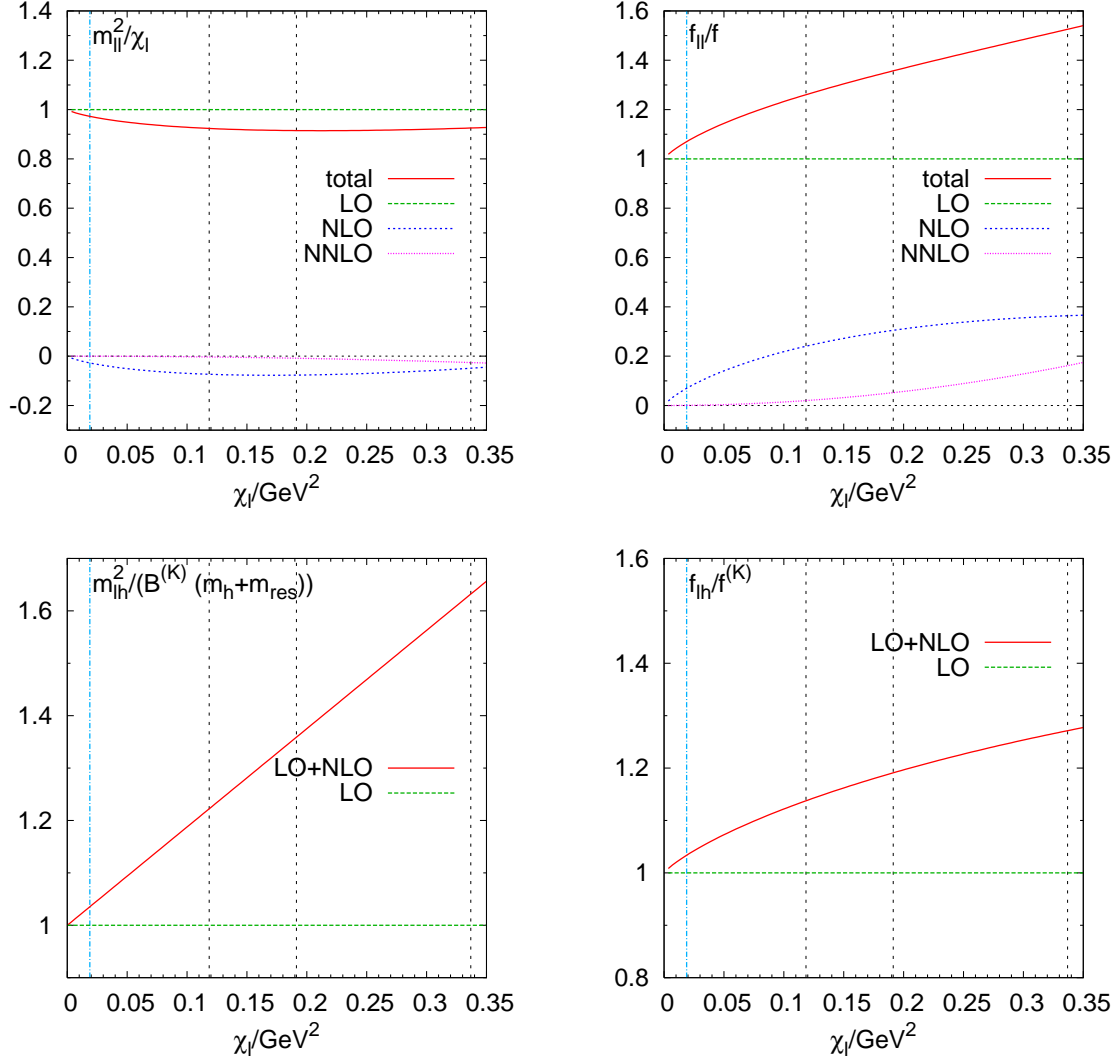


FIG. 14: Comparison of the size of the LO, NLO, and NNLO contributions in the  $SU(2) \times SU(2)$  fits for unitary degenerate meson masses squared  $m_{H'}^2$  (*upper left panel*) and decay constants  $f_{H'}$  (*upper right panel*) as a function of the the light sea quark mass parameter  $\chi_l$  (for details see Sec. VIC 1). The LO-contribution is normalized to one. *Vertical dashed lines* indicate quark masses of  $m_l = m_{ud}, 0.005, 0.01, 0.02$  (from left to right). The lower panels give a comparison of the size of the LO and NLO contributions in kaon ChPT for the kaon mass squared  $m_{H'}^2$  (*lower left panel*) and kaon decay constant  $f_{H'}$  (*lower right panel*) as a function of the the light sea quark mass.

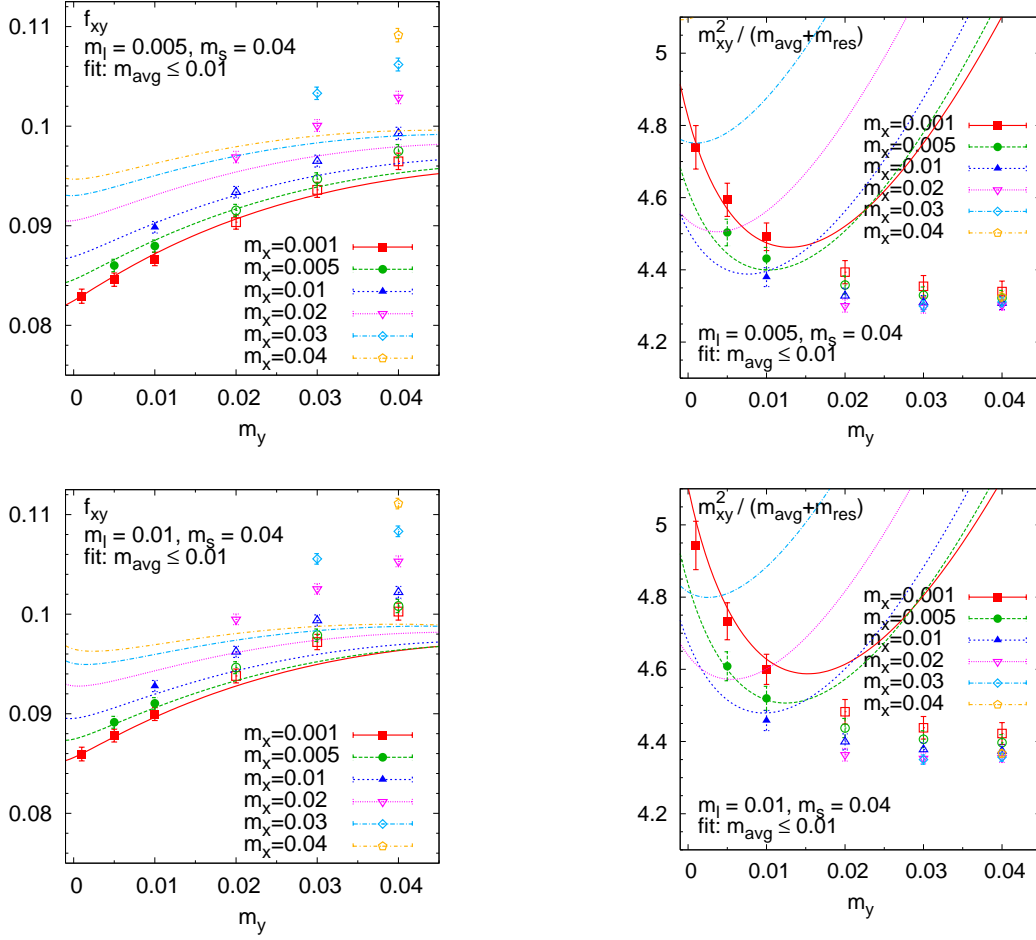


FIG. 15: Combined  $SU(3) \times SU(3)$  fits for the meson decay constants (*left panels*) and masses (*right panels*) at two different values for the light sea quark mass, with valence mass cut  $m_{\text{avg}} \leq 0.01$ . Points marked by *filled symbols* were included in the fit, while those with *open symbols* were excluded.

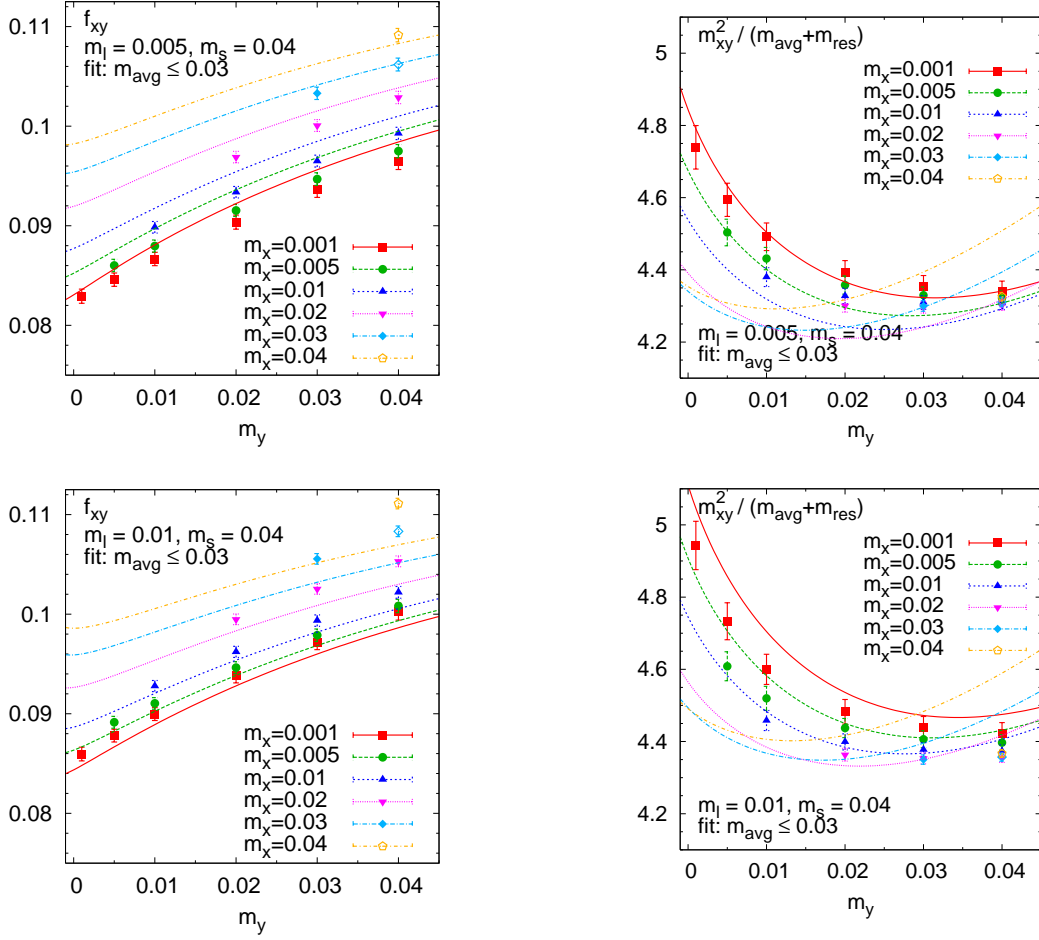


FIG. 16: Combined  $SU(3) \times SU(3)$  fits for the meson decay constants (*left panels*) and masses (*right panels*) at two different values for the light sea quark mass, with valence mass cut  $m_{\text{avg}} \leq 0.03$ . Points marked by *filled symbols* were included in the fit, while those with *open symbols* were excluded.

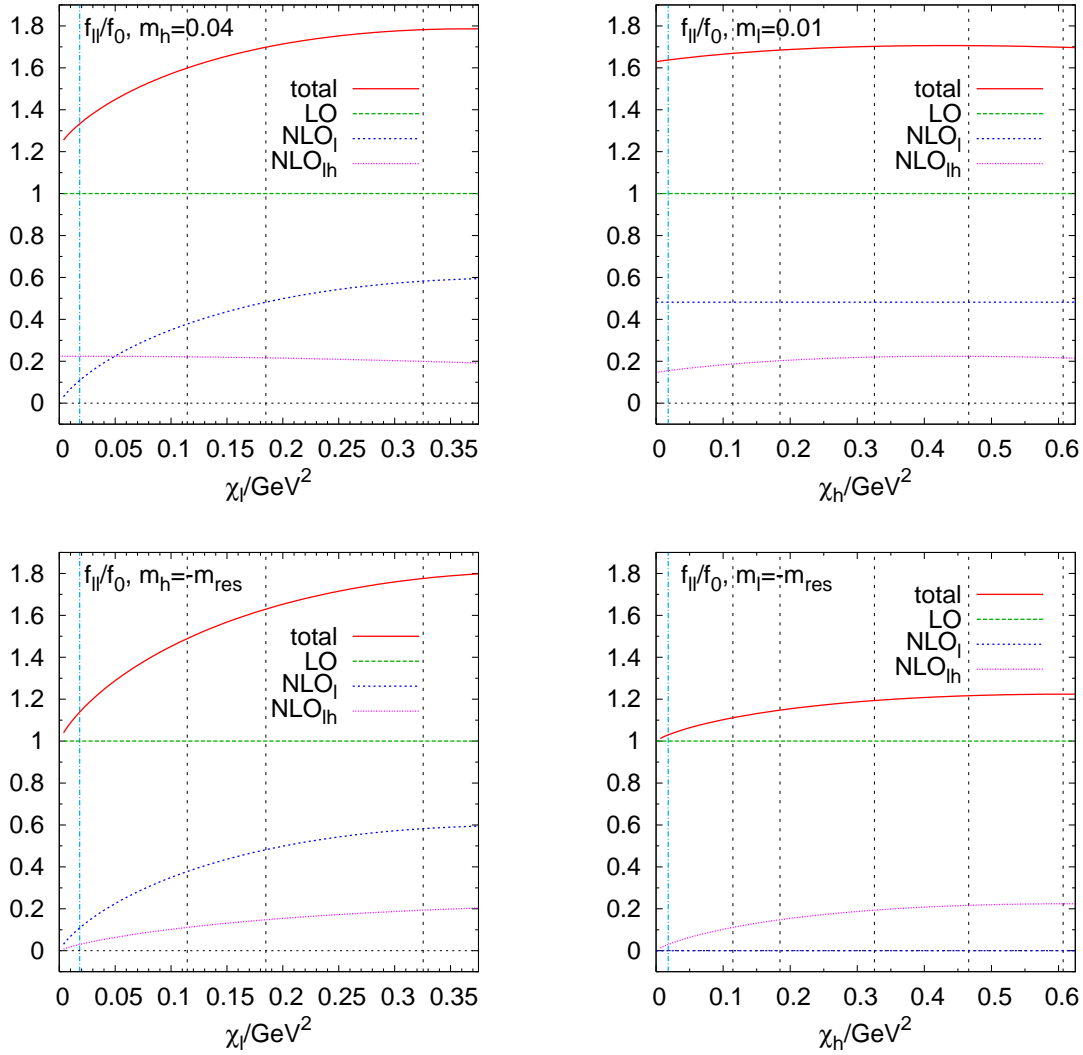


FIG. 17: Leading order (LO) and Next-to-Leading order (NLO) contributions in the unitary meson decay constant fit in SU(3) PQChPT as function of the light quark mass parameter (*left panels*) and the heavy quark mass parameter (*right panels*). In the plots in the *top panels* the other quark mass parameter was set to our highest value used in the fits ( $m_l = 0.01$  or  $m_h = 0.04$ ), while in those in the *bottom panels* the remaining quark mass parameter was set to zero ( $m_l$  or  $m_h = -m_{\text{res}}$ ). NLO<sub>l</sub> denotes the NLO contribution proportional to  $\log \chi_l$  and NLO<sub>lh</sub> the NLO contribution proportional to  $\log(\chi_l + \chi_h)/2$ . The LO contribution is always normalized to one. *Vertical dashed lines* indicate quark masses of  $m_l = m_{ud}, 0.005, 0.01, 0.02, 0.03, \text{ and } 0.04$  (from left to right, left panels only show quark masses up to 0.02).

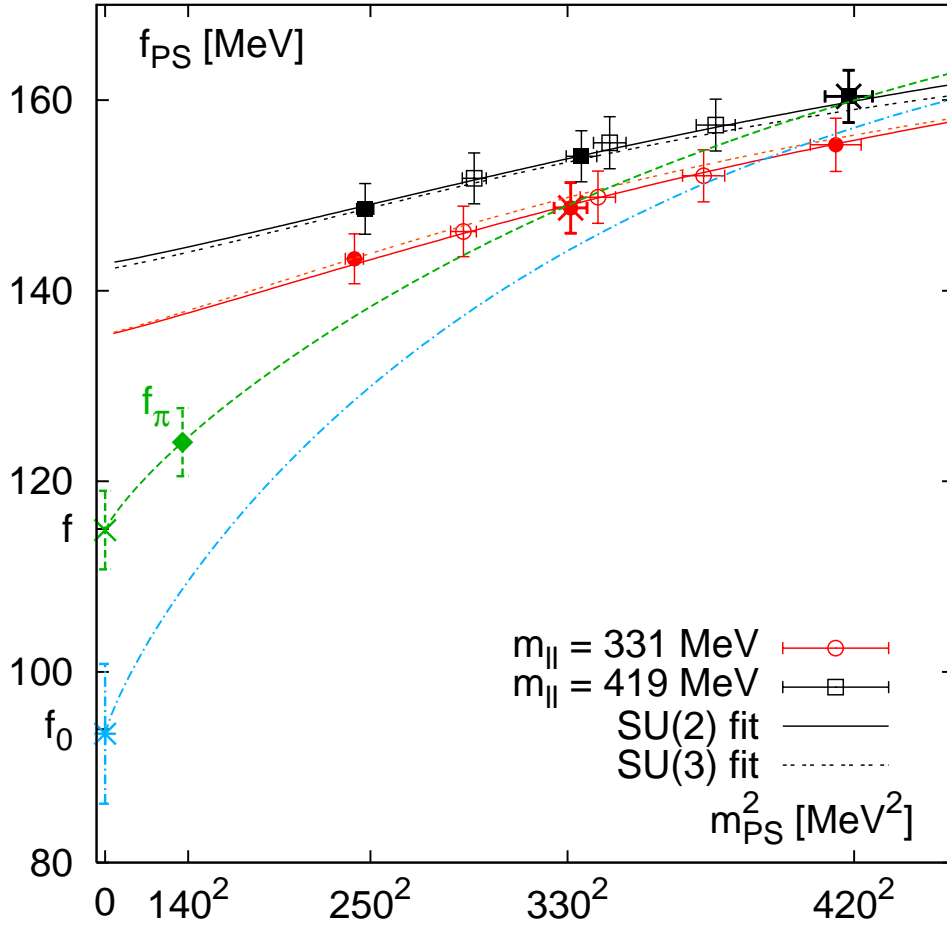


FIG. 18: A plot of our measured values for the decay constant, converted to physical units, versus the degenerate valence pseudoscalar mass squared. The data for degenerate quarks is denoted by filled symbols and for non-degenerate quarks, open symbols are used. The graph shows that we see small effects for non-degenerate quarks. The results of SU(2) and SU(3) partially quenched ChPT fits to our data are shown, and both fits agree well with the data. The unitary SU(2) chiral extrapolation is also given, along with our value of  $f$ , and two of our data points lie on this curve, as expected. The value of  $f$  differs by  $\approx 30\%$  from the decay constant measured at  $m_\pi = 420 \text{ MeV}$ . We also plot the SU(3) chiral limit curve, for which the horizontal axis is the unitary meson mass for three degenerate mass quarks. None of our measured values must lie on this line. The large difference between  $f_0$  and our measurements is apparent, showing the poor convergence of NLO SU(3) ChPT, with LECs as determined from our data.

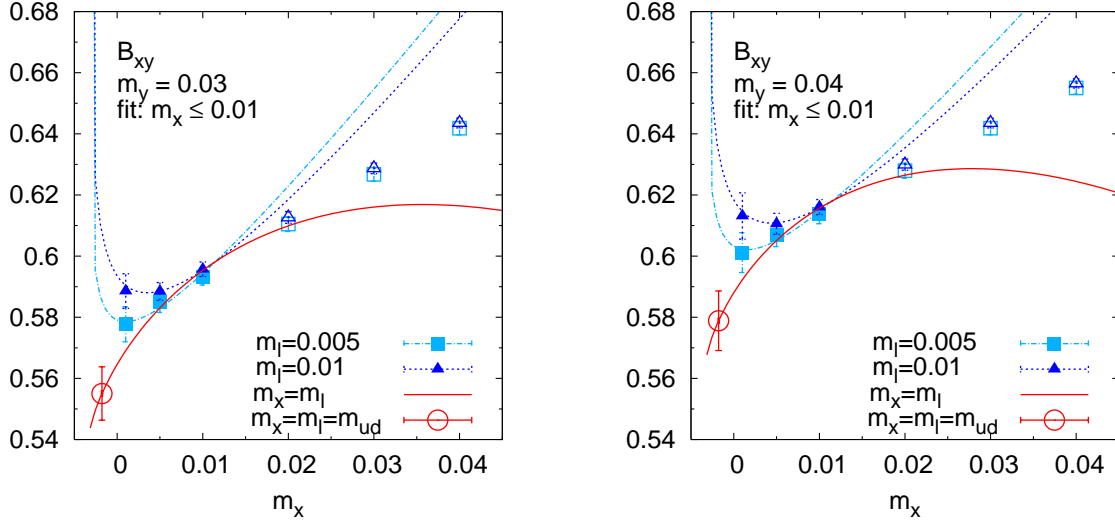


FIG. 19: Extrapolation of the pseudoscalar bag parameter  $B_{xy}$  in the light quark mass  $m_x$  to the physical point  $m_{ud}$  for  $m_y = 0.03$  (left panel) and  $m_y = 0.04$  (right panel). Points with *filled symbols* are included in the fit while those marked by *open symbols* are excluded. For fit parameters see Table XXII.



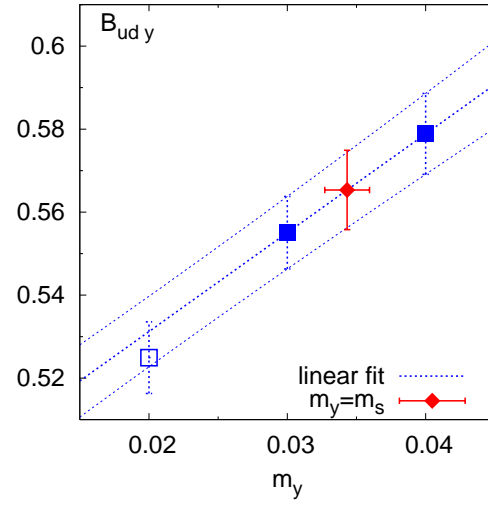


FIG. 20: Linear interpolation in  $m_y$  of the pseudoscalar bag parameter  $B_{udy}$  to the physical strange quark mass  $m_s$  (red diamond). The open symbol at  $m_y = 0.02$  was excluded from the interpolation.

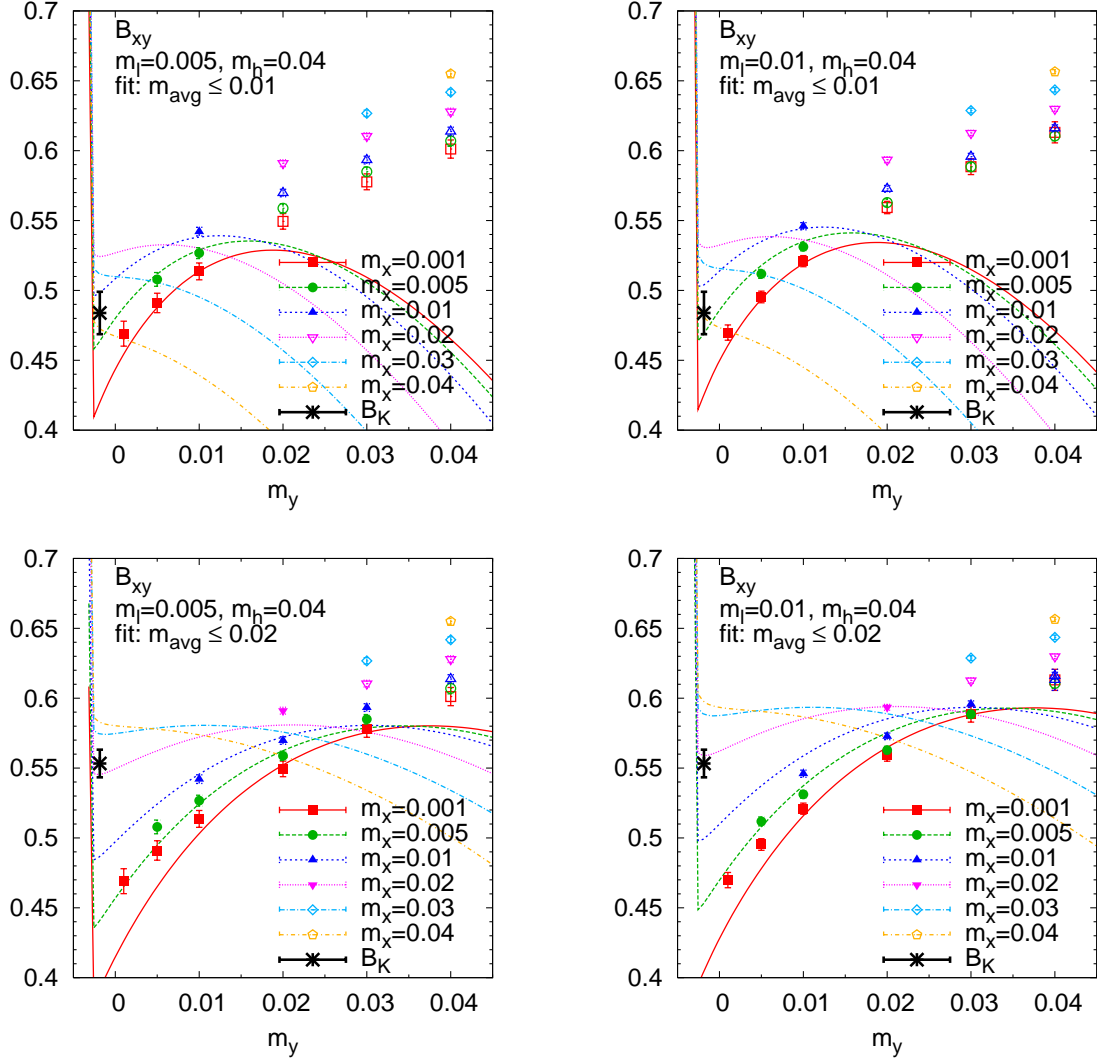


FIG. 21: Fitting the pseudoscalar bag parameter  $B_{xy}$  to the  $SU(3) \times SU(3)$   $\chi$ PT formulae with a cut in the average valence mass value of 0.01 (*top panels*) and 0.02 (*bottom panels*). Points marked by *open symbols* are excluded from the fit. The *left panels* are for light sea quark masses  $m_l = 0.005$ , the *right panels* for  $m_l = 0.01$ .

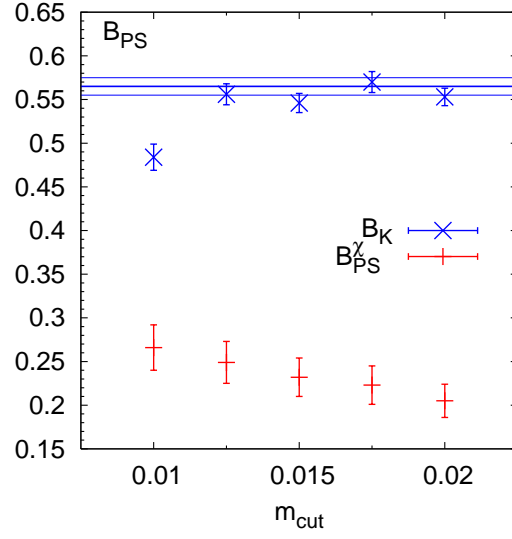


FIG. 22: Dependence of the fit parameter  $B_{\text{PS}}^{\chi}$  (red bars) and the extrapolated physical value of  $B_K$  (blue crosses) on the average valence mass cut, when fitting to the  $\text{SU}(3) \times \text{SU}(3)$  fit formula. The blue lines indicate the result (with statistical error) for  $B_K$  obtained from the  $\text{SU}(2) \times \text{SU}(2)$  fit.

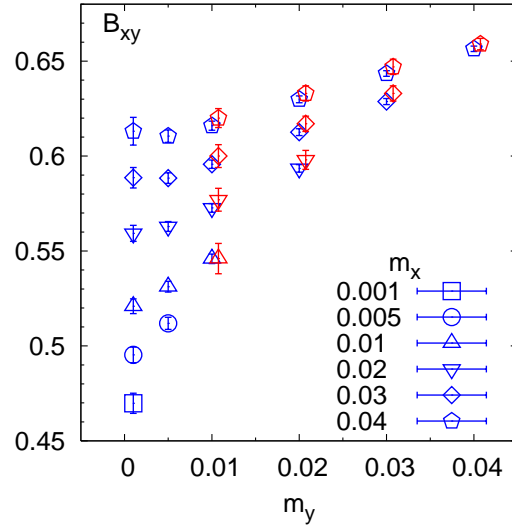


FIG. 23: Comparison of the pseudoscalar bag parameter  $B_{xy}$  for valence quark masses  $m_x$ ,  $m_y$  measured on  $16^3 \times 32$  (red symbols) and  $24^3 \times 64$  (blue symbols) lattices at  $m_l = 0.01$ ,  $m_h = 0.04$ . (Red symbols are slightly shifted to the right on this plot.)

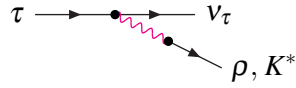


FIG. 24: The diagram illustrating how  $\tau$  decays can be used to deduce  $f_\rho$  and  $f_{K^*}$ .

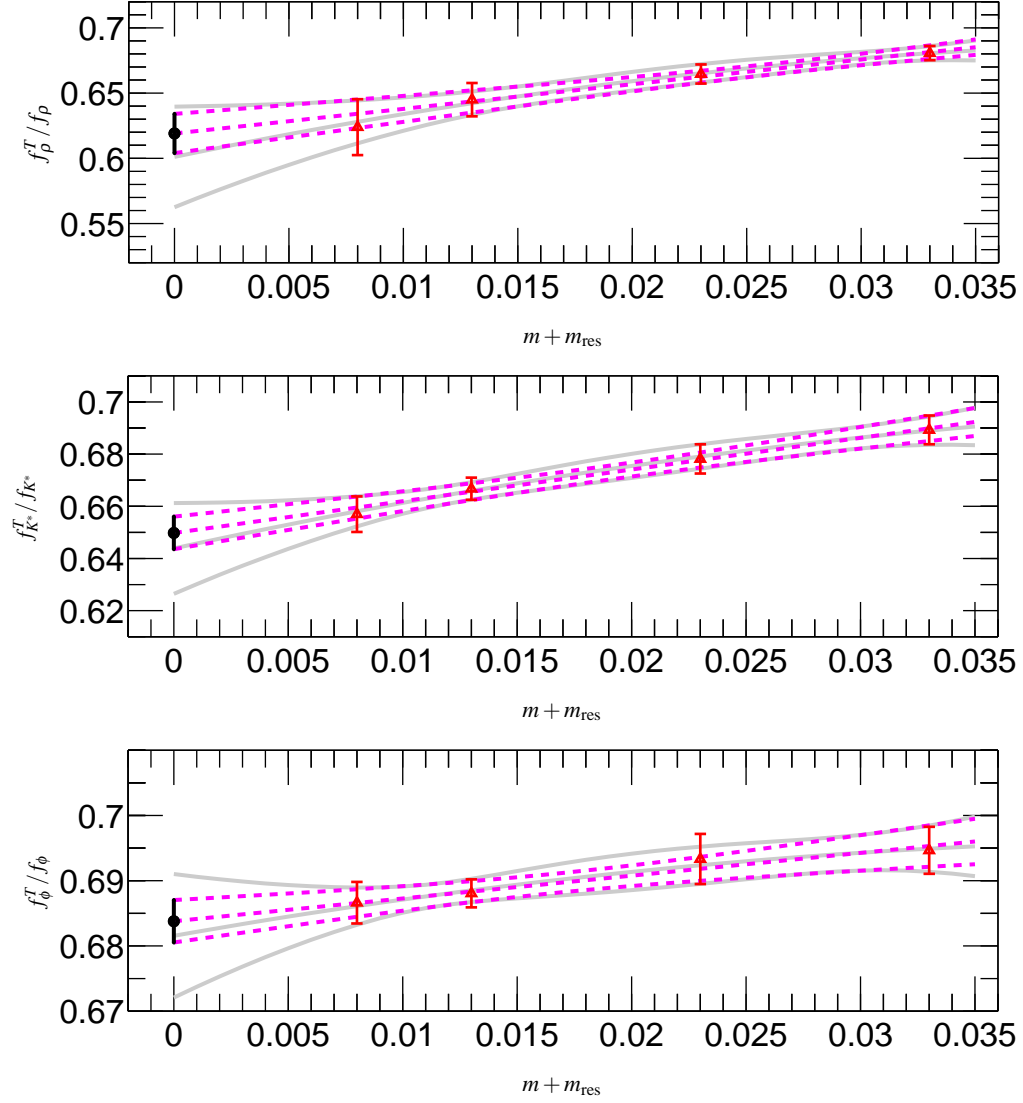


FIG. 25: Chiral extrapolations for  $f_{\rho}^T/f_{\rho}$ ,  $f_{K^*}^T/f_{K^*}$  and  $f_{\phi}^T/f_{\phi}$  respectively. The broken red lines represent a linear fit to the mass behaviour and the solid grey lines a quadratic fit.